

A Comprehensive Study on Multiphase Flow through Pipeline and Annuli using CFD

Approach

by

© Rasel A Sultan

A Thesis submitted to the

School of Graduate Studies

in partial fulfilment of the requirements for the degree of

Master of Engineering

Faculty of Engineering and Applied Science

Memorial University of Newfoundland

May 2018

St. John's

Newfoundland

Abstract

The physical phenomenon of more than one state or phase (i.e. gas, liquid or solid) simultaneously flowing is defined as multiphase flow. The overall performance of multiphase flow is more complex compared to single phase flow through pipeline or annuli. Calculation accuracy of pressure drop, and particle concentration is very important to design pipeline or annular geometry for multiphase flow. The objectives in the present study are to design a CFD model that can be used to predict multiphase fluid flow properties with more accuracy; to validate proposed CFD model with experimental data and existing empirical correlations at different orientations of geometry and combination of fluids; and to investigate the effects of pipe diameter, wall roughness, fluid velocity, fluid type, particle size, particle concentration, drill pipe rotation speed and drill pipe eccentricity on pressure losses and settling conditions. Three distinct phases of working fluids are used to fulfill the project. Simulation process is conducted using ANSYS fluent version 16.2 platform. Eulerian model with Reynolds Stress Model (RSM) turbulence closure is selected as optimum to analyze multiphase fluid flow. Pressure gradient and sand concentration profile are the primary output parameters to analyze. This article combines validation work at all possible cases to verify the developed model and parametric study to observe the effects of selected parameters on particle deposition. In parametric analysis, eccentricity of the annular pipe is varied from 0 – 50% and rotated about its own axis from 0 – 150 rpm. The diameter ratio of the simulated annuli is 0.56. Results show very good agreement with existing experiments and developed correlations. Also, the effects of different parameters are briefly analyzed with proper explanations. Fluid Structure Interaction (FSI) is introduced to observe the fluid flow effect on pipeline deformation.

Acknowledgement

First and foremost, I am very grateful to my supervisor Dr. Mohammad Azizur Rahman, co-supervisors Dr. Sohrab Zendehboudi and Dr. Vassilios C. Kelessidis, for the continuous support, guidance, and encouragement they gave me and also for the financial support provided. I acknowledge with gratitude the valuable suggestions and feedback in preparation of the manuscripts given by Dr. Vandad Talimi from C-Core Canada and Dr. M M A Rushd from Texas A&M University at Qatar. Also, I greatly acknowledge the funding received by Natural Science and Engineering Research Council (NSERC) of Canada, Research and Development Corporation Newfoundland and Labrador (RDC, newly called InnovateNL) and School of Graduate Studies (SGS) of Memorial University.

Furthermore, I highly appreciate the support given by the research and administration staff of the Faculty of Engineering and Applied Science, Memorial University. Especially Dr. Faisal Khan, Dr. Leonard Lye, Moya Crocker, Colleen Mahoney, and everyone who helped me in some way. My heartfelt thanks also go to all my friends and colleagues for their continuous support from the beginning, specially Mohammad Masum Jujuly who supported me to learn ANSYS software.

Finally, I would like to thank my mother Aleya Begum, my father Mohammed Tipu Sultan and my sister Rahana Sultana for all the love and support. Thank you.

Table of Contents

| | |
|---|------|
| Abstract | ii |
| Acknowledgement | iii |
| Table of Contents | iv |
| List of Tables | vi |
| List of Figures | vii |
| List of Appendices | xii |
| List of Symbols, Nomenclature or Abbreviations | xiii |
| Introduction..... | 1 |
| Co-authorship Statement..... | 5 |
| Chapter 1. Validation of CFD Simulation Model with Multiphase Fluid Flow through Pipeline and Annular Geometry..... | 6 |
| Introduction | 6 |
| Theory | 7 |
| Multiphase Model..... | 9 |
| Turbulence Model..... | 12 |
| Simulation Methodology..... | 16 |
| Results and Discussions | 21 |
| Single Phase Flow through Pipeline | 22 |
| Single Phase Flow through Annuli..... | 23 |
| Two Phase (solid-liquid) flow through Pipeline..... | 24 |
| Two Phase (solid-liquid) flow through Annuli..... | 31 |
| Two Phase (gas-liquid) flow through Pipeline | 32 |
| Three Phase (solid-liquid-gas) flow through Pipeline..... | 34 |
| Future Plan | 37 |
| Conclusion..... | 37 |
| Acknowledgments | 40 |
| Reference..... | 40 |
| Chapter 2. Pressure Losses and Settling Conditions in a Horizontal Annulus | 49 |
| Introduction | 49 |

| | |
|---|-----|
| Literature Review | 50 |
| Methods | 51 |
| CFD Simulation | 51 |
| Turbulence Model Selection | 54 |
| Length Independence Study | 59 |
| Mesh analysis | 60 |
| CFD Model Validation | 62 |
| Single Phase Flow through Annuli | 62 |
| Two Phase (solid-liquid) flow through Annuli | 64 |
| Results and Discussion | 65 |
| Effect of Flow Rate | 66 |
| Effect of Drill Pipe Rotation and Eccentricity | 71 |
| Effect of Particle Size | 72 |
| Conclusions | 73 |
| References | 74 |
| Chapter 3. CFD Simulation of Three Phase Gas-Liquid-Solid Flow in Horizontal Pipes | 80 |
| Introduction | 81 |
| Mathematical Model | 82 |
| Simulation Methodology | 88 |
| Simulation Validation | 89 |
| Parametric Sensitivity Study | 92 |
| Conclusion | 98 |
| References | 99 |
| Summary | 106 |
| Appendices | 108 |

List of Tables

Tables in Chapter 1

| | |
|---|----|
| Table 1. Variable Parameter Ranges..... | 21 |
|---|----|

Tables in Chapter 2

| | |
|--|----|
| Table 1. Analysis of Turbulence Model Performance..... | 55 |
|--|----|

Tables in Chapter 3

| | |
|--|----|
| Table 1. Mesh Distribution Statistics..... | 88 |
|--|----|

List of Figures

Figures in Chapter 1

| | |
|--|----|
| Figure 1. Presentation of the comparative analysis of different turbulence models: (a) Kelessidis et al., 2011, (b) Skudarnov et al., 2004..... | 14 |
| Figure 2. Presentation of Mesh Independence from Fukuda and Shoji, 1986..... | 17 |
| Figure 3. Mesh distribution in (a) pipe geometry, (b) annular geometry..... | 19 |
| Figure 4. Pressure Gradient variation along pipe length..... | 20 |
| Figure 5. Optimum convergence rate analysis from Camçi, 2003..... | 20 |
| Figure 6. Comparison of simulated pressure gradient with Wood (1966) correlation, experimental data from Kaushal et al. (2005) and Skudarnov et al. (2004) at different inlet velocity..... | 22 |
| Figure 7. Comparison of simulated pressure gradient with Haaland (1983) correlation and experimental data from Kelessidis et al. (2011) and Camçi (2003) at different inlet velocity..... | 24 |
| Figure 8. Particle size distribution of different particle used in Kaushal et al. (2005)... | 26 |
| Figure 9. Comparison of simulated pressure gradient with experimental data from Skudarnov et al. (2001), Kaushal et al. (2005) and Skudarnov et al. (2004) at different inlet slurry velocity..... | 27 |
| Figure 10. Comparison of simulated solid local volumetric concentration across vertical centerline with Gillies and Shook, 1994..... | 28 |
| Figure 11. Comparison of simulated and measured solid local volumetric concentration across vertical centerline with Roco and Shook, 1983..... | 29 |

| | |
|--|----|
| Figure 12. Particle size distribution of different particle used in Roco and Shook (1983)..... | 30 |
| Figure 13. Solid concentration distribution in the vertical cross section plane (data from Roco and Shook, 1983)..... | 31 |
| Figure 14. Comparison of simulated two-phase frictional pressure gradient at different mixture velocity and volume concentration of slurry with Ozbelge and Beyaz, 2001..... | 32 |
| Figure 15. Comparison of simulated axial liquid velocity at vertical position with experimental data from Kocamustafaogullari and Wang, 1991..... | 33 |
| Figure 16. Comparison of simulated axial liquid velocity at horizontal position with experimental data from Kocamustafaogullari and Wang, 1991..... | 34 |
| Figure 17. Comparison of simulated pressure gradient as a function of gas velocity with experimental data from Fukuda and Shoji, 1986..... | 35 |
| Figure 18. Comparison of simulated pressure gradient as a function of gas volume fraction with Gillies et al., 1997..... | 36 |
| Figure 19. Particle size distribution of different particle used in Fukuda and Shoji (1986)..... | 37 |
| Figure 20. Overall simulation predictions of different experiment data..... | 39 |

Figures in Chapter 2

| | |
|---|----|
| Figure 1. Performance of turbulence models in predicting pressure loss (Data Source: Kaushal et al., 2005)..... | 54 |
|---|----|

| | |
|---|----|
| Figure 2. Length independence analysis (A) 75% eccentric, 150 RPM inner pipe rotation speed and 400 kg/min flow rate; (B) Concentric, stationary inner pipe and 200 kg/min flow rate..... | 59 |
| Figure 3. Mesh distribution..... | 61 |
| Figure 4. Mesh independence analysis..... | 61 |
| Figure 5. An example of optimum convergence rate analysis..... | 62 |
| Figure 6. Comparison of simulated pressure gradient with Haaland (1983) correlation and experimental data from Kelessidis et al. (2011) and Camçi (2003) at different inlet velocity..... | 63 |
| Figure 7. Comparison of simulated two-phase frictional pressure gradient at different mixture velocity and volume concentration of slurry with Ozbelge and Beyaz, 2001... | 65 |
| Figure 8. Effect of fluid flow on particle concentration profile (Concentric annuli with stationary inner pipe)..... | 66 |
| Figure 9. Effect of fluid flow on particle concentration profile (Concentric annuli with 150 rpm rotating inner pipe)..... | 67 |
| Figure 10. Effect of fluid flow on particle concentration profile (50% eccentric annuli with stationary inner pipe)..... | 67 |
| Figure 11. Effect of fluid flow on particle concentration profile (50% eccentric annuli with 150 rpm inner pipe)..... | 68 |
| Figure 12. Contour distribution of sand concentration profile: (a) $Re = 4 \cdot 10^4$, (b) $Re = 7 \cdot 10^4$, (c) $Re = 10^5$ and (d) $Re = 2 \cdot 10^5$ | 70 |
| Figure 13. Effect of inner pipe rotation on pressure loss..... | 71 |

| | |
|--|----|
| Figure 14. Effect of inner pipe eccentricity on pressure loss at different rotational speed..... | 72 |
|--|----|

| | |
|---|----|
| Figure 15. Effect of sand particle size on bed concentration near wall..... | 73 |
|---|----|

Figures in Chapter 3

| | |
|--|----|
| Figure 1. Optimum turbulence model analysis..... | 85 |
|--|----|

| | |
|---|----|
| Figure 2. Mesh distribution in the pipe geometry..... | 88 |
|---|----|

| | |
|--|----|
| Figure 3. Optimum convergence rate analysis..... | 89 |
|--|----|

| | |
|--|----|
| Figure 4. Comparison of simulation data with correlations (Wood, 1966) and experimental data of Skudarnov et al. (2004)..... | 90 |
|--|----|

| | |
|--|----|
| Figure 5. Comparison of pressure gradient as a function of gas velocity with 24.7% solid volume concentration in slurry (C_v) and 3 m/s slurry velocity..... | 91 |
|--|----|

| | |
|---|----|
| Figure 6. Pressure Gradient at different gas velocity and solid volume concentration in slurry with other variables constant..... | 92 |
|---|----|

| | |
|---|----|
| Figure 7. Sand concentration distribution in vertical plane at outlet with 1.14 m/s air inlet. (a) $C_v = 8.8\%$ and (b) $C_v = 13.3\%$ | 94 |
|---|----|

| | |
|--|----|
| Figure 8. Sand concentration distribution in vertical plane at outlet with $C_v = 24.7\%$. (a) 0.643 m/s air inlet, (b) 1.36 m/s air inlet and (c) 1.9 m/s air inlet..... | 95 |
|--|----|

| | |
|--|----|
| Figure 9. Pressure Gradient at different gas velocity and pipe diameter with other variables constant..... | 96 |
|--|----|

| | |
|---|----|
| Figure 10. Pressure Gradient at different gas velocity and pipe wall roughness with other variables constant..... | 96 |
|---|----|

| | |
|---|----|
| Figure 11. Pressure Gradient at different gas velocity and water viscosity with other variables constant..... | 97 |
| Figure 12. Contour of pipeline deformation..... | 99 |

List of Appendices

| | |
|---|-----|
| Appendix 1. Sensitivity Analysis of A CFD Model for Simulating Slurry Flow Through Pipeline..... | 108 |
| Appendix 2. A Computational Fluid Dynamics Study of Two-Phase Slurry and Slug Flow in Horizontal Pipelines..... | 139 |
| Appendix 3. CFD and Experimental Approach on Three Phase Gas-Liquid-Solid Newtonian Fluid flow in Horizontal Pipes..... | 152 |
| Appendix 4. Data Tables..... | 173 |

List of Symbols, Nomenclature or Abbreviations

| | |
|---------------|--|
| CFD | Computational Fluid Dynamics |
| RSM | Reynolds Stress Model |
| SST | Shear Stress Transport |
| RANS | Reynolds Averaged Navier–Stokes |
| LES | Large Eddy Simulation |
| FSI | Fluid Structure Interaction |
| SIMPLE | Semi-Implicit Method for Pressure Linked Equations |
| ANN | Artificial Neural Network |
| d_m | Sand Particle Diameter |
| C_v | Sand Volumetric Concentration |
| D | Pipe Diameter |
| D_h | Hydraulic Diameter |
| d_a | Air Bubble Diameter |
| C_a | Air Volumetric Concentration |
| v | Fluid Velocity |
| v_a | Air Velocity |
| v_w | Water Velocity |
| v_s | Sand Velocity |
| ε | Wall Roughness |
| Re | Reynolds Number |
| f | Friction Factor |

Introduction

The use of multiphase flow like liquid-gas, liquid-solid and even solid-liquid-gaseous three-phase flow through pipeline or annuli is increasing every day. Flow through pipeline and annular pipe makes it simpler to transport required materials to destined places. The overall performance of multiphase flow is more complex compared to single phase flow as this flow must combat various problems such as corrosion, erosion, slugging etc. to get optimum result. Also, the chemical and physical interactions between phases, non-linearity of governing equations compared to the single phase flow, large variations in flow characteristics with respect to process and operating conditions are the main challenges while studying multiphase flow and designing the corresponding equipment. This complexity presents a major challenge in the study of multiphase flows and a lot more extravagant researches are required before even a shallow understanding is achieved.

Applications of this research work with multiphase flow through pipeline or annuli can be listed as below –

- Transportation of Raw Materials, Wastes and Sludge.
- Mining Plants.
- Coal Processing Plants.
- Food and Chemical Plants.
- Petroleum Industries (oil and gas transportation & oil and gas or oil and sand production in pipelines or production wells where the pressure drop and temperature change are not that much significant.)
- Nuclear Plants.

- Power Plants.
- Biomedical Engineering Applications.
- Micro-Scale Fluid Dynamics Studies.

The existing empirical correlations become less accurate as those involve many simplifying assumptions. CFD simulations help to minimize such kind of assumptions. More limitations found from literature reviews are –

- Developed empirical correlations along with experimental studies of two and three phase flow in pipeline and annuli are based on limited scopes, data and application ranges (Hernández et al., 2008 and Rahman et al., 2013).
- CFD approaches are not validated and acceptable in wide range of operating conditions. In most of the previous CFD studies, the numerical model is validated using a very limited number of data sets (for example, Dewangan and Sinha, 2016, Chen et al., 2009 and Kumar and Kaushal, 2016).

In this study a CFD model is developed by using Navier Stokes equations to model the hydrodynamics of the flow system. Present work is focused on developing a CFD model capable of taking into consideration the effects of all important multiphase flow parameters, such as fluid velocity, fluid type, particle size, particle concentration, annular pipe rotational speed and annular pipe eccentricity. Before conducting parametric study, our model is validated with twelve different experimental data sets which involve flow conditions significantly different from each other.

Objectives of the present work are:

- ❖ To develop a CFD model which will be highly reliable to researchers and engineers at different applications and different conditions related to pipeline or annular pipe flow with multiphase fluids.
- ❖ To validate the model with wide ranges of experimental and empirical data sets.
- ❖ To conduct parametric study with developed CFD model to predict frictional pressure loss and settling conditions through annular pipe.
- ❖ To analyze the validity of the developed model with three phase gas-liquid-solid flow through pipeline and introduce Fluid Structure Interaction (FSI) for further research.

This thesis is written in manuscript format and is divided into three main chapters excluding the introduction and summary. Appendices are added which include related published works and data tables. The following paragraphs briefly shows outline the chapters.

Chapter 1 is on extensive literature reviews and validation processes of our developed CFD model at different operating conditions with multiphase fluid flow through pipeline and annuli. Twelve different data sources are used to validate our developed model. Comprehensive theoretical analysis is also done to explain the proposed model and its validity. This chapter is submitted in Particulate Science and Technology journal and received a minor review. The chapter is updated according to the received reviews.

Chapter 2 is on analyzing frictional pressure loss and settling conditions through annular pipe. Finding ‘deposition velocity’ is the main goal of this chapter. Effect of fluid velocity, fluid type, particle size, particle concentration, annular pipe rotational speed and annular pipe eccentricity on pressure gradient and particle deposition are studied for a wide range of conditions. Few results are discussed and all findings are shared for further investigation. This chapter is projected to submit in SPE Drilling & Completion Journal.

Chapter 3 is on three phase gas-liquid-solid flow in horizontal pipes using developed CFD model. Three phase flow analysis is very rare and new in multiphase flow research area. Our model shows very good agreement with three phase experimental data and thus we approached three phase flow analysis showing few findings from our model. Fluid Structure Interaction (FSI) is discussed which eventually will lead to find several hazards (e.g. pipe deformation, leakage, fire explosions, material losses etc.) due to multiphase fluid flow through pipeline and annuli. This chapter is accepted and presented at ASME 2017 Fluids Engineering Division Summer Meeting (FEDSM2017).

In Summary section, the outcomes are presented, and future recommendations are suggested.

Appendix 1, 2 and 3 present published works related to the chapters. Appendix 1 is accepted and presented at International Conference on Petroleum Engineering 2016 (ICPE-2016) where two phase slurry flow through pipeline is analyzed. Appendix 2 is accepted and will be presented at 3rd Workshop and Symposium on Safety and Integrity Management of Operations in Harsh Environments (C-RISE3) where two phase slug flow is analyzed with FSI concept. Appendix 3 is accepted in International Journal of Computational Methods and Experimental Measurements (in press) where experimental approach with our developed model is discussed. Appendix 4 presents data tables from parametric analysis.

Co-authorship Statement

In all the papers presented in the following chapters, myself, Rasel A Sultan, is the principle author. My supervisor Dr. Mohammad Azizur Rahman, co-supervisors Dr. Sohrab Zendehboudi, and Dr. Vassilios C. Kelessidis provided theoretical and technical guidance, support with analysis, reviewing and revising of the manuscripts. I have carried out most of the data collection and analysis. I have prepared the first drafts of the manuscripts and subsequently revised the manuscripts based on the co-authors' feedback and the peer review process. Co-authors and supervisors assisted in developing the concepts and testing of the models. As co-authors, Dr. Vandad Talimi, Dr. M M A Rushd, Dr. John Shirokoff, Hassn Hadia and Serag Alfarek contributed through support in development of model, introducing experimental setup, reviewing and revising the manuscripts.

Chapter 1. Validation of CFD Simulation Model with Multiphase Fluid Flow through Pipeline and Annular Geometry

Rasel A Sultan¹, M. A. Rahman², Sayeed Rushd², Sohrab Zendehboudi¹, Vassilios C. Kelessidis³

¹Faculty of Engineering and Applied Science, Memorial University of Newfoundland, Canada

²Texas A&M University at Qatar, Doha, Qatar

³Petroleum Institute, Abu Dhabi, UAE

Abstract

Accuracy of prediction of pressure losses plays a vital role in the design of multiphase flow systems. The present study focused on the development of a computational fluid dynamics (CFD) model to predict these parameters conveniently and accurately. The main objective was to validate the developed model through comparison of its simulation results with existing experimental data and empirical correlations. Both pipeline and annular geometries were considered for the validation. A number of datasets that involved a significant variation in process conditions were used for the validation. All three phases—liquid (water), gas (air), and solid (sand)—were taken into account. The simulations were conducted using the workbench platform of ANSYS Fluent 16.2. The Eulerian model of multiphase flow and the Reynolds stress model (RSM) of turbulence closure available in this version of Fluent were used for the present study. The average velocities and volumetric concentrations of involved phases were specified as the inlet boundary conditions. The stationary surfaces of the flow channels were hydrodynamically considered as either smooth or rough walls, and the outlets were regarded as being open to the atmosphere. The simulation results of pressure loss showed good agreement with the corresponding measured values as well as with the predictions of well-established correlations.

Introduction

Multiphase flows in pipelines or annuli are of great importance and widely employed in various industries and applications, such as chemical process and petroleum industries, nuclear plants, pipeline engineering, power plants, biomedical engineering, microscale fluid dynamics studies, mining plants, food processing industries, geothermal flows, and extrusion of molten plastics (Roco and Shook, 1983; Dewangan and Sinha, 2016). In particular, slurry flow or solid–liquid two-phase flow has become increasingly popular owing to its manifold applications in various industries. This kind of two-phase flow through a pipeline is being studied since the third decade of the 20th century with focus on the development of general solutions based on available experimental data for solid volumetric or mass concentration profiles, pressure drops, and slurry velocity profiles. Among the initial studies, those of O’Brien and Morrough (1933) and Rouse (1937) focused on slurry flows in an open channel with low solid concentrations. They used a diffusion model to predict the concentration distribution. Durand (1951), Durand and Condolios (1952), and Newitt et al. (1955) are also considered as pioneers in describing the frictional pressure losses in slurry flow. Correlations established by Thomas (1965) and Krieger (1972) for homogeneous slurry and the model proposed by Ling et al. (2003) for heterogeneous slurry provided a new dimension to the study of pressure losses in this kind of multiphase flow. Some other important works on empirical correlations for slurry pressure losses include those of Govier and Aziz (1972), Vocadlo and Charles (1972), Aude et al. (1974), Aude et al. (1975), and Seshadri (1982). It is important to note that most of the studies conducted prior to 2000 had a limited application range, scope, and data (Lahiri and Ghanta, 2007). Different computational fluid dynamics (CFD)-based models were proposed later in an effort to address these limitations. A number of such studies were conducted on slurry flow in a pipeline (Ling et al., 2003; Cornelissen

et al., 2007; Hernández et al., 2008; Lin and Ebadian, 2008; Chen et al., 2009; Kaushal et al., 2013; Gopaliya and Kaushal, 2015; Kumar and Kaushal, 2016). However, the outcomes of studies on pipeline slurry flows are not necessarily applicable to similar flows in annuli. Annular slurry flows have not been studied as extensively as the counterpart flows in pipeline. Some remarkable works on annular slurry flows include those of Özbelge and Köker (1996), Özbelge and Beyaz (2001), Eraslan and Özbelge (2003), Özbelge and Eraslan (2006), Camçi and Özbelge (2006), Kelessidis et al. (2007), and Özbelge and Ünal (2008). Furthermore, Escudier et al. (2002) presented a bibliographic list of works on annular flows.

Govier and Aziz (1972) well presented two-phase flow of liquid and gas in a pipeline. Addition of solid particles to the two-phase pipeline flow was found to lead to a reduction in the pump size and an increase in the flow rate (Orell, 2007; Pouranfard et al., 2015). This kind of three-phase system helps to reduce air pollution, noise, and accidents and also provides energy savings. Addition or injection of air in a two-phase slurry system was also reported to reduce pumping cost and enhance bitumen recovery from oil-sand fields (Sanders et al., 2007). Numerous studies were conducted on three-phase pipeline flow (Scott and Rao, 1971; Toda et al., 1978, Hatate et al., 1986; Fukuda and Shoji, 1986; Kago et al., 1986; Gillies et al., 1997; Bello et al., 2005; Rahman et al., 2013; Li et al., 2015; Pouranfard et al., 2015). Most of these studies were experimental works that focused on measurement of frictional pressure losses, deposition velocity (i.e., the minimum superficial velocity of a mixture to prevent accumulation of solids or wastes in the pipeline), and in situ concentration of each phase. Despite being many in number, these experimental works cover a narrow range of operating conditions (Orell, 2007; Rahman et al., 2013). Research works based on CFD or numerical simulation are a new addition in this field. A few notable examples of

such works include those of Van Sint Annaland et al. (2005), Washino et al. (2011), Baltussen et al. (2013), and Liu et al. (2015).

In the present study, a CFD model is used to simulate multiphase fluid flows through pipelines and annuli. The model is validated through comparison of its simulation results with experimental data of one-, two-, and three-phase flows. In most of the previous CFD studies, the numerical model was validated using a very limited number of datasets; the number of datasets was typically as low as one or two (see, for example, Dewangan and Sinha (2016), Chen et al. (2009), and Kumar and Kaushal (2016)). In contrast, our modeling approach is validated through comparison with 12 different experimental datasets involving flow conditions that are significantly different from each other. The CFD results are also compared with the predictions of well-established correlations. In view of the fact that process conditions vary over a wide span in the industry, the objective of the present study is to verify the suitability of a commercially available CFD model to simulate multiphase flows in both pipelines and annuli under a wide range of process conditions.

Theory

Multiphase Model

The Eulerian model based on the Euler-Euler approach is used in the present CFD study as the multiphase model (Fluent, 2009). This is because this investigation includes solid–liquid–gas three-phase flows, in which both granular (fluid–solid) and non-granular (fluid–fluid) flows are involved. The Eulerian model is known to be capable of addressing different kinds of couplings with individual momentum and continuity equations quite effectively (Anderson and Jackson, 1967).

Volume fractions represent the space occupied by each phase, and the laws of conservation of mass and momentum are satisfied by each phase individually. The conservation equations can be

derived by averaging the local instantaneous balance for each of the phases (Anderson and Jackson, 1967) or by using the mixture theory approach (Bowen, 1976).

The volume of phase q , V_q , is defined by

$$V_q = \int a_q dV \quad (1)$$

where,

a_q = volume fraction

$$\text{and } \sum_{q=1}^n a_q = 1 \quad (2)$$

Continuity equation for mixture is as below -

$$\frac{\partial}{\partial t} (a_q \rho_q) + \nabla \cdot (a_q \rho_q \overline{\vartheta}_q) = 0 \quad (3)$$

where, ρ_q is the phase reference density, or the volume averaged density of the q^{th} phase in the solution domain. $\overline{\vartheta}_q$ indicates velocity vector.

The conservation of momentum for a fluid phase q is –

$$\begin{aligned} \frac{\partial}{\partial t} (a_q \rho_q \overline{\vartheta}_q) + \nabla \cdot (a_q \rho_q \overline{\vartheta}_q \overline{\vartheta}_q) = & -a_q \nabla p + \nabla \cdot \overline{\tau}_q + a_q \rho_q \vec{g} + \sum_{p=1}^n \{K_{pq} (\overline{\vartheta}_p - \overline{\vartheta}_q) + \\ & \dot{m}_{pq} \overline{\vartheta}_{pq} - \dot{m}_{qp} \overline{\vartheta}_{qp}\} + (\overline{F}_q + \vec{F}_{lift,q} + \vec{F}_{vm,q}) \end{aligned} \quad (4)$$

Here \vec{g} is the acceleration due to gravity, $\overline{\tau}_q$ is the q^{th} phase stress-strain tensor, \overline{F}_q is an external body force, $\vec{F}_{lift,q}$ is a lift force and $\vec{F}_{vm,q}$ is a virtual mass force.

Considering the work of Alder and Wainwrigth (1960), Chapman and Cowling (1970) and Syamlal et al. (1993), a multi-fluid granular model is used to describe the flow behavior of a fluid-solid mixture.

The conservation of momentum for the solid phase is -

$$\frac{\partial}{\partial t} (a_s \rho_s \vec{v}_s) + \nabla \cdot (a_s \rho_s \vec{v}_s \vec{v}_s) = -a_s \nabla p - \nabla p_s + \nabla \cdot \bar{\tau}_s + a_s \rho_s \vec{g} + \sum_{l=1}^N \{K_{ls} (\vec{v}_l - \vec{v}_s) + \dot{m}_{ls} \vec{v}_{ls} - \dot{m}_{sl} \vec{v}_{sl}\} + (\vec{F}_s + \vec{F}_{lift,s} + \vec{F}_{vm,s}) \quad (5)$$

where, p_s is the s^{th} solids pressure, $K_{ls} = K_{sl}$ is the momentum exchange coefficient between fluid or solid phase l and solid phase s , N is the total number of phases.

For granular flows, the solids pressure is composed of a kinetic term and a second term due to particle collisions –

$$p_s = a_s \rho_s \theta_s + 2\rho_s (1 + e_{ss}) a_s^2 g_{0,ss} \theta_s \quad (6)$$

where e_{ss} is the coefficient of restitution for particle collisions, $g_{0,ss}$ is the radial distribution function and θ_s is the granular temperature. A default value of 0.9 for e_{ss} is used but the value can be adjusted for different particle type. This value is selected based on Fluent (2009) and a trial & error process during validation. The function $g_{0,ss}$ is a distribution function that control the transition from the compressible condition to incompressible condition. A value of 0.63 is the default for $a_{s,max}$.

Equation 7 is showing the form of the coefficient of restitution (Wakeman and Tabakoff, 1982).

$$e_{ss} = \frac{v_2}{v_1} \quad (7)$$

where v_2 = particle velocity after collision, and v_1 = particle velocity before collision.

The solids stress tensor contains shear and bulk viscosities arising from particle momentum exchange due to translation and collision. A frictional component of viscosity can also be included to account for the viscous-plastic transition that occurs when particles of a solid phase reach the maximum solid volume fraction.

The solids stress viscosity term contains shear viscosity due to collision ($\mu_{s,col}$), kinetic viscosity ($\mu_{s,kin}$) and frictional viscosity ($\mu_{s,fr}$). It can be written as -

$$\mu_s = \mu_{s,col} + \mu_{s,kin} + \mu_{s,fr} \quad (8)$$

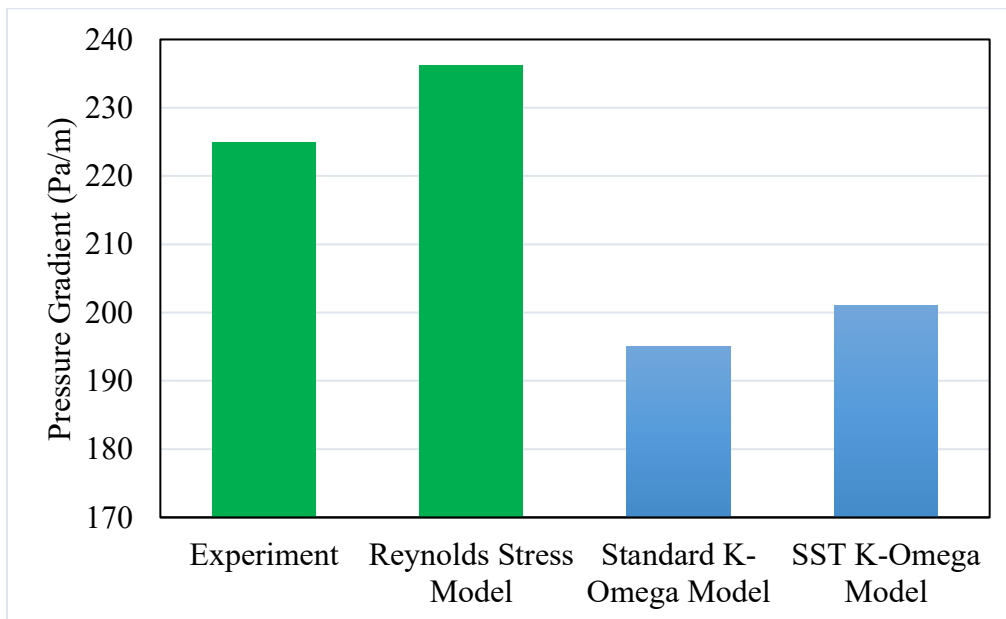
Turbulence Model

The choice of turbulence model for a CFD problem relies on the physics of the flow, the level of accuracy needed, the availability of computational resources, and the time requirement for the solution. To make an appropriate selection, it is necessary to understand the capabilities and limitations of the available options. A few points are discussed below in this regard.

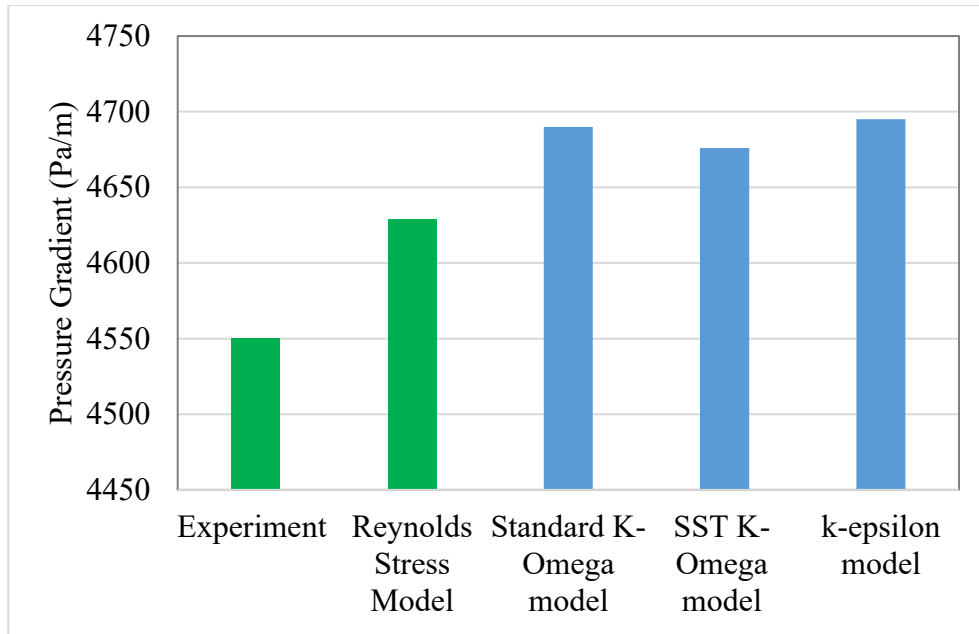
- Comparative studies on the performance of popular Reynolds-averaged Navier–Stokes (RANS) turbulence models such as the $k-\epsilon$ model, $k-\omega$ model, and Reynolds stress model (RSM) and on that of large-eddy simulation (LES) of steady fluid flow through pipelines or annuli are available in the open literature (e.g., Vijiapurapu and Cui, 2010; Markatos, 1986). Vijiapurapu and Cui (2010) compared the results obtained using different turbulence models with the experimental results of Zagarola and Smits (1997) and Nourmohammadi et al. (1985). The $k-\epsilon$ and $k-\omega$ models were able to provide acceptable results with low computational cost and minimal effort. The LES model solved large-scale turbulence eddies by averaging smaller-scale ones. This model was found to be more acceptable and universal. However, it required extensively large computational resources and time. In comparison to these

turbulence models, the performance of the RSM was optimum for turbulence flow through pipelines or annuli. The computational cost of the RSM was much lower than that of the LES model, and the results of the RSM were more accurate than those of the $k-\epsilon$ and $k-\omega$ models.

- Lien and Leschziner (1994) proposed a value of 0.82 for the adjustable constant σ_k by applying the gradient-diffusion model to the diffusion term of the RANS equation. This particular value of σ_k is used in the RSM, and it is different from corresponding values used in different versions of the $k-\epsilon$ and $k-\omega$ models.
- In the RSM, the pressure-strain term (Φ_{ij}) is designed according to the proposals of Gibson and Launder (1978) and Fu et al. (1987). Closure coefficients (C_1 and C_2) are modified to make the RSM more acceptable than the $k-\omega$ model as well as other RANS models.



(a)



(b)

Figure 1. Presentation of the comparative analysis of different turbulence models: (a) Kelessidis et al., 2011 (Pipe inner diameter 0.04 m, pipe outer diameter 0.07 m, concentric annuli, water as fluid, water flow velocity 1.12 m/s), (b) Skudarnov et al., 2004 (Pipe diameter 0.023m, water and glass spheres as fluid, $C_v = 15\%$, $d_m = 0.14$ mm, slurry flow velocity 1.724 m/s) [$d_m =$ sand particle diameter, $C_v =$ sand volumetric concentrations]

- A comparative analysis of the performance of different turbulence models was conducted as part of the present study. Four different models were used to predict the pressure losses of multiple data points. Invariably, the RSM provided better results than the other models. The agreement between the RSM prediction and the measured value of pressure loss was less than 10%. Two examples of the comparison are depicted in Figure 1.

The Reynolds stress model resolves the RANS equations by solving transport equations for the Reynolds stresses together with an equation for the dissipation rate. Modelling approach of RSM

is originated from Launder et al. (1975). The exact transport equation of Reynolds Stress (R_{ij} or $\overline{u'_i u'_j}$) is as follows:

$$\frac{DR_{ij}}{Dt} = P_{ij} + D_{ij} - \epsilon_{ij} + \Phi_{ij} + \theta_{ij} \quad (9)$$

where,

$\frac{DR_{ij}}{Dt}$ is the summation of changing rate of R_{ij} and transport of R_{ij} by convection,

P_{ij} is production rate of R_{ij} ,

D_{ij} is diffusion transport of R_{ij} ,

ϵ_{ij} is rate of dissipation,

Φ_{ij} is pressure strain correlation term, and

θ_{ij} is rotation term.

D_{ij} can be modeled assuming rate of transport of Reynolds stresses by diffusion is proportional to gradients of Reynolds stresses. Diffusion term used in simulation is presented as:

$$D_{T,ij} = \frac{\partial}{\partial x_k} \left(\frac{\mu_t}{\sigma_k} \frac{\partial R_{ij}}{\partial x_k} \right) \quad (10)$$

where $\sigma_k = 0.82$, $\mu_t = C_\mu \frac{k^2}{\epsilon}$ and $C_\mu = 0.09$.

Production rate P_{ij} of R_{ij} or $\overline{u'_i u'_j}$ can be expressed as:

$$P_{ij} = - \left(\overline{u'_i u'_m} \frac{\partial U_j}{\partial x_m} + \overline{u'_j u'_m} \frac{\partial U_i}{\partial x_m} \right) \quad (11)$$

The pressure-strain term, Φ_{ij} on Reynold stresses consists of three major components and those are $\Phi_{ij,1}$ = slow pressure-strain term or the return-to-isotropy term, $\Phi_{ij,2}$ = rapid pressure-strain term and $\Phi_{ij,w}$ = wall-reflection term:

$$\Phi_{ij} = \Phi_{ij,1} + \Phi_{ij,2} + \Phi_{ij,w} \quad (12)$$

$$\Phi_{ij,1} = -C_1 \frac{\epsilon}{k} \left[\overline{u'_i u'_j} - \frac{2}{3} \delta_{ij} k \right] \quad (13)$$

$$\Phi_{ij,2} = -C_2 \left[P_{ij} - \frac{2}{3} \delta_{ij} P \right] \quad (14)$$

where $C_1 = 1.8$ and $C_2 = 0.6$.

The wall-reflection term, $\Phi_{ij,w}$ is responsible for the normal stresses distribution near the wall.

The dissipation rate ϵ_{ij} or destruction rate of R_{ij} is modeled as:

$$\epsilon_{ij} = \frac{2}{3} \delta_{ij} \epsilon \quad (15)$$

$$\epsilon = 2\nu \overline{s'_{ij} \cdot s'_{ij}} \quad (16)$$

where s'_{ij} = fluctuating deformation rate

Rotation term is expressed as:

$$\theta_{ij} = -2\omega_k (R_{jm} e_{ikm} + R_{im} e_{jkm}) \quad (17)$$

where,

ω_k = rotation vector, and

e_{ikm} = alternating symbol, +1, -1 or 0 depending on i, j and k.

Simulation Methodology

The computational grids for horizontal pipelines and annuli were generated using ANSYS Fluent 16.2. Meshing was finalized after proper checking of the mesh independency of simulation results.

The mesh analysis performed in the present study is illustrated in Figure 2 with an example. Data for the analysis were collected from Fukuda and Shoji (1986). As shown in the figure, the output

pressure drop became almost constant with an increase in the number of nodes to above a certain value (~150000). Simulation of many other similar data points revealed that the minimum number of nodes required to ensure mesh independency for pipelines was 135000 and the corresponding value for annuli was 540000. Inflations near all walls were added for the precise solution of different parameters. Although the use of unsymmetrical meshes was computationally more challenging, it was expected to yield better results than symmetrical meshes (Gopaliya and Kaushal, 2015). Samples of computational grid distributions of the pipelines and annular geometries are shown in Figure 3. Each cross-section had 10 inflation layers near the wall(s), with a growth rate of 20%.

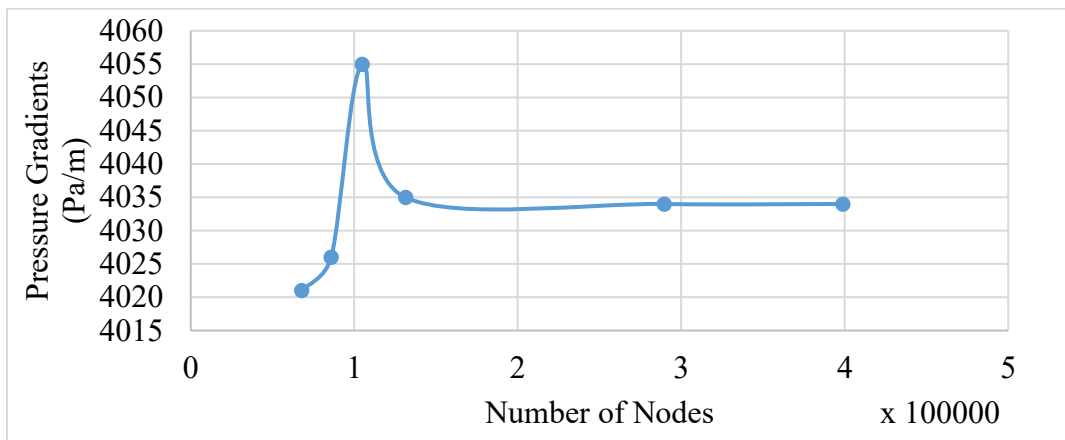


Figure 2. Presentation of Mesh Independence from Fukuda and Shoji, 1986 (0.0416 m pipe diameter, 0.074 mm sand particle diameter, 2 mm air bubble diameter, 3 m/s slurry velocity)

The minimum length from the entrance to a fully developed flow section, i.e., the entrance length, is around $50D_h$, where D_h is the hydraulic diameter (Wasp et al., 1977). The length of the pipelines/annulus was maintained to be long enough ($>50D_h$) to achieve length-independent results of pressure losses at the fully developed flow section. An example of length independence analyses is shown in Figure 4.

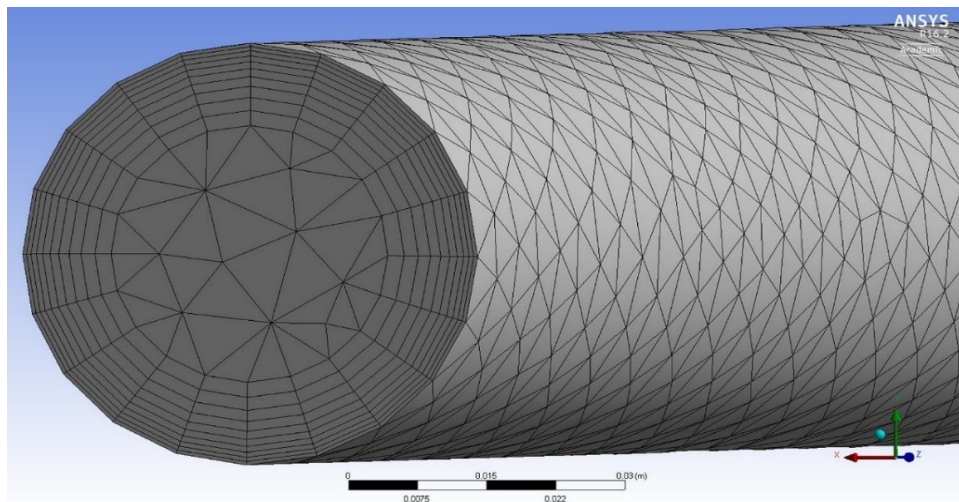
It should be mentioned that the values of dimensionless wall distance (y^+) are defined only in the wall-adjacent cells in consideration of the convergence requirement of y^+ for cells adjacent to the wall. The value of y^+ changes with the wall shear stress, fluid density, hydraulic diameter, and molecular viscosity:

$$y^+ = \frac{y}{\mu} \sqrt{\rho \tau_w} \quad (18)$$

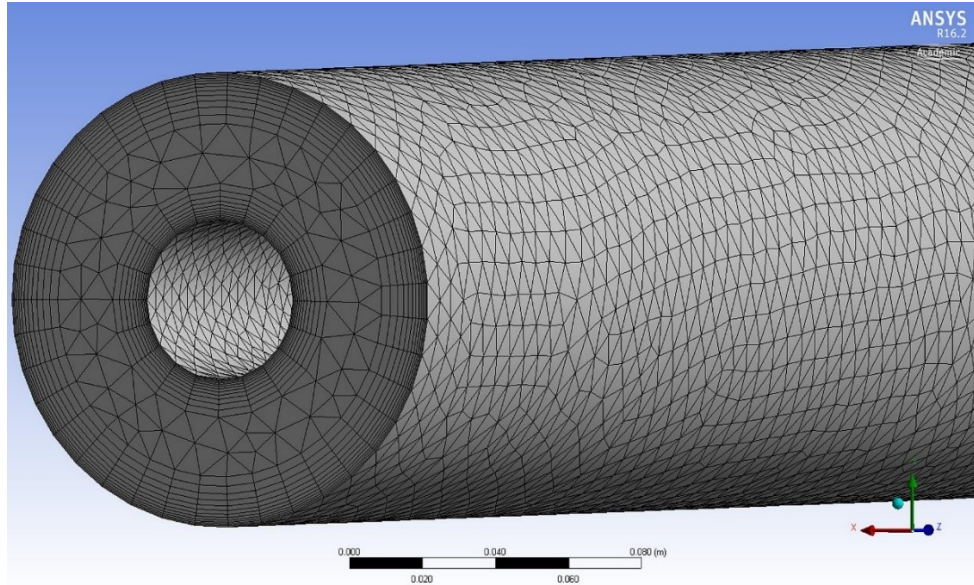
$$\text{or, } y^+ \equiv \sqrt{Re}$$

$$[\tau_w = \mu \frac{\partial u}{\partial y} \text{ and } Re = \frac{\rho u y}{\mu}]$$

where y is the distance from the wall to the cell center; u , the fluid velocity; μ , the molecular viscosity; ρ , the fluid density; and τ_w , the wall shear stress. Eventually, y^+ depends on the mesh resolution (changing the value of y) and the flow Reynolds number. Default standard wall functions are generally applicable if the first cell center adjacent to the wall has a y^+ value larger than 30 (Fluent, 2009). In view of the minimum requirement ($y^+ > 30$), the value of y^+ in our study was maintained above 45.



(a)



(b)

Figure 3. Mesh distribution in (a) pipe geometry (number of nodes 135000, wall inflation layers 10), (b) annular geometry (number of nodes 540000, wall inflation layers 10)

A convergence value of 10^{-5} was used to terminate the iterations for the solution. This is the optimum value that ensures satisfactory accuracy and computation time. Figure 5 shows an example of the analyses performed to determine the optimum convergence rate within a range of 10^{-4} to 10^{-6} . On an average, 30 min of computational time was required for each simulation (computer specifications: Dell Precision T7810, Intel Xeon 3.00 GHz, 16.0 GB RAM).

The SIMPLE algorithm for single-phase flow and the phase-coupled SIMPLE (PC-SIMPLE) algorithm for multiphase flow were applied with the first and second order upwind discretization method to achieve stability and convergence of the governing equations (Vasquez, 2000). Upwind discretization refers to a method that numerically simulates the direction of the normal velocity in the flow field. The no-slip boundary condition was adopted to simulate the interaction between the fluid and the wall.

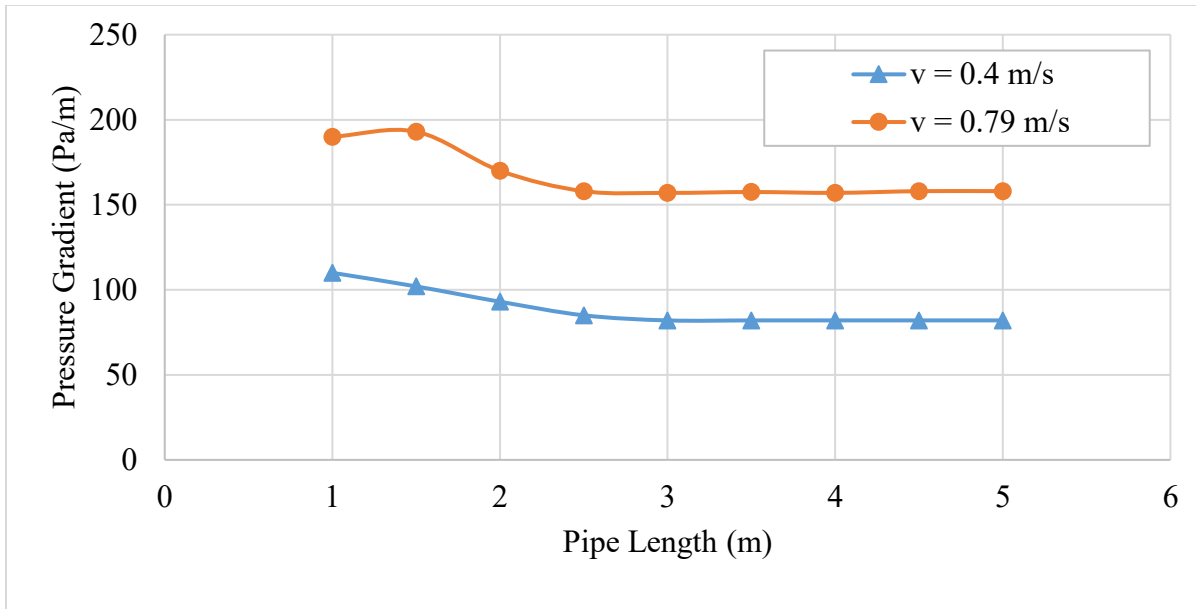


Figure 4. Pressure Gradient variation along pipe length (where arbitrarily boundary conditions are taken as - length 5 m, inner diameter 0.0635 m, outer diameter 0.1143 m and water as fluid).

['v' indicating flow velocity]

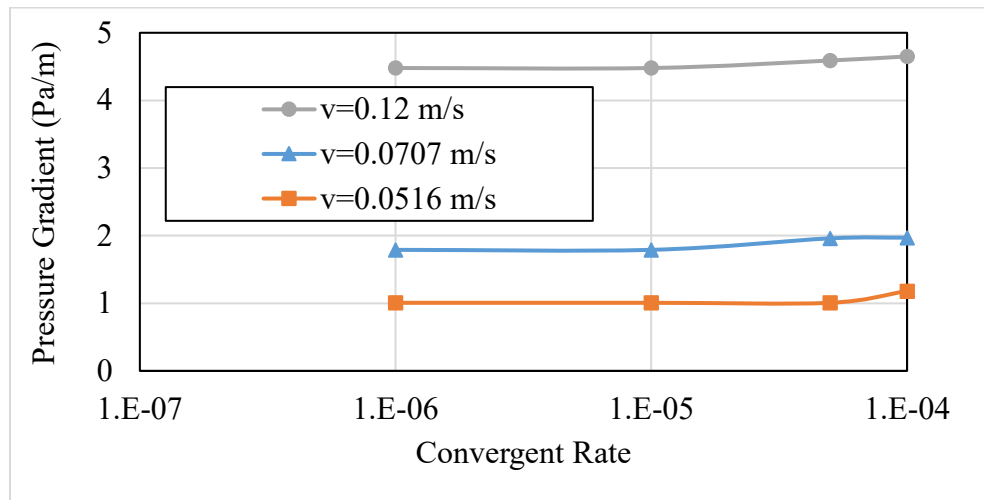


Figure 5. Optimum convergence rate analysis (from Camçi, 2003 experiment data where inner diameter 0.0432 m, outer diameter 0.123 m, length 5 m, wall material aluminum, concentric annuli) ['v' indicates inlet velocity of fluid]

Results and Discussions

As mentioned earlier, the results of the CFD model were compared with the values measured in different experiments and the predictions of relevant correlations to validate the simulation methodology. The total analysis covered a wide range of different parameters, including a Reynolds number range of 10^4 – 10^7 . The ranges of the parametric values used for the investigation are presented in Table 1.

Table 1. Variable Parameter Ranges

| Parameters | Ranges | Unit |
|----------------------------------|-----------------|---------------|
| Outer Diameter | 0.023 – 0.263 | m |
| Inner Diameter | 0 – 0.06 | m |
| Length | 2.9 – 22 | m |
| Pipe Wall Roughness | 0 – 0.2 | mm |
| Sand Concentration | 0.8 – 50 | % |
| Sand Particle Diameter | 30 – 440 | μm |
| Air Concentration | 4.3 – 38.78 | % |
| Air Bubble Diameter | 0.1 – 2 | mm |
| Input Water Superficial Velocity | 0.05 – 5 | m/s |
| Input Sand Superficial Velocity | 0.07 – 5 | m/s |
| Input Air Superficial Velocity | 0.2 – 3 | m/s |
| Water Equivalent Reynolds Number | 10^4 – 10^7 | Unit less |

Single Phase Flow through Pipeline

The CFD model was verified, at first, using the experimental measurements of pressure losses for the single-phase water flow through horizontal pipeline. The data were collected from Skudarnov et al. (2004) and Kaushal et al. (2005). In Skudarnov et al. (2004), pipe length was 17 m, pipe diameter was 0.023 m, water (density: 998.2 kg/m^3 , viscosity: 0.001003 kg/m-s) was the working fluid and stainless steel (roughness 0.032 mm) was the wall material. Similarly, pipe length was 22 m and pipe diameter was 0.0549 m for the data set available in Kaushal et al. (2005). The fluid and the wall material were same as those of Skudarnov et al. (2004). Simulation results of pressure gradients, i.e., pressure drops per unit length at different fluid velocities through the pipelines are compared with the experimental measurements in Figure 6. The figure also includes the predictions of an empirical correlation proposed by Wood (1966).

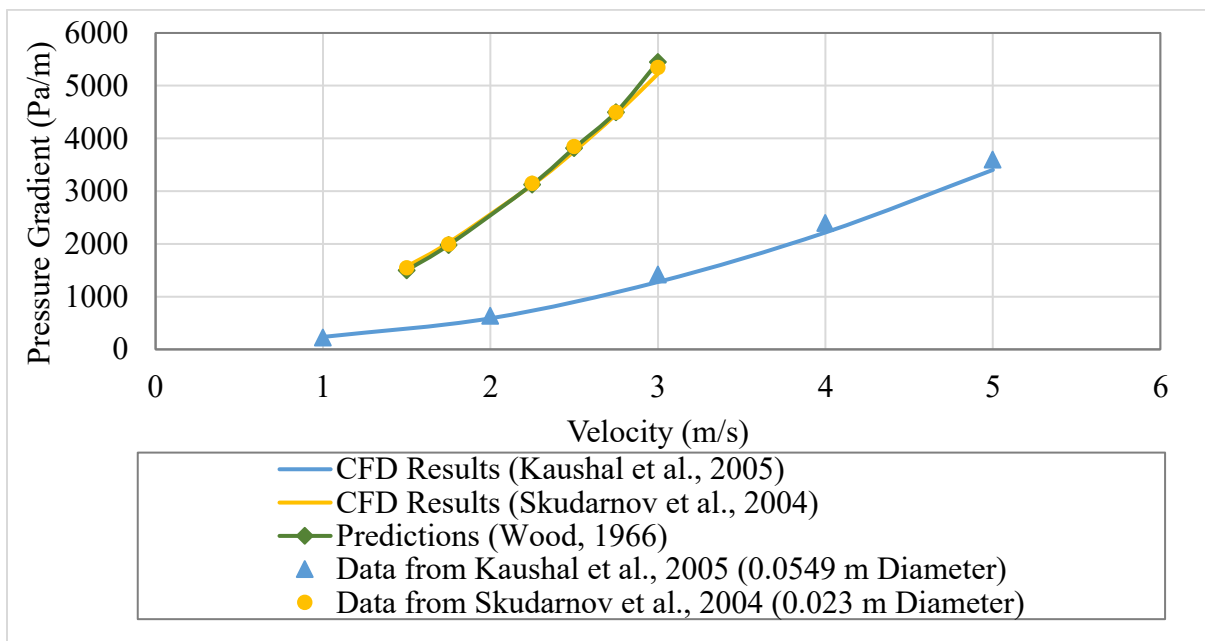


Figure 6. Comparison of simulated pressure gradient with Wood (1966) correlation, experimental data from Kaushal et al. (2005) and Skudarnov et al. (2004) at different inlet velocity

According to the correlation, the friction factor (f) or the dimensionless expression of pressure loss is as follows:

$$f = a + b.Re^{-c} \quad (19)$$

$$a = 0.0026\left(\frac{e}{D}\right)^{0.225} + 0.133\left(\frac{e}{D}\right)$$

$$b = 22\left(\frac{e}{D}\right)^{0.44}$$

$$c = 1.62\left(\frac{e}{D}\right)^{0.134}$$

$$Re = \frac{\rho v D}{\mu}$$

where e is wall roughness, Re is Reynolds Number, D is pipe diameter, ρ is fluid density, μ is fluid viscosity, and v is fluid velocity. It is a well-accepted empirical formula in case of any simple pipe flow with wall roughness.

The results shown in Figure 6 demonstrate an acceptable agreement of the CFD results with the experimental values and also with the predictions of Wood's correlation. The average difference was 2% from Skudarnov et al. (2004) data, 5% from Kaushal et al. (2005) data and 2% from the predictions of Wood (1966) correlation.

Single Phase Flow through Annuli

Two sets of experimental data from Kelessidis et al. (2011) and Camçi (2003) along with the predicted values of the correlation proposed by Haaland (1983) are compared to the CFD results in Figure 7. The geometry was horizontal concentric annuli. Kelessidis et al. (2011) used an inner diameter (ID) of 0.04 m, an outer diameter (OD) of 0.07 m and an annulus length of 5 m. For the

data set of Camçi (2003), the ID was 0.0432 m, the OD was 0.123 m and the length was 5 m. The flowing fluid was water for both setups. The wall materials were Plexiglas and Aluminum, both of which were hydrodynamically smooth.

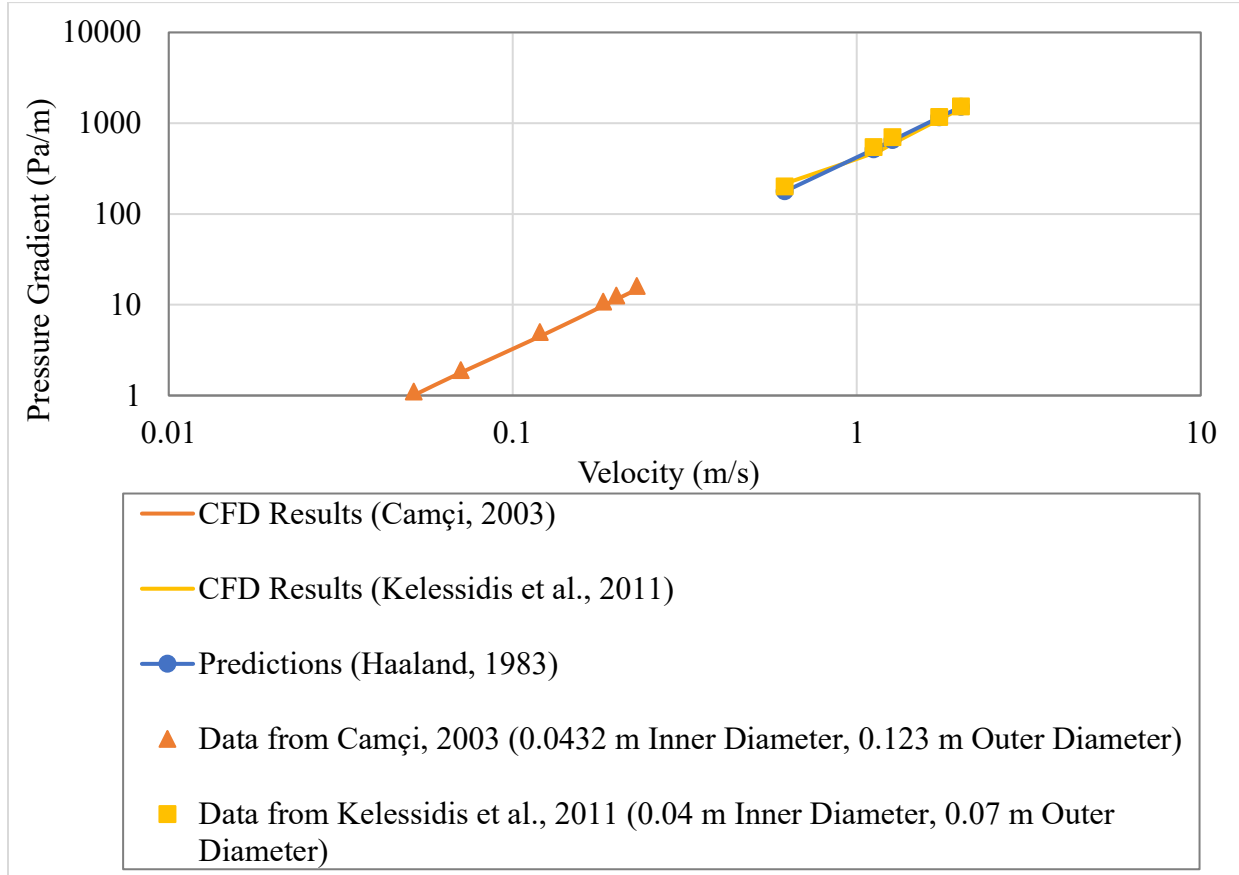


Figure 7. Comparison of simulated pressure gradient with Haaland (1983) correlation and experimental data from Kelessidis et al. (2011) and Camçi (2003) at different inlet velocity

Correlation of Haaland (1983) is as follows-

$$\frac{1}{\sqrt{f}} = -3.6 \left\{ \left(\frac{\epsilon_a}{3.7d_e} \right)^{1.1} + \frac{6.9}{Re} \right\} \quad (20)$$

where f = friction factor, d_e = OD - ID, Re = Reynolds Number, ϵ_a = absolute roughness.

On an average, the CFD results differ from the measured and predicted values by 10%. It should be mentioned that the error associated with the experimental data was $\pm 10\%$.

Two Phase (solid-liquid) flow through Pipeline

The simulation results of pressure gradients for water-sand two phase slurry flow through horizontal pipeline are compared with the data published by Skudarnov et al. (2001), Skudarnov et al. (2004) and Kaushal et al. (2005). Experimental details of Skudarnov et al. (2004) was previously presented with respect to discussing the results shown in Figure 6 for single phase water flow. They used glass spheres (double-species slurry with densities of 2490 kg/m^3 and 4200 kg/m^3 , 50% volume mixtures, $d_m = 0.14 \text{ mm}$) as solid particles, stainless steel (roughness 0.032 mm) as wall material, and 15% solid volumetric concentration (C_v). Similarly, geometry and other properties of Kaushal et al. (2005) related to single phase water flow (Figure 6) are used for simulating the corresponding slurry flow conditions. They used spherical glass beads (double-species slurry with 0.125 mm and 0.44 mm diameter, mean density 2470 kg/m^3 , 50% volume mixtures) as the solid phase. Particle Size Distribution (PSD) in Kaushal et al. (2005) is shown in Figure 8. In the literature, they used two different sized fresh samples in average size of 0.125 mm and 0.44 mm ; mix them up and using laser scattering analyzer determined PSD. For the experiments reported by Skudarnov et al. (2001), diameter of pipe was 22.1 mm , length was 1.4 m and pipe material was Aluminum (0.05 mm roughness). They used water as liquid phase and silica (20% concentration, mean particle diameter 0.03 mm and density 2381 kg/m^3) as solid phase. Figure 9 demonstrates the comparative results which show very good compliance between simulated and measured values. The average difference was less than 10% which can be attributed to the experimental errors (calculated accuracy of the pressure gradient is $\pm 50 \text{ Pa/m}$ in experiment) and the numerical errors (considering different models and assumptions).

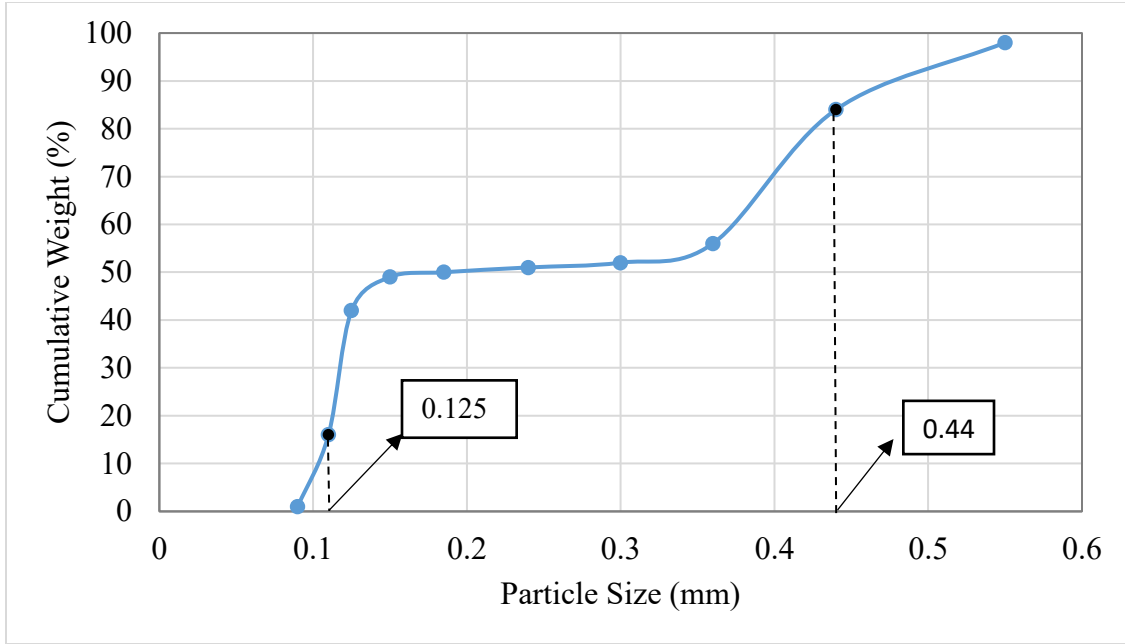


Figure 8. Particle size distribution of different particle used in Kaushal et al. (2005)

In addition to pressure losses, local solid concentration profiles of water-sand slurry flows were also obtained from the CFD solutions to validate with the experimental data published by Gillies and Shook (1994) and Roco and Shook (1983). The comparative results are presented in Figure 10 and Figure 11, respectively. For Gillies and Shook (1994) data set (Figure 10), length of pipe was 2.7 m (horizontal), diameter was 53.2 mm, water (density 998.2 kg/m^3 , viscosity 0.001003 kg/m-s) was the liquid phase, Silica (chemical formula SiO_2 , density 2650 kg/m^3 , $d_m = 0.18 \text{ mm}$) was the solid phase, slurry ($C_v = 14\%$, 29% and 45%) velocity was 3.1 m/s and wall material was aluminum (roughness 0.2 mm ,). Similarly, pipe length was 13.15 m , and diameter was 263 mm for Roco and Shook (1983) data set (Figure 11). The fluid (slurry of water and sand) and the wall material were same as the previous reference. Grain size or mean particle diameter of sand (d_m) was 0.165 mm . Particle Size Distribution (PSD) from literature is shown in Figure 12 from where 0.165 mm is selected as mean size. Mixture velocity 3.5 m/s and four different solid volumetric concentrations (C_v) 9.95% , 18.4% , 26.8% and 33.8% respectively were considered for analysis.

The contours of local volumetric concentration distributions of solid particles in the vertical cross section planes (data from Roco and Shook (1983)) are shown in Figure 13. The contours were collected from the CFD simulation results. It is understandable by analyzing the contours that the regions of highest solid concentrations are located near the wall in the lower half of pipe cross section which is due to the downward gravitational force.

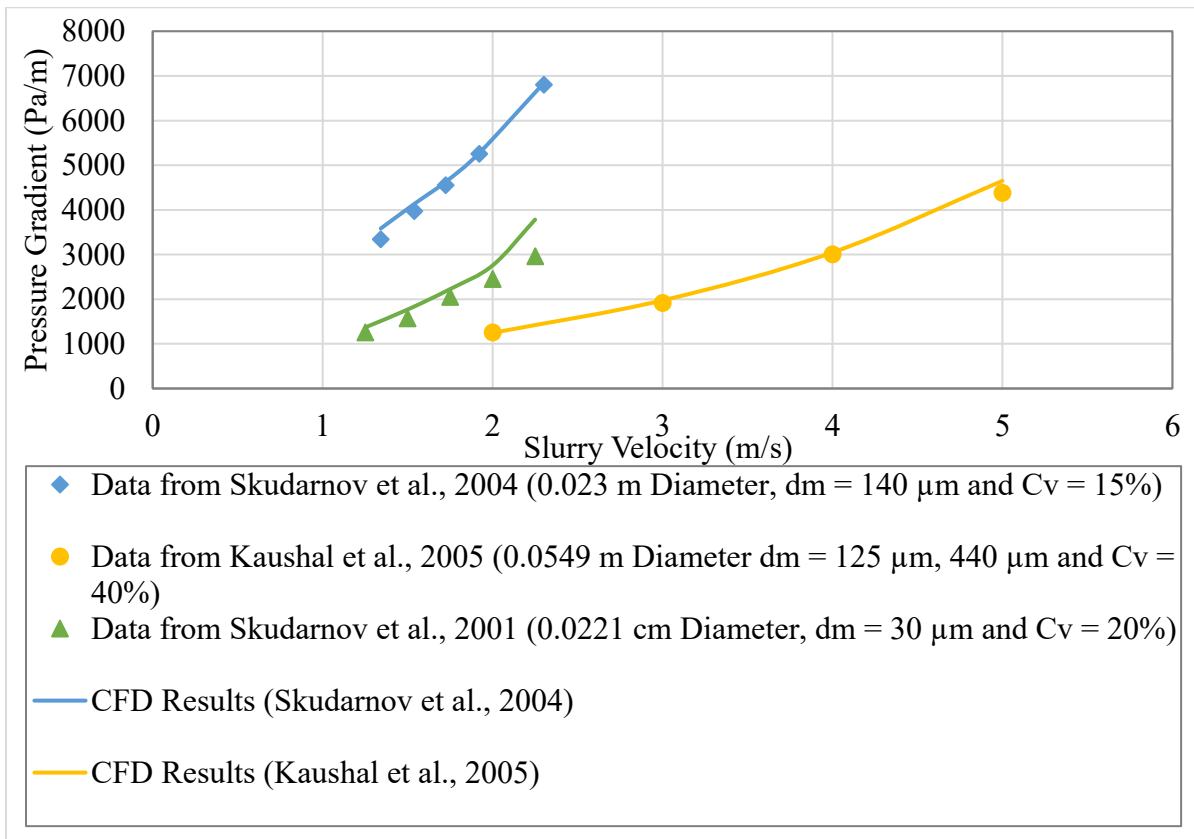


Figure 9. Comparison of simulated pressure gradient with experimental data from Skudarnov et al. (2001), Kaushal et al. (2005) and Skudarnov et al. (2004) at different inlet slurry velocity [d_m = sand particle diameter, C_v = sand volumetric concentrations]

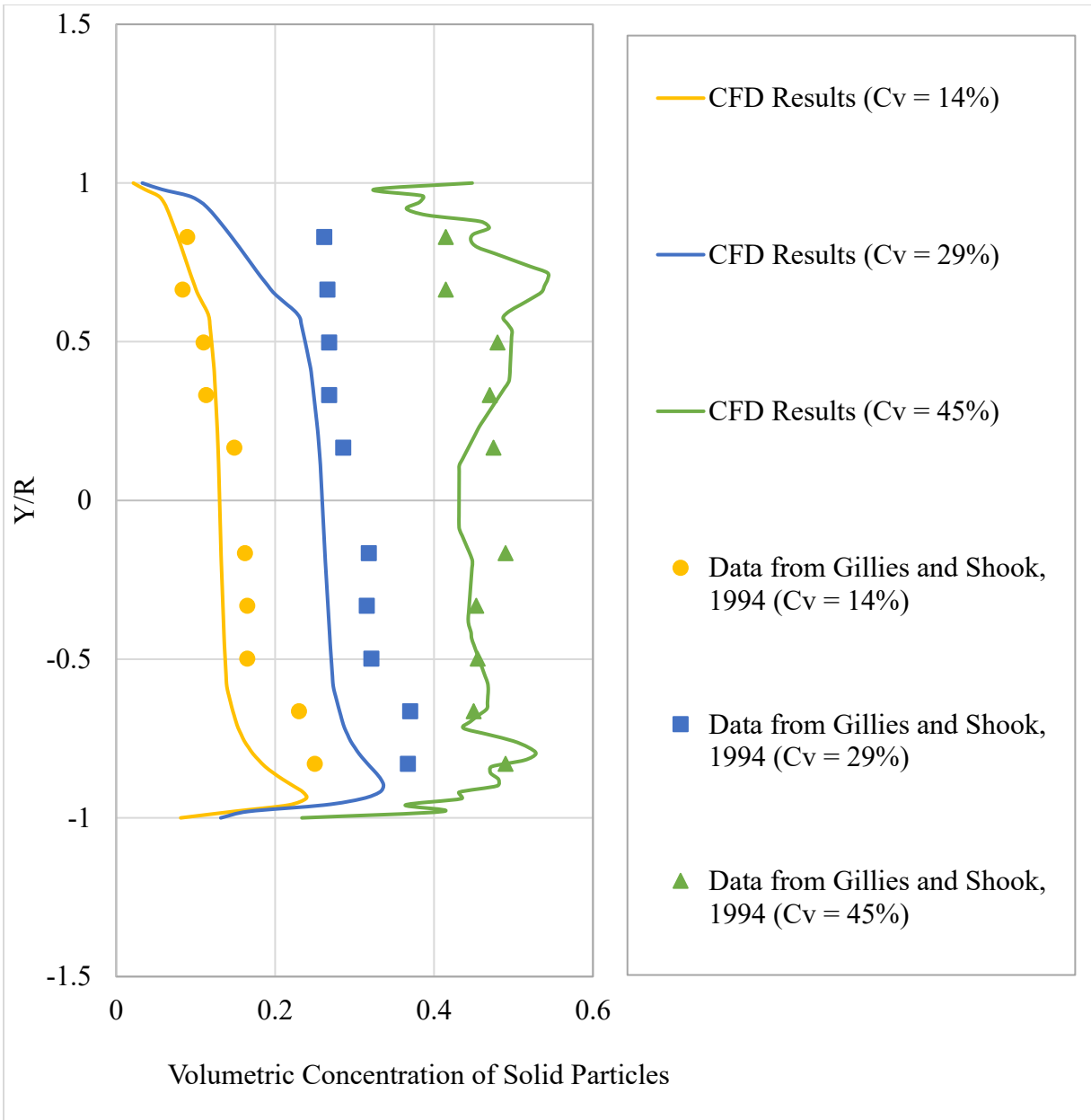


Figure 10. Comparison of simulated solid local volumetric concentration across vertical centerline with Gillies and Shook, 1994 (263 mm pipe diameter, $d_m = 0.18$ mm, slurry velocity 3.1 m/s) [d_m = sand particle diameter, C_v = sand volumetric concentrations]

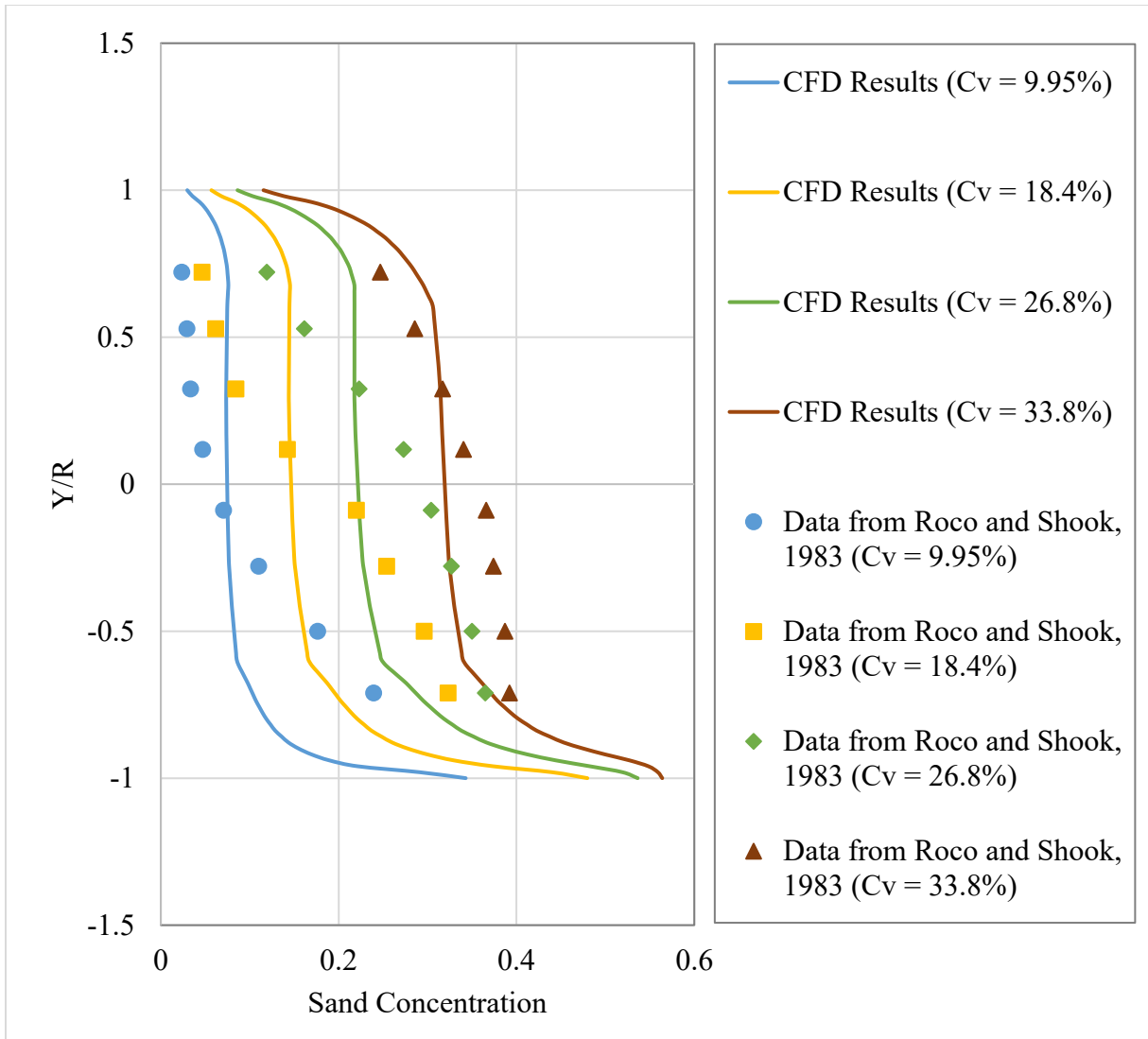


Figure 11. Comparison of simulated and measured solid local volumetric concentration across vertical centerline with Roco and Shook, 1983 (53.2 mm pipe diameter, $d_m = 0.165$ mm, slurry velocity 3.5 m/s) [d_m = sand particle diameter, C_v = sand volumetric concentrations]

Although simulated results are in good agreement with experimental values in general, it should be noted that the deviations are noticeable near the wall in the lower half of the cross-section (Figure 10). One of the possible reasons could be abrasive rounding of these generous size particles by repeated passages during experiment. This resulted in significant quantities of fines which were

distributed uniformly within the pipe and might have led to increase in carrier fluid density. New boundary conditions (e.g. enhanced wall treatment, scalable wall function, non-equilibrium wall functions etc.) at the wall for pipeline flows of slurries with larger grain sizes can be applied to minimize the deviations.

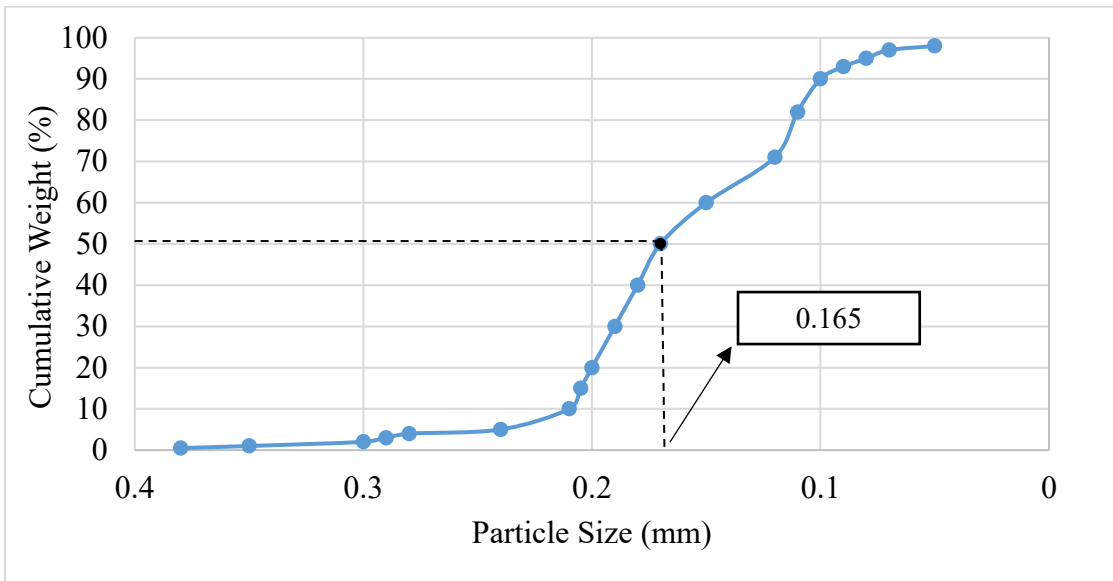
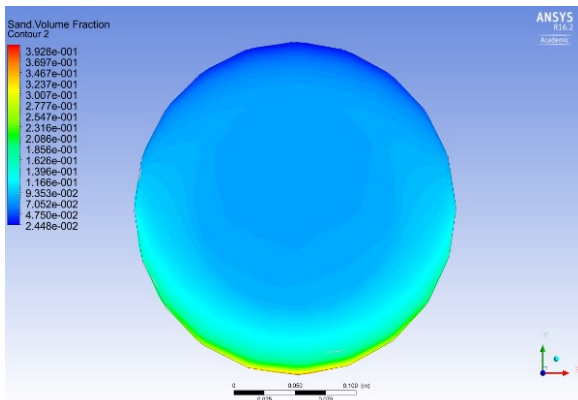
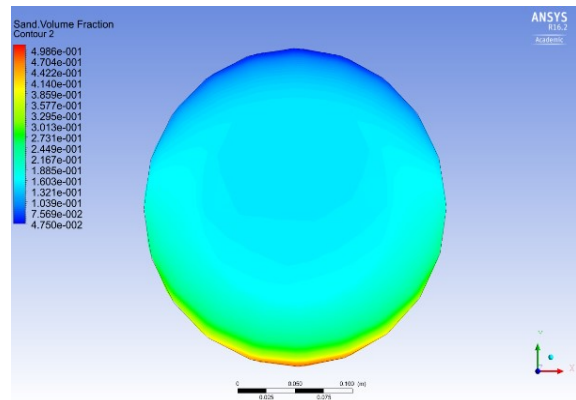


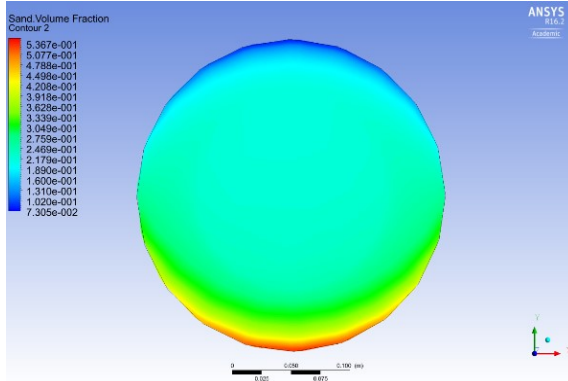
Figure 12. Particle size distribution of different particle used in Roco and Shook (1983)



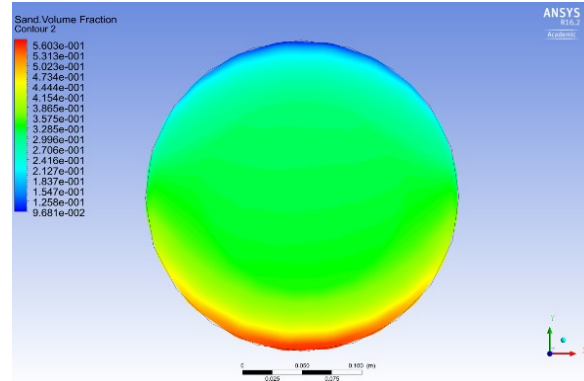
(a) solid volumetric concentration 9.95%



(b) solid volumetric concentration 18.4%



(c) solid volumetric concentration 26.8%



(d) solid volumetric concentration 33.8%

Figure 13. Solid concentration distribution in the vertical cross section plane (data from Roco and Shook, 1983 where 53.2 mm pipe diameter, $d_m = 0.165$ mm, slurry velocity 3.5 m/s) [$d_m =$ sand particle diameter, $C_v =$ sand volumetric concentrations]

Two Phase (solid-liquid) flow through Annuli

Pressure gradient (Pa/m) profiles of water-sand slurry flows through vertical concentric annuli are compared with Ozbelge and Beyaz (2001) experimental data in Figure 14. For the CFD simulation, the liquid phase was considered as water (density 9982 kg/m^3 , viscosity 0.001003 kg/m-s) and solid phase was taken as feldspar (symbol $\text{K}_2\text{O} \cdot \text{Al}_2\text{O}_3 \cdot \text{SiO}_2$, mean particle diameter 0.23 mm, mean density 2500 kg/m^3 , range of slurry volumetric concentration 0.8%–1.8%). Length, OD and ID of the annulus were 5 m, 0.125 m, and 0.025 m, respectively. As the inlet boundary conditions, average velocities were specified in the range of 0.0738–0.197 m/s. In compliance to the experimental conditions, a smooth pipe of stainless steel (density 8030 kg/m^3) was used for the simulation. The pipe was assumed to be vertical, i.e., gravity effect was included and gravitational acceleration was directed opposite to outlet. No slip boundary conditions for liquid and solid phase were used at the walls. Figure 14 shows the comparison among simulated and measured two-phase

frictional pressure drops. Very similar to the previous analyses, the simulated results are in good agreement with the experimental values with an average discrepancy of only 3%.

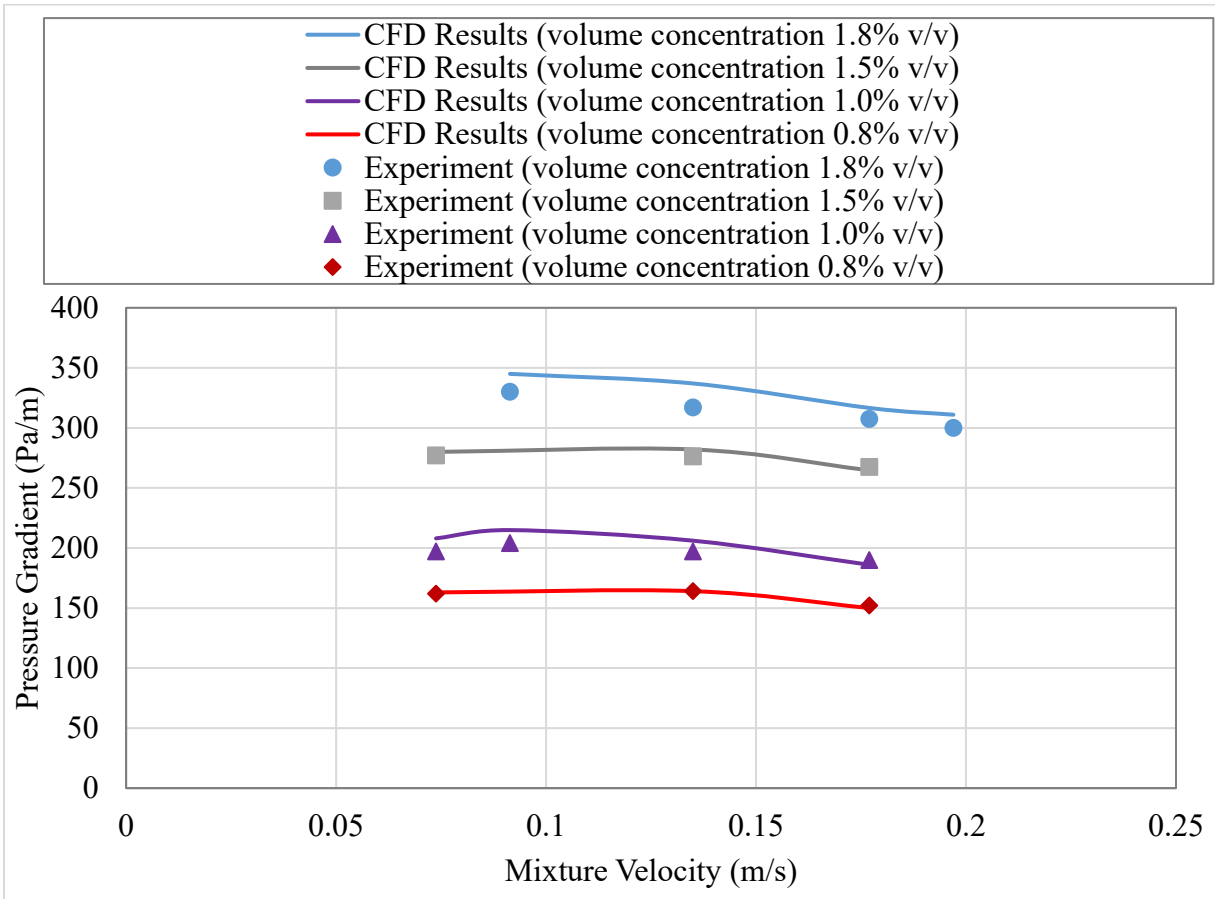


Figure 14. Comparison of simulated two-phase frictional pressure gradient at different mixture velocity and volume concentration of slurry with Ozbelge and Beyaz, 2001 (0.125 m outer diameter, 0.025 m inner diameter, $d_m = 0.23$ mm) [d_m = sand particle diameter, C_v = sand volumetric concentrations]

Two Phase (gas-liquid) flow through Pipeline

Figure 15 and Figure 16 show the comparisons of liquid water velocity profiles in two phase air-water flow through horizontal pipeline. Axial velocities of vertical and horizontal positions are presented in Figure 15 and Figure 16, respectively. The data presented by Kocamustafaogullari

and Wang (1991) were used for these comparisons. For the experiments, diameter of pipeline was 50.4 mm, pipe length was 9000 mm, water was the liquid phase (mean velocity: 5.1 m/s), air was gaseous phase (mean velocity: 0.25 m/s, volume fraction: 0.043), bubble size was 2 mm, temperature was 25°C, and pipe roughness was 0.1 mm.

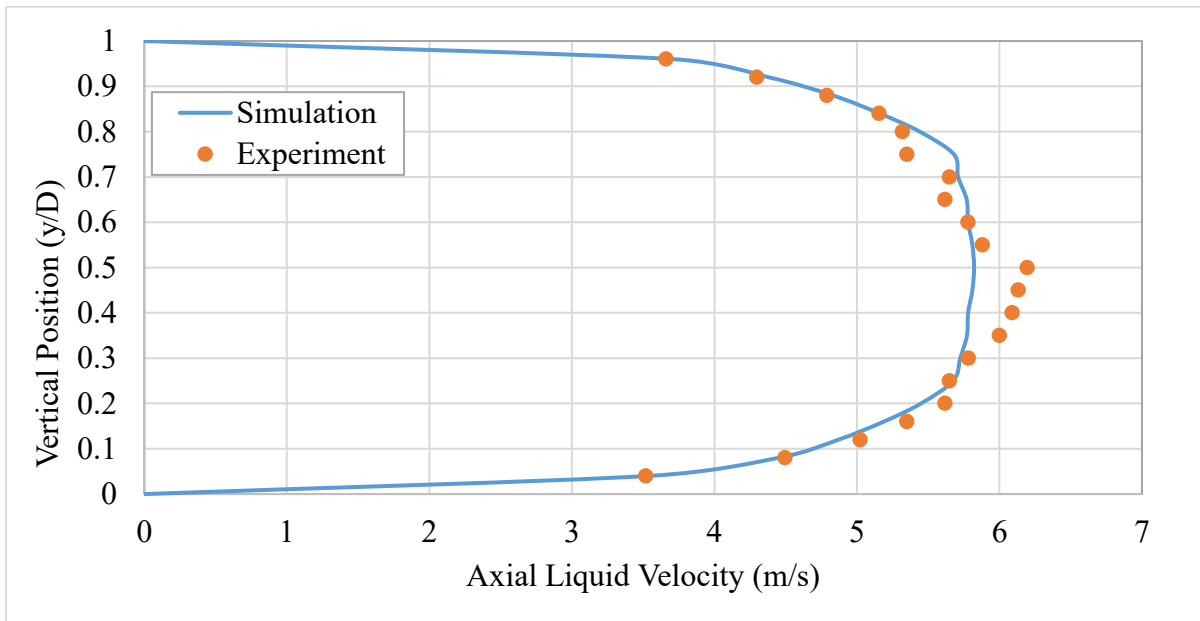


Figure 15. Comparison of simulated axial liquid velocity at vertical position with experimental data from Kocamustafaogullari and Wang, 1991 (50.4 mm pipe diameter, $d_a = 2$ mm, $C_a = 4.3\%$, $v_a = 0.25$ m/s, $v_s = 5.1$ m/s) [d_a = air bubble diameter, C_a = air volumetric concentrations, v_a = air velocity, v_w = water velocity]

From the analysis, simulated local velocity profile is agreeing with experiment having considerable errors. The velocity profile from experiment has slight degree of asymmetry where velocity in the pipe top region is lower than pipe bottom region. Due to the presence of gas particles and gravitational effect on gas, liquid concentration is lower at top region of pipe. This results in decreasing mixture velocity at upper half of pipe (gas velocity 0.25 m/s and water velocity 5.1 m/s).

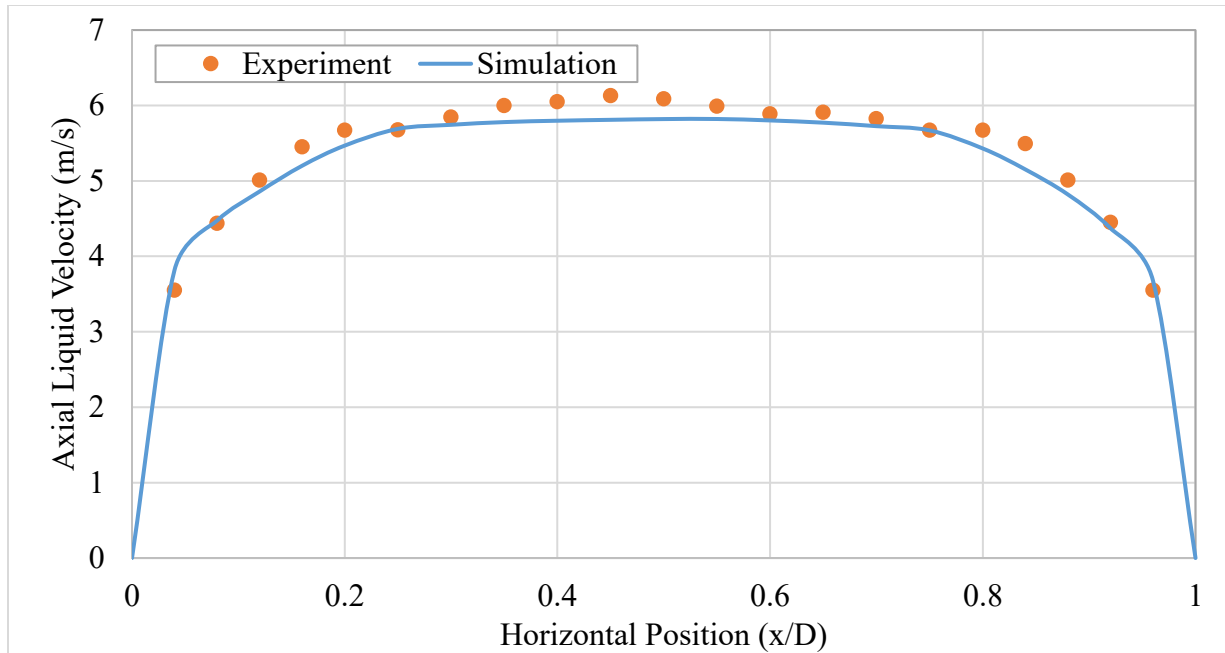


Figure 16. Comparison of simulated axial liquid velocity at horizontal position with experimental data from Kocamustafaogullari and Wang, 1991 (50.4 mm pipe diameter, $d_a = 2$ mm, $C_a = 4.3\%$, $v_a = 0.25$ m/s, $v_s = 5.1$ m/s) [d_a = air bubble diameter, C_a = air volumetric concentrations, v_a = air velocity, v_w = water velocity]

Three Phase (solid-liquid-gas) flow through Pipeline

The simulation results of pressure gradients for air-water-sand three phase flows through horizontal pipelines are compared in Figure 17 and Figure 18 with the experimental data available in Fukuda and Shoji (1986), Kago et al. (1986) and Gillies et al. (1997). In the experiments conducted by Fukuda and Shoji (1986), length of pipe was 2.9 m, diameter of pipe was 0.0416 m, water was the liquid phase (density 998.2 kg/m³, viscosity 0.001 kg/m-s), silica sand particle was the solid phase (density 2650 kg/m³, mean particle diameter 0.074 mm) and air was the gaseous phase (density 1.225 kg/m³, viscosity 1.789×10^{-5} kg/m-s). Mean particle diameter of sand particle was selected from particle size distribution chart (Figure 19). Pipe wall material was Polycarbonate (transparent, smooth pipe). Fukuda and Shoji (1986) used solid volume concentrations of 8.8% ,

13.3% and 24.7% in slurry and 3 m/s slurry velocity with different velocities of gas. For the experiments reported in Kago et al. (1986), length of pipe was 5.95 m, diameter of pipe was 51.5 mm and the three phase fluid was comprised of water, air and sand (Silica Alumina catalyst particle with density 1520 kg/m³, mean particle diameter 0.059 mm and 40% volumetric concentration in slurry). Wall material was similar to the one used by Fukuda and Shoji (1986). Slurry velocity was maintained at 0.5 m/s. In case of Gillies et al. (1997), length of pipe was 5 m, diameter of pipe was

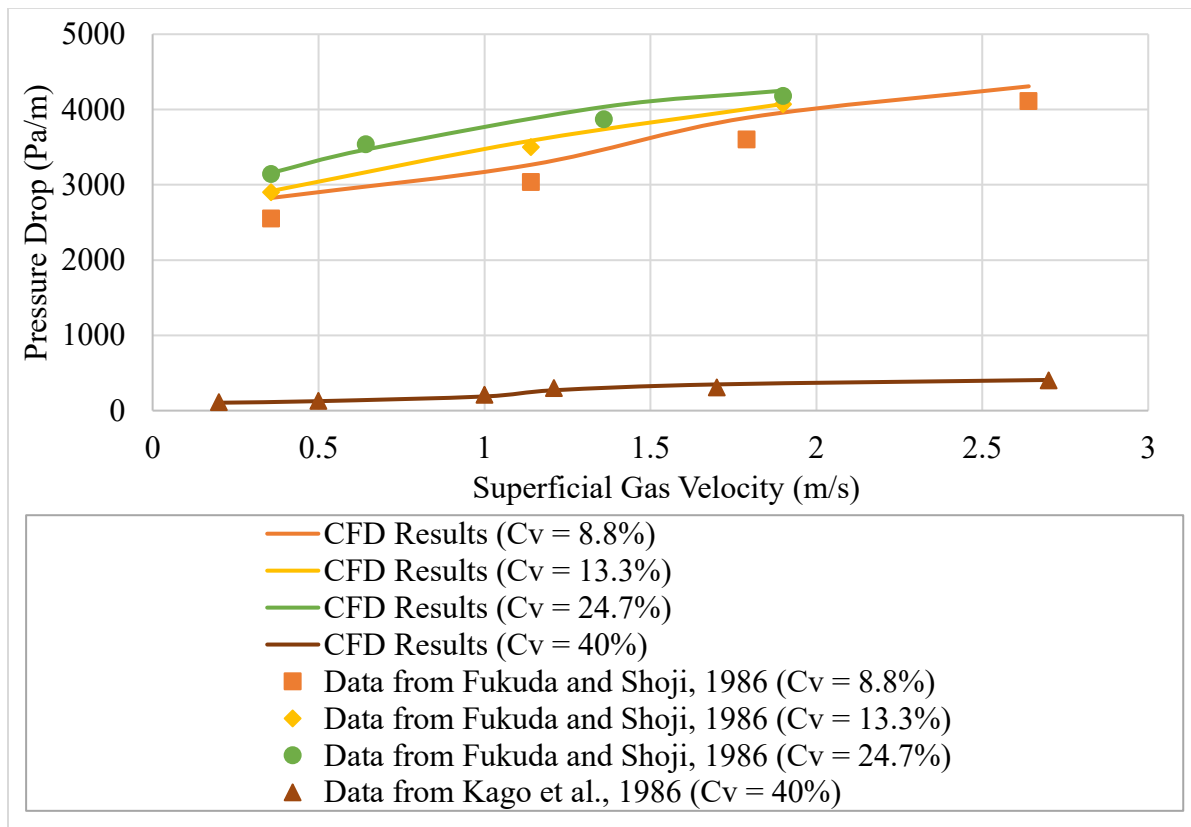


Figure 17. Comparison of simulated pressure gradient as a function of gas velocity with experimental data from Fukuda and Shoji, 1986 (0.0416 m pipe diameter, 0.074 mm sand particle diameter, 2 mm air bubble diameter, 3 m/s slurry velocity) and Kago et al., 1986 (0.0515 m pipe diameter, 0.059mm sand particle diameter, 2 mm air bubble diameter, 0.5 m/s slurry velocity)

52 mm and, similar to Kago et al. (1986), the three phase fluid was comprised of water, air and sand (density 2650 kg/m^3 , mean particle diameter 0.2 mm, 26% volumetric concentration). Wall material was same as two previous references and two different slurry velocities (0.25 m/s and 0.5 m/s) were used.

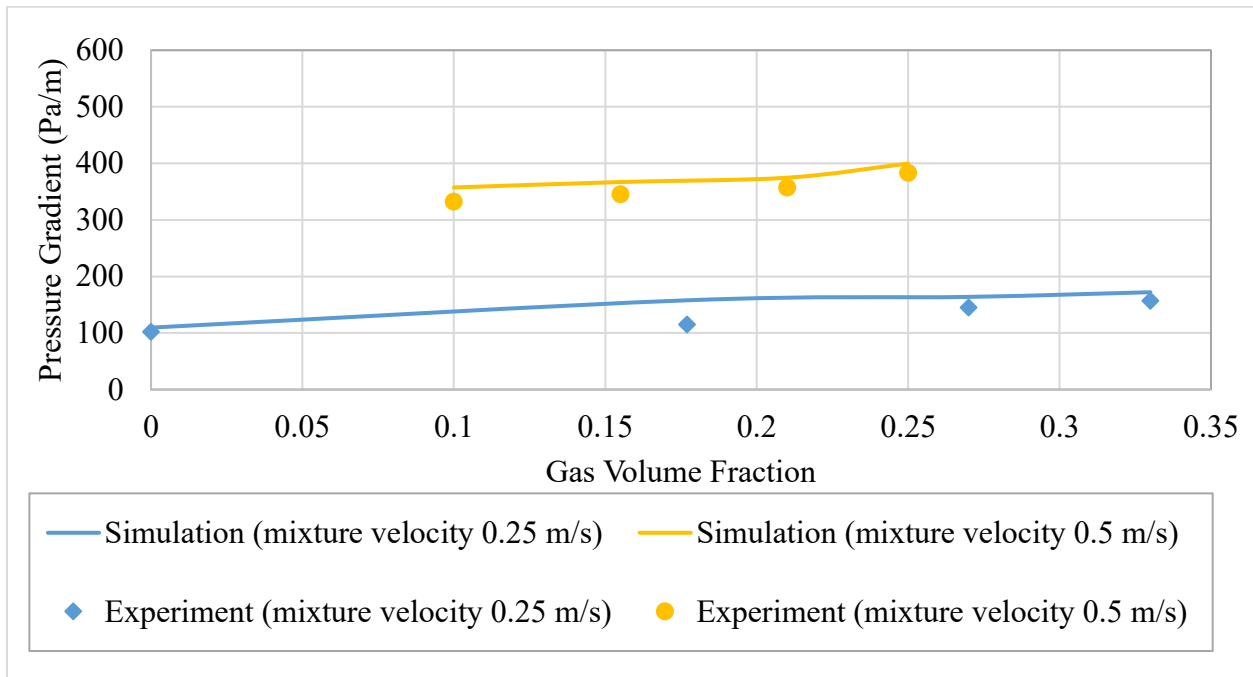


Figure 18. Comparison of simulated pressure gradient as a function of gas volume fraction with Gillies et al., 1997 experimental data (0.052 m pipe diameter, 0.2 mm sand particle diameter, 2 mm air bubble diameter, 0.5 m/s slurry velocity, 26% slurry volumetric concentration)

As presented in Figure 17, the average difference of the simulation results from the Fukuda and Shoji (1986) data was 1% and that from the Kago et al. (1986) data was 8%. Similar discrepancy for the Gillies et al. (1997) data set (Figure 18) was 11%. That is, the CFD simulation results agreed very well with the measured values for the three phase flows through pipelines.

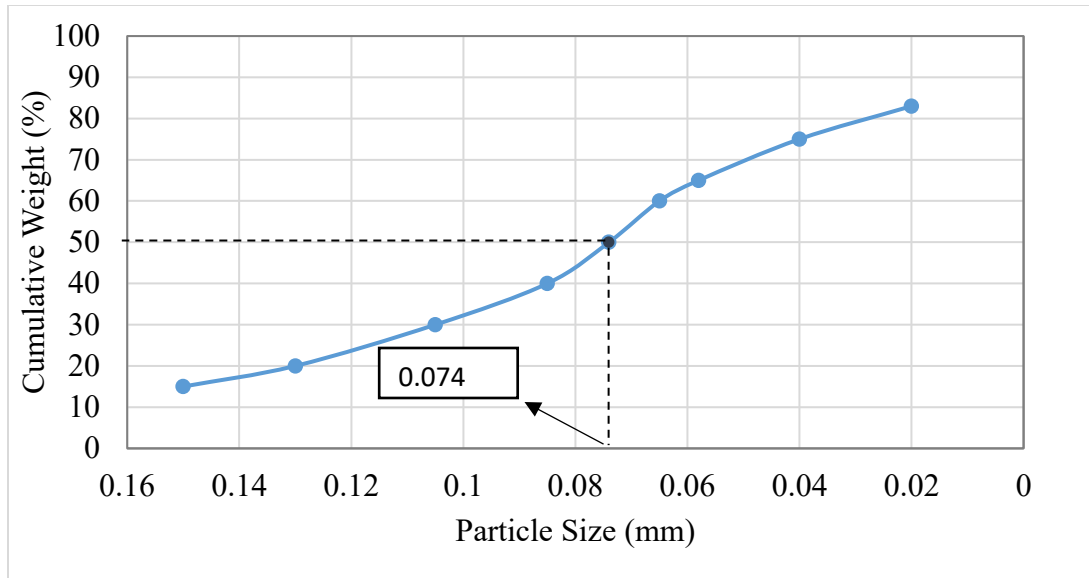


Figure 19. Particle size distribution of different particle used in Fukuda and Shoji (1986)

Future Plan

Continuation of the current work is in progress. It is expected to lead to find out numerical dependencies of different parameters by conducting parametric studies in details. Also, analyzing solid concentration profile of slurry will help to find out the deposition velocity, i.e., the minimum superficial velocity of mixture required to prevent accumulation of solids. Experimental facilities have already been developed in Texas A&M University at Qatar (TAMUQ) to comprehensively study the drilling and hole-cleaning process conditions. Applying the current CFD model to predict various experimentally tested process conditions, the next step is to elaborately study the parametric effects on the pressure losses and the concentration profiles of multiphase flows through pipelines and annuli involving both Newtonian and non-Newtonian fluids. Apart from this, another ongoing research is to analyze Fluid Structure Interaction (FSI). Due to multiphase flows through pipelines and annuli under different conditions, pressure stresses are formed which may deform the pipe/annulus. This study is expected to be significant for the process safety of different multiphase flow systems.

Conclusion

The current study helps to validate a CFD model of multiphase flow through pipeline and annuli. The model can be applied to different applications, especially the ones related to oil and gas industry. The analysis can give idea of selecting optimum range of particle size, volumetric concentration of slurry and mixture velocity during operation using this model. It demonstrated an acceptable agreement with experimental results from single phase to three phase flow, which eventually validates the developed CFD model for further applications. The present investigation can be summarized as follows:

- On the basis of related literatures and experimental validations, the Eulerian model as the multiphase model and the Reynolds stress model (RSM) as the turbulence model were selected as the optimum models in this study.
- Mesh size and inflation layers near the wall were finalized after proper checking of the mesh independency of the simulation results and in consideration of the convergence requirement of the dimensionless wall distance ($y^+ > 30$). The minimum numbers of nodes for the pipeline and annular geometries were 135000 and 540000, respectively. Furthermore, 10 inflation layers with a growth rate of 20% were used near the boundaries.
- Length-independent results were ensured through analysis of the output parameter, i.e., pressure gradient at different cross-sections of the pipeline and annuli (Figure 3). This was done to verify the minimum flow development section or entrance length ($50D_h$) and to analyze the variation of pressure gradients along the length.
- Good agreement of the simulation results with the corresponding experimental values were found over a wide range of properties and flow conditions (Table 1). Considering pressure gradient results from all cases, the average difference was less than 15% with a maximum

value of 30% (Figure 20). Also, velocity profile and sand concentration profile along cross section provided a reasonable discrepancy ($< 15\%$). These indicate the validity of our model within the given range of process conditions which is wide enough to cover different types of operating conditions at several industries.

- Future works are underway to ensure that the present CFD model is applicable to the simulation of industrially important multiphase flow conditions. The following industries are expected to benefit from the use of this model: chemical process plants, petroleum industries, food processing industries, and nuclear plants. Further analysis is required to select the values of different coefficients and constants, such as the coefficient of lift, coefficient of drag, restitution coefficient, and wall boundary conditions, to minimize errors and widen the application range of this model.

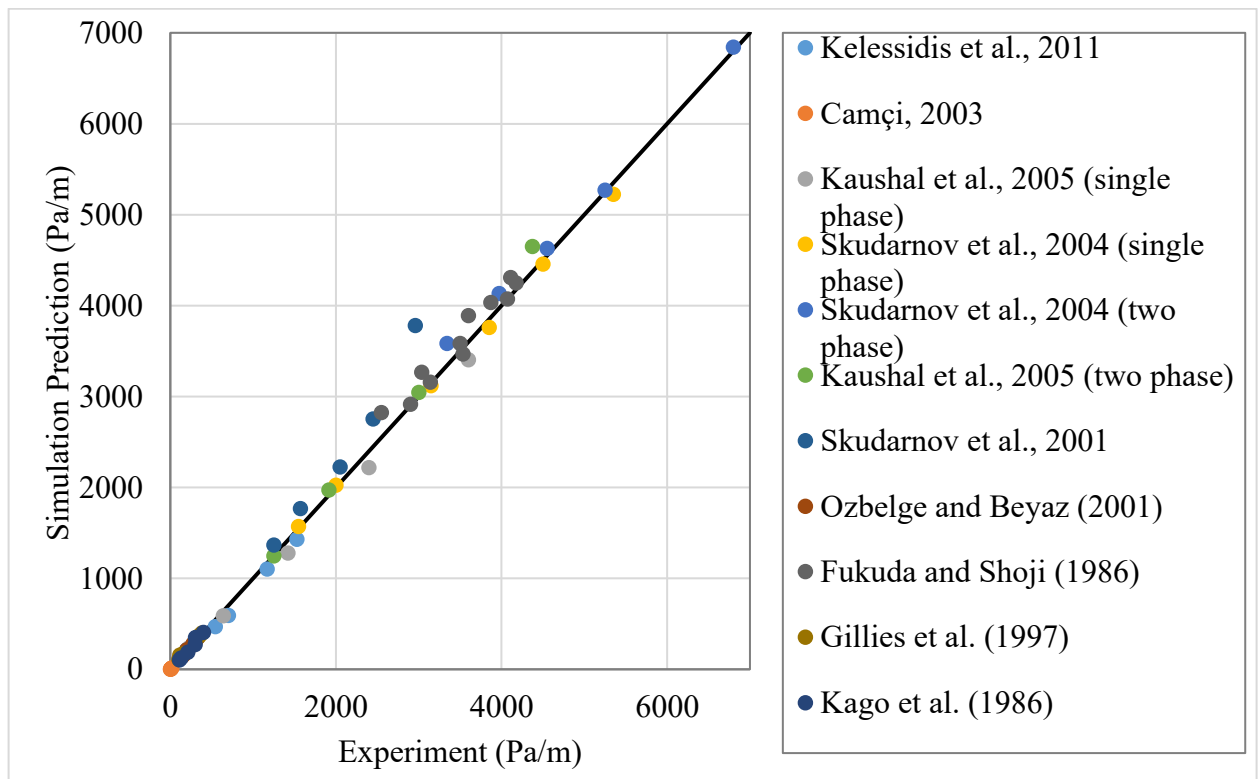


Figure 20. Overall simulation predictions of different experiment data

Acknowledgments

The authors are thankful to Faculty of Engineering and Applied Science of Memorial University, Texas A&M University at Qatar and ANSYS Inc. (License Server Machine: lmserver2.engr.mun.ca) for helping this project.

Reference

- Alder, B. J., and T. E. Wainwright. "Studies in molecular dynamics. II. Behavior of a small number of elastic spheres." *The Journal of Chemical Physics* 33, no. 5 (1960): 1439-1451.
- Anderson, T. Bo, and Roy Jackson. "Fluid mechanical description of fluidized beds. Equations of motion." *Industrial & Engineering Chemistry Fundamentals* 6, no. 4 (1967): 527-539.
- Aude, T. C., T. L. Thompson, and E. J. Wasp. "Economics of slurry pipeline systems." *Publication of: Cross (Richard B) Company* 15, no. Proc Paper (1974).
- Aude, T. C., T. L. Thompson, and E. J. Wasp. "Slurry-pipeline systems for coal; other solids come of age." *Oil Gas J.:(United States)* 73, no. 29 (1975).
- Baltussen, M. W., L. J. H. Seelen, J. A. M. Kuipers, and N. G. Deen. "Direct Numerical Simulations of gas-liquid-solid three phase flows." *Chemical Engineering Science* 100 (2013): 293-299.
- Bello, Oladele O., Kurt M. Reinicke, and Catalin Teodoriu. "Particle Holdup Profiles in Horizontal Gas-liquid-solid Multiphase Flow Pipeline." *Chemical engineering & technology* 28, no. 12 (2005): 1546-1553.
- Bowen, R. M. "Theory of Mixtures in Continuum Physics, Vol. III, Eringen, A. C, ed." (1976).
- Camçı, Gülden. "Application of isokinetic sampling technique for local solid densities in upward liquid-solid flows through an annulus." PhD diss., METU, 2003.

- Camçi, Gülден, and Tülay A. Özbelge. "Determination of dilute slurry densities in a vertical annulus using isokinetic sampling." *Chem. Eng. Comm.* 193, no. 11 (2006): 1482-1501.
- Chapman, Sydney, and Thomas George Cowling. *The mathematical theory of non-uniform gases: an account of the kinetic theory of viscosity, thermal conduction and diffusion in gases.* Cambridge university press, 1970.
- Chen, Ning Hsing. "An explicit equation for friction factor in pipe." *Industrial & Engineering Chemistry Fundamentals* 18, no. 3 (1979): 296-297.
- Chen, Liangyong, Yufeng Duan, Wenhao Pu, and Changsui Zhao. "CFD simulation of coal-water slurry flowing in horizontal pipelines." *Korean journal of chemical engineering* 26, no. 4 (2009): 1144-1154.
- Cornelissen, Jack T., Fariborz Taghipour, Renaud Escudié, Naoko Ellis, and John R. Grace. "CFD modelling of a liquid–solid fluidized bed." *Chemical Engineering Science* 62, no. 22 (2007): 6334-6348.
- Dewangan, Satish K., and Shobha L. Sinha. "Exploring the hole cleaning parameters of horizontal wellbore using two-phase Eulerian CFD approach." *The Journal of Computational Multiphase Flows* 8, no. 1 (2016): 15-39.
- Durand, Robert. "Transport hydraulique de graviers et galets en conduite." *La Houille Blanche* (1951): 609-619.
- Durand, R., and E. Condolios. "The hydraulic transportation of coal and solid material in pipes." *In Processing of Colloquium on Hransport of Coal, National Coal Board, Nov*, vol. 5. 1952.
- Eraslan, Ahmet N., and Tülay A. Özbelge. "Assessment of flow and heat transfer characteristics for proposed solid density distributions in dilute laminar slurry upflows through a concentric annulus." *Chemical engineering science* 58, no. 17 (2003): 4055-4069.

- Escudier, M. P. P. J., P. J. Oliveira, F. Pinho, and S. Smith. "Fully developed laminar flow of non-Newtonian liquids through annuli: comparison of numerical calculations with experiments." *Experiments in fluids* 33, no. 1 (2002): 101-111.
- Fluent, A. N. S. Y. S. "12.0/12.1 Documentation." *Users Guide Manual, Ansys Inc* (2009).
- Fu, S., B. E. Launder, and M. A. Leschziner. "Modelling strongly swirling recirculating jet flow with Reynolds-stress transport closures." In *6th Symposium on Turbulent Shear Flows*, pp. 17-6. 1987.
- Fukuda, Tadashi, and Yasuo Shoji. "Pressure Drop and Heat Transfer for Tree Phase Flow: 1st Report, Flow in Horizontal Pipes." *Bulletin of JSME* 29, no. 256 (1986): 3421-3426.
- Gibson, M. M., and B. E. Launder. "Ground effects on pressure fluctuations in the atmospheric boundary layer." *Journal of Fluid Mechanics* 86, no. 3 (1978): 491-511.
- Gillies, R. G., M. J. McKibben, and C. A. Shook. "Pipeline flow of gas, liquid and sand mixtures at low velocities." *Journal of Canadian Petroleum Technology* 36, no. 09 (1997).
- Gillies, R. G., and C. A. Shook. "Concentration distributions of sand slurries in horizontal pipe flow." *Particulate science and technology* 12, no. 1 (1994): 45-69.
- Gopaliya, Manoj Kumar, and D. R. Kaushal. "Analysis of effect of grain size on various parameters of slurry flow through pipeline using CFD." *Particulate Science and Technology* 33, no. 4 (2015): 369-384.
- Govier, George Wheeler, and Khalid Aziz. *The flow of complex mixtures in pipes*. Vol. 469. New York: Van Nostrand Reinhold, 1972.
- Haaland, Skjalg E. "Simple and explicit formulas for the friction factor in turbulent pipe flow." *Journal of Fluids Engineering* 105, no. 1 (1983): 89-90.

- Hatate, Yasuo, Hiroshi Nomura, Takanori Fujita, Shuichi Tajiri, and Atsushi Ikari. "Gas holdup and pressure drop in three-phase horizontal flows of gas-liquid-fine solid particles system." *Journal of chemical engineering of Japan* 19, no. 4 (1986): 330-335.
- Hernández, Franz H., Armando J. Blanco, and Luis Rojas-Solórzano. "CFD modeling of slurry flows in horizontal pipes." In *ASME 2008 Fluids Engineering Division Summer Meeting collocated with the Heat Transfer, Energy Sustainability, and 3rd Energy Nanotechnology Conferences*, pp. 857-863. American Society of Mechanical Engineers, 2008.
- Kago, Tokihiro, Tetsuya Saruwatari, Makoto Kashima, Shigeharu Morooka, and Yasuo Kato. "Heat transfer in horizontal plug and slug flow for gas-liquid and gas-slurry systems." *Journal of chemical engineering of Japan* 19, no. 2 (1986): 125-131.
- Kaushal, D. R., A. Kumar, Yuji Tomita, Shigeru Kuchii, and Hiroshi Tsukamoto. "Flow of mono-dispersed particles through horizontal bend." *International Journal of Multiphase Flow* 52 (2013): 71-91.
- Kaushal, D. R., Kimihiko Sato, Takeshi Toyota, Katsuya Funatsu, and Yuji Tomita. "Effect of particle size distribution on pressure drop and concentration profile in pipeline flow of highly concentrated slurry." *International Journal of Multiphase Flow* 31, no. 7 (2005): 809-823.
- Kelessidis, V. C., G. E. Bandelis, and J. Li. "Flow of dilute solid-liquid mixtures in horizontal concentric and eccentric annuli." *Journal of Canadian Petroleum Technology* 46, no. 05 (2007).
- Kelessidis, Vassilios C., Panagiotis Dalamarinis, and Roberto Maglione. "Experimental study and predictions of pressure losses of fluids modeled as Herschel–Bulkley in concentric and eccentric annuli in laminar, transitional and turbulent flows." *Journal of Petroleum Science and Engineering* 77, no. 3 (2011): 305-312.

- Kocamustafaogullari, G., and Z. Wang. "An experimental study on local interfacial parameters in a horizontal bubbly two-phase flow." *International journal of multiphase flow* 17, no. 5 (1991): 553-572.
- Krieger, Irvin M. "Rheology of monodisperse latices." *Advances in Colloid and Interface Science* 3, no. 2 (1972): 111-136.
- Kumar Gopaliya, Manoj, and D. R. Kaushal. "Modeling of sand-water slurry flow through horizontal pipe using CFD." *Journal of Hydrology and Hydromechanics* 64, no. 3 (2016): 261-272.
- Lahiri, S. K., and K. C. Ghanta. "Computational technique to predict the velocity and concentration profile for solid-liquid slurry flow in pipelines." In *17th International Conference on Hydrotransport*, pp. 149-175. 2007.
- Lauder, B. E., G. Jr Reece, and W. Rodi. "Progress in the development of a Reynolds-stress turbulence closure." *Journal of fluid mechanics* 68, no. 3 (1975): 537-566.
- Li, Li, Hai-liang Xu, and Fang-qiong Yang. "Three-phase flow of submarine gas hydrate pipe transport." *Journal of Central South University* 22, no. 9 (2015): 3650-3656.
- Lien, Fue-Sang, and M. A. Leschziner. "Assessment of turbulence-transport models including non-linear RNG eddy-viscosity formulation and second-moment closure for flow over a backward-facing step." *Computers & Fluids* 23, no. 8 (1994): 983-1004.
- Lin, C. X., and M. A. Ebadian. "A numerical study of developing slurry flow in the entrance region of a horizontal pipe." *Computers & Fluids* 37, no. 8 (2008): 965-974.
- Ling, J., P. V. Skudarnov, C. X. Lin, and M. A. Ebadian. "Numerical investigations of liquid–solid slurry flows in a fully developed turbulent flow region." *International Journal of Heat and Fluid Flow* 24, no. 3 (2003): 389-398.

- Liu, Xiaoxing, Yuki Aramaki, Liancheng Guo, and Koji Morita. "Numerical simulation of gas–liquid–solid three-phase flow using particle methods." *Journal of Nuclear Science and Technology* 52, no. 12 (2015): 1480-1489.
- Markatos, N. C. "The mathematical modelling of turbulent flows." *Applied Mathematical Modelling* 10, no. 3 (1986): 190-220.
- Newitt, D. D. "Hydraulic conveying of solids in horizontal pipes." *Trans. Inst. Chem. Engrs.* 33 (1955): 93-103.
- Nourmohammadi, Khosrow, P. K. Hopke, and J. J. Stukel. "Turbulent air flow over rough surfaces. II. Turbulent flow parameters." *ASME, Transactions, Journal of Fluids Engineering* 107 (1985): 55-60.
- O'Brien, Morrrough P. "Review of the theory of turbulent flow and its relation to sediment-transportation." *Eos, Transactions American Geophysical Union* 14, no. 1 (1933): 487-491.
- Orell, Aluf. "The effect of gas injection on the hydraulic transport of slurries in horizontal pipes." *Chemical Engineering Science* 62, no. 23 (2007): 6659-6676.
- Özbelge, T. A., and A. Beyaz. "Dilute solid–liquid upward flows through a vertical annulus in a closed loop system." *International journal of multiphase flow* 27, no. 4 (2001): 737-752.
- Özbelge, Tülay A., and Ahmet N. Eraslan. "A computational hydrodynamic and heat transfer study in turbulent up-flows of dilute slurries through a concentric annulus." *Turkish Journal of Engineering and Environmental Sciences* 30, no. 1 (2006): 1-13.
- Özbelge, Tülay A., and Sema H. Köker. "Heat transfer enhancement in water—feldspar upflows through vertical annuli." *International journal of heat and mass transfer* 39, no. 1 (1996): 135-147.

- Özbelge, Tülay A., and Gülden Camçı Ünal. "A new correlation for two-phase pressure drops in fully developed dilute slurry up-flows through an annulus." *Chemical Engineering Communications* 196, no. 4 (2008): 491-498.
- Page, Chester H. "The International System of Units [SI]." *The Physics Teacher* 9, no. 7 (1971): 379-381.
- Pouranfard, A. R., D. Mowla, and F. Esmailzadeh. "An experimental study of drag reduction by nanofluids in slug two-phase flow of air and water through horizontal pipes." *Chinese Journal of Chemical Engineering* 23, no. 3 (2015): 471-475.
- Rahman, M. A., K. Freeman Adane, and R. Sean Sanders. "An improved method for applying the lockhart–martinelli correlation to three-phase gas–liquid–solid horizontal pipeline flows." *The Canadian Journal of Chemical Engineering* 91, no. 8 (2013): 1372-1382.
- Roco, M. C., and C. A. Shook. "Modeling of slurry flow: the effect of particle size." *The Canadian Journal of Chemical Engineering* 61, no. 4 (1983): 494-503.
- Roco, M. C., and C. A. Shook. "Computational method for coal slurry pipelines with heterogeneous size distribution." *Powder Technology* 39, no. 2 (1984): 159-176.
- Rouse, Hunter. "Modern conceptions of the mechanics of turbulence." *Trans. ASCE* 102 (1937): 463-543.
- Rushd, Sayeed, Sultan, Rasel A., Kelessidis, Vassilios C., and Rahman, M. A. "Investigation of Pressure Losses in Eccentric Inclined Annuli." In *36th International Conference on Ocean, Offshore & Arctic Engineering*. American Society of Mechanical Engineering, 2017.
- Sanders, R. Sean, Jason Schaan, and Melissa M. McKibben. "Oil sand slurry conditioning tests in a 100 mm pipeline loop." *The Canadian Journal of Chemical Engineering* 85, no. 5 (2007): 756-764.

- Scott, D. S., and P. K. Rao. "Transport of solids by gas-liquid mixtures in horizontal pipes." *The Canadian Journal of Chemical Engineering* 49, no. 3 (1971): 302-309.
- Seshadri, V. "Basic process design for a slurry pipeline." *Proc. The Short Term Course on Design of pipelines for transporting liquid and solid materials, IIT, Delhi* (1982).
- Seshadri, V. "Concentration and size distribution of solids in a slurry pipeline." In *Proc. 11th Nat. Conference on Fluid Mechanics and Fluid Power, BHEL, Hyderabad, 1982*. 1982.
- Silva, Moises A., and Subhash N. Shah. "Friction pressure correlations of Newtonian and non-Newtonian fluids through concentric and eccentric annuli." In *SPE/ICoTA Coiled Tubing Roundtable*. Society of Petroleum Engineers, 2000.
- Skudarnov, P. V., H. J. Kang, C. X. Lin, M. A. Ebadian, P. W. Gibbons, F. F. Erian, and M. Rinker. "Experimental investigation of single-and double-species slurry transportation in a horizontal pipeline." In *Proc. ANS 9th International Topical Meeting on Robotics and Remote Systems, Seattle, WA*. 2001.
- Skudarnov, P. V., C. X. Lin, and M. A. Ebadian. "Double-species slurry flow in a horizontal pipeline." *Journal of fluids engineering* 126, no. 1 (2004): 125-132.
- Syamlal, Madhava, William Rogers, and Thomas J. O'Brien. "MFIx documentation: Theory guide." *National Energy Technology Laboratory, Department of Energy, Technical Note DOE/METC-95/1013 and NTIS/DE95000031* (1993).
- Thomas, David G. "Transport characteristics of suspension: VIII. A note on the viscosity of Newtonian suspensions of uniform spherical particles." *Journal of Colloid Science* 20, no. 3 (1965): 267-277.
- Toda, M., K. Shimazaki, and S. Maeda. "Pressure drop of three-phase flow in horizontal pipes." *Kagaku Kogaku Ronbunshu* 4 (1978): 56-62.

- Van Sint Annaland, M., N. G. Deen, and J. A. M. Kuipers. "Numerical simulation of gas–liquid–solid flows using a combined front tracking and discrete particle method." *Chemical engineering science* 60, no. 22 (2005): 6188-6198.
- Vasquez, Sergio. "A Phase Coupled Method for Solving Multiphase Problems on Unstructured Mesh." In *ASME Fluids Engineering Division Summer Meeting*. 2000.
- Vijiapurapu, Sowjanya, and Jie Cui. "Performance of turbulence models for flows through rough pipes." *Applied Mathematical Modelling* 34, no. 6 (2010): 1458-1466.
- Vocadlo, J. J., and M. E. Charles. "Transportation of slurries." *Canadian Mining and Metallurgical Bulletin* 65, no. 726 (1972).
- Wakeman, T., and W. Tabakoff. "Measured particle rebound characteristics useful for erosion prediction." In *ASME 1982 International Gas Turbine Conference and Exhibit*, pp. V003T05A005-V003T05A005. American Society of Mechanical Engineers, 1982.
- Washino, K., H. S. Tan, A. D. Salman, and M. J. Hounslow. "Direct numerical simulation of solid–liquid–gas three-phase flow: Fluid–solid interaction." *Powder technology* 206, no. 1 (2011): 161-169.
- Wasp, Edward J., John P. Kenny, and Ramesh L. Gandhi. "Solid–liquid flow: slurry pipeline transportation. [Pumps, valves, mechanical equipment, economics]." *Ser. Bulk Mater. Handl.; (United States)* 1, no. 4 (1977).
- Lin, C. X. "Double-Species Slurry Flow in a Horizontal Pipeline." (2004).
- Zagarola, M. V., and A. J. Smits. "Scaling of the mean velocity profile for turbulent pipe flow." *Physical review letters* 78, no. 2 (1997): 239.

Chapter 2. Pressure Losses and Settling Conditions in a Horizontal Annulus

Rasel A Sultan¹, M. A. Rahman², Sayeed Rushd², Sohrab Zendehboudi¹, Vassilios C. Kelessidis³

¹Faculty of Engineering and Applied Science, Memorial University of Newfoundland, Canada

²Texas A&M University at Qatar, Doha, Qatar

³Petroleum Institute, Abu Dhabi, UAE

Abstract

Estimation of pressure losses and settling conditions are vital in the hydraulic design of annular drill holes in Petroleum Industry. The present study investigates the effects of fluid velocity, fluid type, particle size, particle concentration, drill pipe rotation speed and drill pipe eccentricity on pressure losses and settling conditions using computational fluid dynamics (CFD). The eccentricity of the drill pipe is varied in the range of 0 – 50% and it rotates about its own axis at 0 – 150 rpm. The diameter ratio of the simulated drill hole is 0.56. This study is about the numerical simulation of turbulent conditions. Experimental data confirmed the validity of current CFD model developed using ANSYS 16.2 platform. The goal of the current work is to develop a comprehensive CFD tool that can be used for modeling the hydraulic conditions associated with hole cleaning in extended reach drilling.

Introduction

In the petroleum industry, predicting frictional pressure losses and settling conditions for the transportation of drilling fluids in the annuli are important for drilling operations. Inaccurate predictions can lead to a number of costly drilling problems. A few examples of such problems are loss of circulation, kicks, blockage, wear, abrasion, and improper rig power selection. The existing empirical models become less accurate as those involve many simplified assumptions. CFD simulations help to minimize such assumptions by using the physics based Navier Stokes

equations to model the hydrodynamics of the flow system. Current work is focused on developing a comprehensive CFD model which is capable of considering the effects of all important drilling parameters, such as fluid velocity, fluid type, particle size, particle concentration, drill pipe rotation speed and drill pipe eccentricity.

Literature Review

The estimation of pressure loss in an annulus is more difficult compared to pipe flow due to the complexities in hydraulics resulting from the complex geometry [1, 2]. From an empirical perspective, the issue is usually addressed by replacing pipe diameter in the pipe flow models with an “effective diameter” of annulus. A number of definitions of “effective diameter” have been proposed till date. However, it is difficult to select a definition for a field application as those were developed and/or applied empirically. A comparison of multiple definitions in predicting pressure losses is presented by Anifowoshe and Osisanya [3]. Other issues that make the estimation of pressure losses in drilling holes difficult are the eccentricity and the rotational speed of inner drill pipe. Many studies have been done on the flow of non-Newtonian fluids in annuli to introduce empirical/analytical models which allow to take these effects into account [1, 3-10]. The results of the previous studies show that the annular pressure losses for non-Newtonian (power law) fluids flowing in a drill hole depend on drill pipe rotation speed, fluid properties, flow regimes (laminar/transitional/turbulent), diameter ratio, eccentricity and equivalent hydrodynamic roughness.

Using commercially available CFD packages like ANSYS FLUENT to predict pressure losses for the annular transportation of drilling fluids is comparatively a new approach. Sorgun and Ozbayoglu [9] demonstrated the better performance of CFD model compared to the existing empirical models in predicting frictional pressure losses. Sorgun [8] investigated the effect of pipe

eccentricity on pressure loss, tangential velocity, axial velocity and effective viscosity by using CFD. Erge et al. [6] presented a CFD modeling approach which is applicable to estimate frictional pressure losses in an eccentric annulus with inner pipe rotation while circulating yield power law fluids. However, most of these CFD studies were limited to the laminar flow of a single phase in hydro dynamically smooth annuli.

Annular flow of drilling fluids containing cuttings, i.e., slurry has not been studied in sufficient details. Examples of works in the field of annular slurry flow are [11-14]. Focus of these studies were to understand the hydrodynamics of the slurry flow in annulus from real time experiments and to produce empirical models based on data analysis. Recently, different researchers [15-17] have used CFD in studying the transportation of slurry in annuli. Ofei [15] examined the effect of the rheological parameters of the carrying fluids on the velocity of solid. Sorgun and Ulker [16] compared the predictions of pressure losses obtained using Artificial Neural Network (ANN) and CFD. Both methods produced comparable results. Sun et al. [17] studied the effects of inclination, rotational speed and flow rate on the distribution of solid concentration and the frictional pressure loss. Similar to the single phase annular flow works, most of these CFD studies were limited to the laminar slurry flow conditions.

Methods

CFD Simulation

In the current work, the CFD simulation model of the annular slurry flow is developed using ANSYS Fluent 16.2 platform. Following previous works [18-20], a multi-fluid granular model is used to describe the flow behavior of a fluid-solid mixture. The granular version of Eulerian model is selected as the multiphase model. This is because high solid volume fraction is expected to be used for this study and the granular version captures the hydrodynamics of high concentration

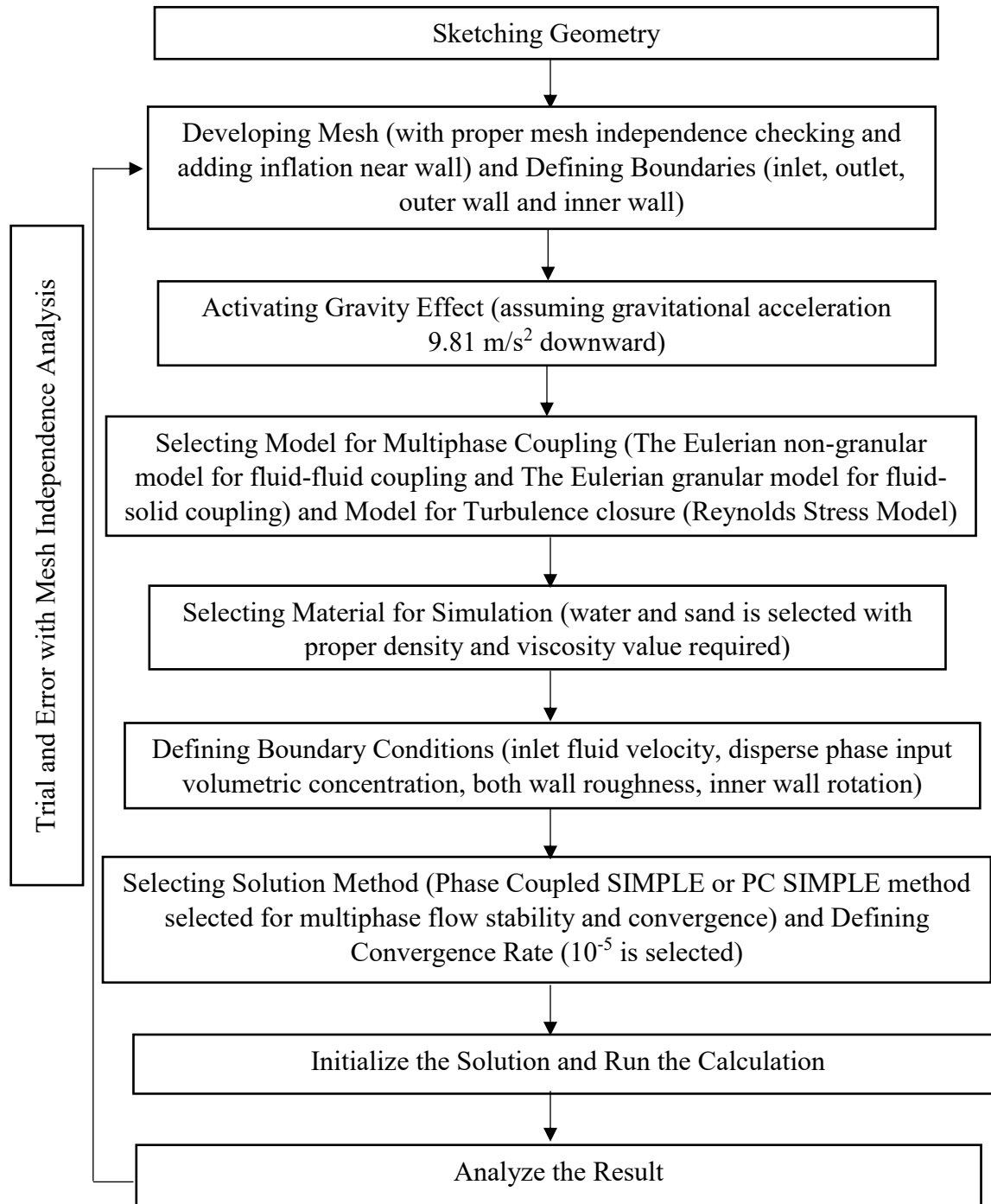
slurries consisting of varying grain sizes. It allows modeling of multiple separate but interacting phases. The phases can be liquids, gases, or solids in nearly any combination. The Eulerian treatment is used for each phase, in contrast to the Eulerian-Lagrangian treatment that is used for the discrete phase model.

The description of multiphase flow as interpenetrating continua incorporates the concept of phasic volume fractions, which represent the space occupied by each phase. Each phase satisfies the laws of conservation of mass and momentum individually. The conservation equations are modified by averaging the local instantaneous balance for each of the phases [21] or by using the mixture theory approach [22]. A detailed description is available in Appendix A.

For Eulerian multiphase calculations, the phase coupled SIMPLE (PC-SIMPLE) algorithm is used for the pressure-velocity coupling. PC-SIMPLE is an extension of the SIMPLE algorithm to multiphase flows [23, 24]. The velocities coupled by phases are solved in a segregated fashion. The block algebraic multigrid scheme used by the density-based solver is used to solve a vector equation formed by the velocity components of all phases simultaneously [25]. Then, a pressure correction equation is built based on total volume continuity. Pressure and velocities are then corrected so as to satisfy the continuity constraints.

To ensure stability and convergence of iterative process, a second order upwind discretization was used for momentum equation and first upwind discretization was employed for volume fraction, turbulent kinetic energy and its dissipation. Upwinding refers to the face value derived from quantities in the cell upstream, or "upwind," relative to the direction of the normal velocity. When first-order accuracy is desired, quantities at cell faces are determined by assuming that the cell-center values of any field variable represent a cell-average value and hold throughout the entire cell; the face quantities are identical to the cell quantities. Thus, the face value is set equal to the

The total simulation process has the following steps –



cell-center value of in the upstream cell when first-order upwinding is selected. In contrast, when second-order accuracy or second-order upwinding is desired, quantities at cell faces are computed using a multidimensional linear reconstruction approach [26]. In this approach, higher-order

accuracy is achieved at cell faces through a Taylor series expansion of the cell-centered solution about the cell centroid.

Turbulence Model Selection

Turbulent quantities for fluid flow are computed using Reynolds Stress Model [27-29]. Abandoning the isotropic eddy-viscosity hypothesis, the RSM closes the Reynolds-averaged Navier-Stokes equations by solving transport equations for the Reynolds stresses, together with an equation for the dissipation rate [30]. Here five additional transport equations are required in 2D flows and seven additional transport equations must be solved in 3D (please see Appendix B for further details). The turbulence model was selected for the current work analyzing the relative performance of different models. A typical example of the analysis is presented in Figure 1. In this figure, % Difference refers to the percentile difference between the experimental measurements of pressure loss and the corresponding CFD predictions. In most cases, the difference was less than 10% when RSM was used. A list of the important results is presented in Table 1.

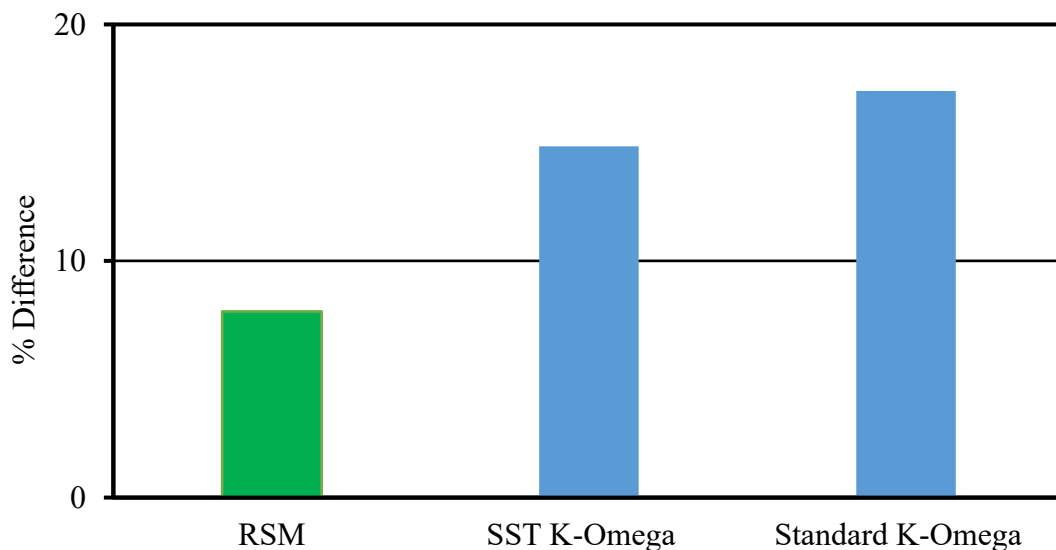


Figure 1. Performance of turbulence models in predicting pressure loss (Data Source: Kaushal et al., 2005 [40])

Table 1. Analysis of Turbulence Model Performance

| Reference | Experimental Conditions | % Difference [100(Experiment – Simulation)/Experiment] | | | |
|----------------------------|---|---|--------------------|-------------------------|---------------------------|
| | | RSM | SST k- ω | Standard k- ω | Standard k- ϵ |
| Kaushal et al. (2005) [40] | <p>Pipe orientation: Horizontal</p> <p>Pipe dia.: 0.0549 m</p> <p>Pipe material of construction: Stainless Steel (density 8030 kg/m³, smooth wall)</p> <p>Fluid: Single phase water (density: 998.2 Kg/m³, viscosity: 0.001003 Kg/m-s)</p> <p>Fluid velocity: 2 m/s</p> | 8 | 15 | 17 | 17.48 |
| Camçi (2003) [41] | <p>Annulus orientation: Horizontal and concentric</p> <p>Annulus dimensions: 0.0432 m ID, 0.123 m OD</p> | 9 | 17 | 20 | 23 |

| | | | | | |
|--|---|----|------|----|------|
| | <p>Material of construction: Aluminum (smooth wall)</p> <p>Fluid: Single phase water</p> <p>Fluid velocity: 0.2 m/s</p> | | | | |
| <p>Kelessidis et al. (2011) [33]</p> | <p>Annulus orientation: Horizontal and concentric</p> <p>Annulus dimensions: 0.04 m ID, 0.07 m OD</p> <p>Material of construction: Plexiglas (smooth wall)</p> <p>Fluid: Single phase water</p> <p>Fluid velocity: 1.12 m/s</p> | 8 | 13 | 16 | 22.2 |
| <p>Skudarnov et al. (2004) [42]</p> | <p>Pipe orientation: Horizontal</p> <p>Pipe diameter: 0.023 m</p> <p>Pipe material of construction: Stainless Steel (Wall roughness: 32 μm)</p> | -2 | -2.8 | -3 | -3.2 |

| | | | | | |
|-------------------------------|--|----|----|----|-------|
| | <p>Fluid: Two phase solid – liquid slurry</p> <p>Liquid: Water (density: 998.2 Kg/m³, viscosity: 0.001003 Kg/m-s)</p> <p>Solid: Glass spheres (double-species with densities of 2490 kg/m³ and 4200 kg/m³, 50% by 50% volume mixture, particle diameter (d_m): 140 μm, volumetric concentration (C_v): 15%)</p> <p>Fluid velocity: 1.724 m/s</p> | | | | |
| Ozbelge and Beyaz (2001) [35] | <p>Annulus orientation: Vertical and concentric</p> <p>Annulus dimensions: 0.125 m OD, 0.025 m ID</p> <p>Material of construction: Stainless Steel (density 8030 kg/m³, smooth wall)</p> | -6 | 14 | 15 | -15.1 |

| | | | | | |
|--------------------------------------|--|----|---|----|----|
| | <p>Fluid: Two phase solid – liquid slurry</p> <p>Liquid: Water (density 998.2 Kg/m³, viscosity 0.001003 Kg/m-s)</p> <p>Solid: Feldspar (mean particle diameter 0.23 mm, mean density 2500 kg/m³, volumetric concentration, C_v = 1.80%)</p> <p>Fluid velocity: 0.135 m/s</p> | | | | |
| <p>Ozbelge and Beyaz (2001) [35]</p> | <p>Annulus orientation: Vertical and concentric</p> <p>Annulus dimensions: 0.125 m OD, 0.025 m ID</p> <p>Material of construction: Stainless Steel (density 8030 kg/m³, smooth wall)</p> <p>Fluid: Two phase solid – liquid slurry</p> | -4 | 8 | 13 | 16 |

| | | | | | |
|--|---|--|--|--|--|
| | Liquid: Water (density 998.2 Kg/m ³ , viscosity 0.001003 Kg/m-s) | | | | |
| | Solid: Feldspar (mean particle diameter 0.23 mm, mean density 2500 kg/m ³ , volumetric concentration, $C_v = 1.80\%$) | | | | |
| | Fluid velocity: 0.197 m/s | | | | |

Length Independence Study

The length of the flow domain is considered long enough to achieve the fully developed flow. Minimum entrance length considered for the flow development is $50D_h$, where hydraulic diameter, $D_h = OD - ID$ [31, 32]. An example of the length independent test is shown in Figure 2. The simulation results were not dependent on length after 3 m from the inlet.

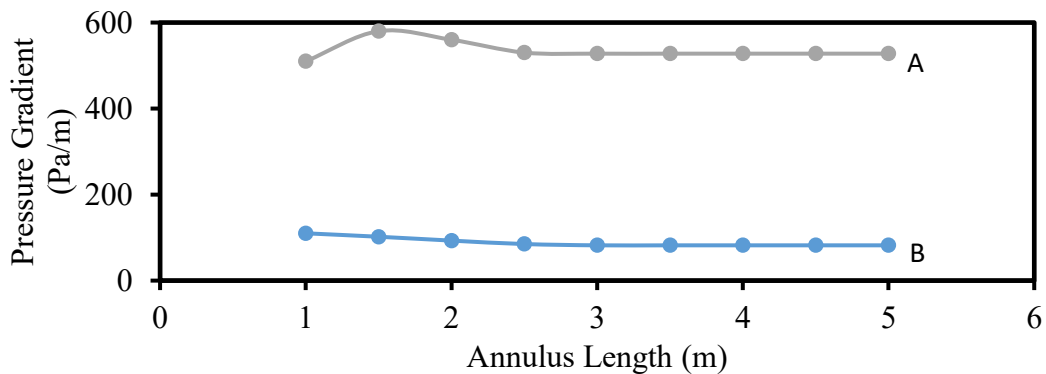
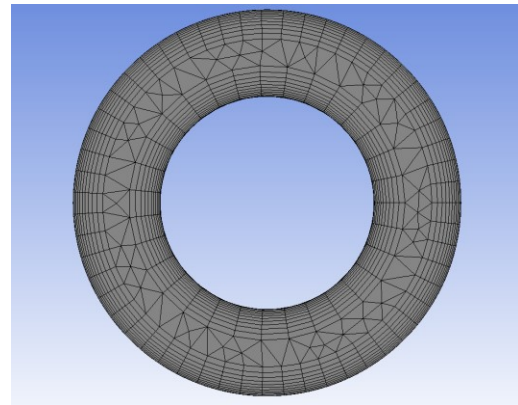
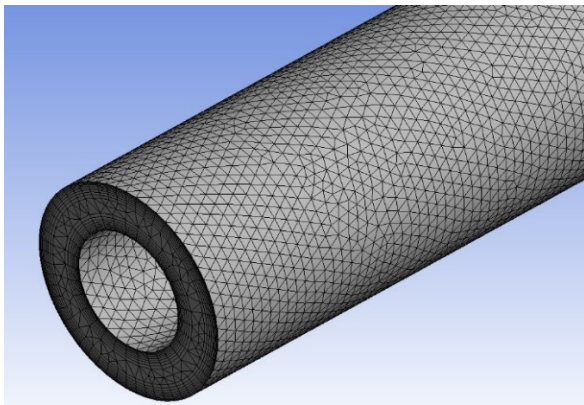


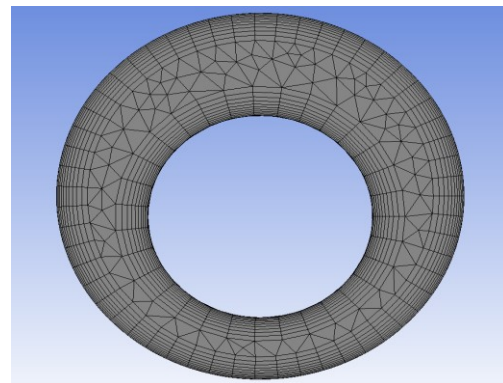
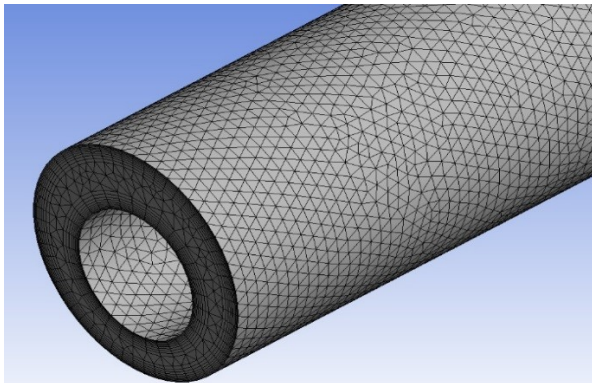
Figure 2. Length independence analysis (A) 75% eccentric, 150 RPM inner pipe rotation speed and 400 kg/min flow rate; (B) Concentric, stationary inner pipe and 200 kg/min flow rate.

Mesh analysis

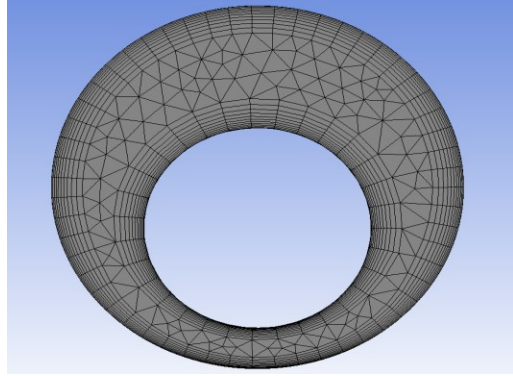
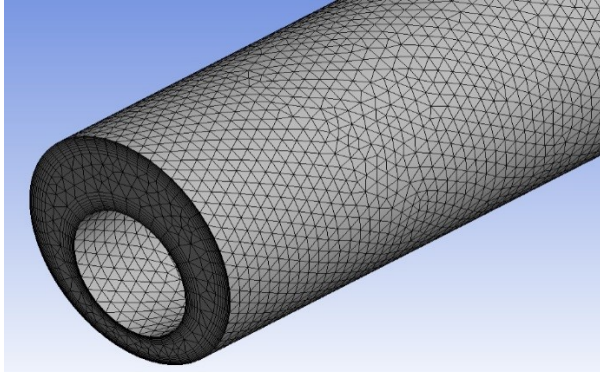
The computational grids for an annular section are generated using ANSYS Fluent and the meshing is finalized on the basis of proper mesh independency check. Multiple layers of Inflation near wall are added from both inner and outer walls to compute the characteristics of different parameters near wall more precisely. Shear stress between wall surface and fluids are much higher and this inflation helps to create denser meshing near wall. An example of computational grid distribution and mesh independence test are shown in Figure 3 and Figure 4. Mesh independent results could be produced for number of nodes more than 800000. All the results presented in the current work were obtained using around 900000 nodes.



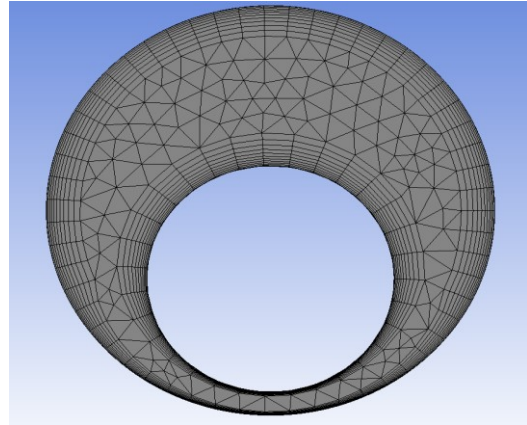
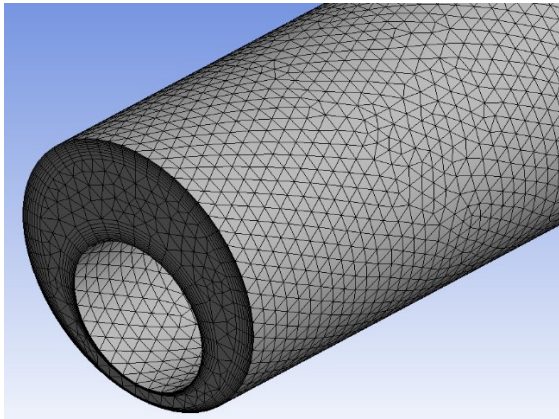
(a) Concentric Inner Pipe (Number of Nodes 901595)



(b) 25% Eccentric Inner Pipe (Number of Nodes 897540)



(c) 50% Eccentric Inner Pipe (Number of Nodes 909730)



(d) 75% Eccentric Inner Pipe (Number of Nodes 919432)

Figure 3. Mesh distribution

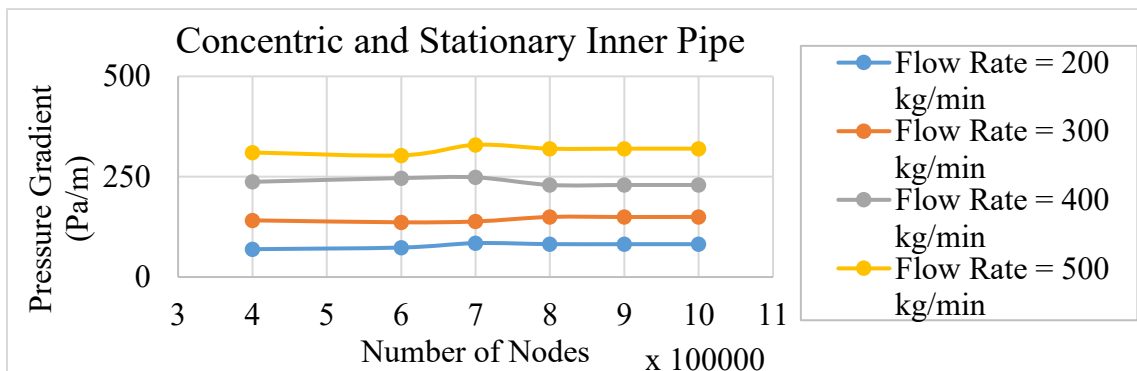


Figure 4. Mesh independence analysis

Convergence rate analysis:

An optimum convergence rate of 10^{-5} was selected for the termination of iteration. Figure 5 shows an example of the analysis used to find out optimum convergence rate within $10^{-6} - 10^{-4}$. The simulation results varied when the convergence value was greater than 10^{-5} . However, the results did not change at all for the values less than 10^{-5} .

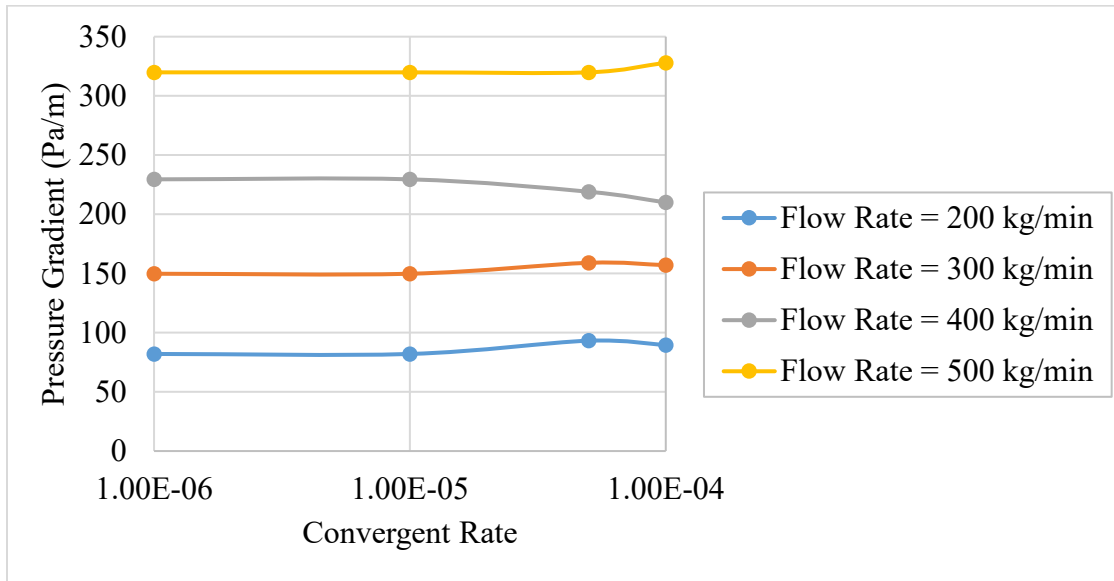


Figure 5. An example of optimum convergence rate analysis

CFD Model Validation

As the preliminary step, the CFD modeling approach is validated with respect to the data available in open literature. Few examples of the validation are presented as follows –

Single Phase Flow through Annuli

Sets of experimental data from Kelessidis et al. (2011) [33] and Camçi (2003) [41] are compared in Figure 6 with the proposed CFD model. The geometry is taken from Kelessidis et al. (2011) where inner diameter (ID) 0.04 m, outer diameter (OD) 0.07 m and length 5 m (horizontal concentric annuli). Fluid is taken as water and wall material is Plexiglas (hydro dynamically

smooth wall, $\epsilon_a=0$). In Camçi (2003) inner diameter 0.0432 m, outer diameter 0.123 m and length 5 m. Wall material is Aluminum (smooth wall).

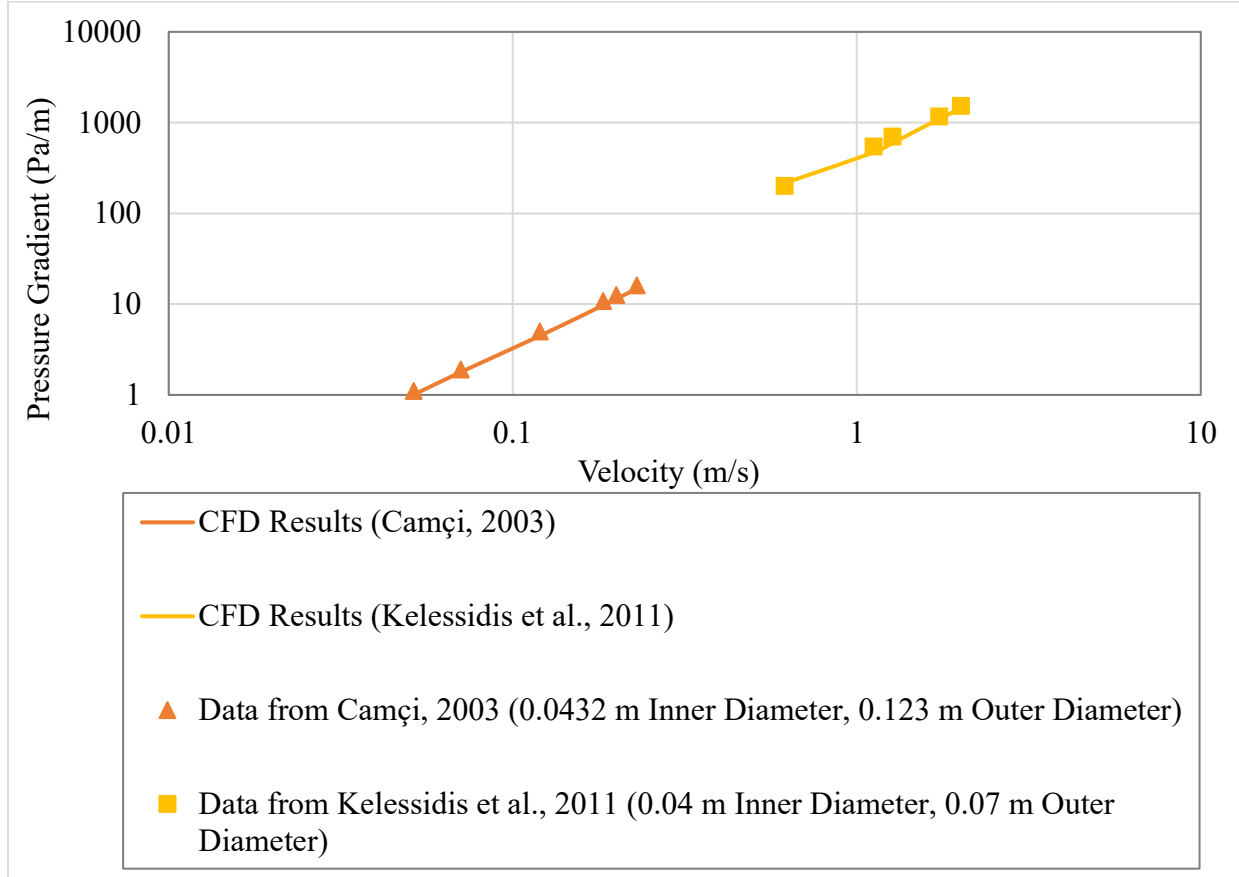


Figure 6. Comparison of simulated pressure gradient with Haaland (1983) correlation and experimental data from Kelessidis et al. (2011) and Camçi (2003) at different inlet velocity

Correlation of Haaland (1983) is as follows-

$$\frac{1}{\sqrt{f}} = -3.6 \left\{ \left(\frac{\epsilon_a}{3.7d_e} \right)^{1.1} + \frac{6.9}{Re} \right\} \quad (1)$$

Where, f = friction factor, d_e = outer diameter- inner diameter, Re = Reynolds Number, ϵ_a = absolute roughness.

In Figure 6, the graph represents log-log scale. Pressure gradient increasing rate in log-log scale is almost linear for both cases. The average percentage error of simulation results from Kelessidis et al. (2011) and Camçi (2003) are 9.88% and 8.46% respectively which indicates very good agreement (it was estimated that the error of the experimental data is approximately $\pm 10\%$ in Kelessidis et al. 2011).

Two Phase (solid-liquid) flow through Annuli

Pressure gradient (Pa/m) profile of water-sand slurry flow through vertical concentric annuli is compared with Ozbelge and Beyaz (2001) [35] experimental data in Figure 7. For the CFD simulation, the liquid phase is considered as water (density 9982 kg/m^3 , viscosity 0.001003 kg/m-s) and solid phase is taken as feldspar (symbol $\text{K}_2\text{O}.\text{Al}_2\text{O}_3.\text{SiO}_2$, mean particle diameter 0.23 mm , mean density 2500 kg/m^3). Length 5 m , outer diameter 0.125 m , inner diameter 0.025 m , inlet velocity range of $0.0738\text{--}0.197 \text{ m/s}$ and overall slurry volumetric concentration range of $0.8\%\text{--}1.8\%$ with 0.23 mm grain size (d_p) are considered as boundary conditions. A smooth pipe of stainless steel (density 8030 kg/m^3) is used for the simulation. The pipe is assumed to be vertical, i.e., gravity effect is included and gravity acceleration is directed opposite to outlet. No slip condition for liquid and solid phase is used at the walls. Figure 14 shows the comparison of simulated and experimental two-phase frictional pressure drop through vertical annuli at different mixture velocity and at different volume concentration of slurry for 0.23 mm mean sand particle diameter (d_p). Simulated results are in good agreement with experimental values with 2.62% average error.

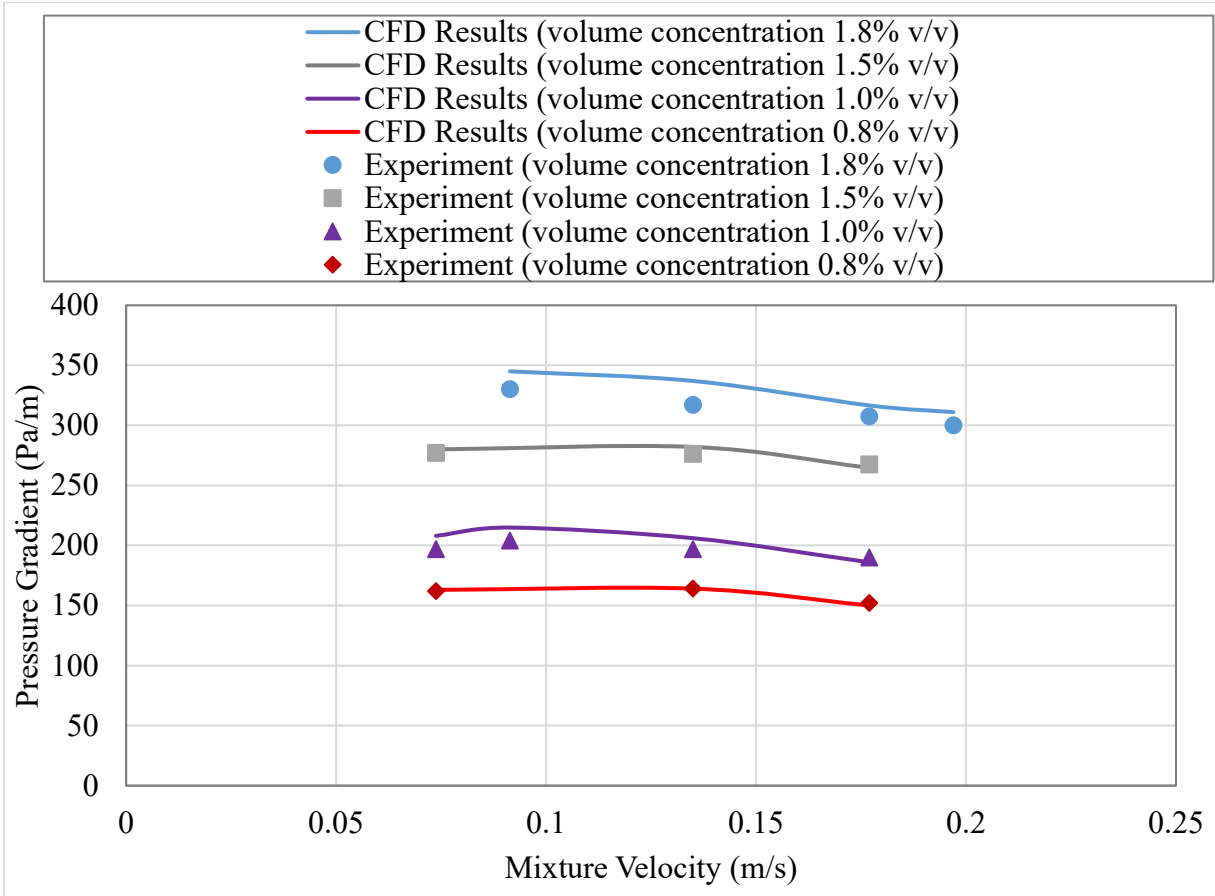


Figure 7. Comparison of simulated two-phase frictional pressure gradient at different mixture velocity and volume concentration of slurry with Ozbelge and Beyaz, 2001 (0.125 m outer diameter, 0.025 m inner diameter, $d_m = 0.23$ mm) [d_m = sand particle diameter, C_v = sand volumetric concentrations]

Results and Discussion

After achieving good validation of proposed model with experimental data, parametric analysis is done to observe the effect of changing flow rate, drill pipe rotation, eccentricity and particle size. (data tables are presented in Appendix 4).

Effect of Flow Rate

The effect of fluid flow on maximum bed concentration is analyzed in Figures 8 – 11. Water with sand particle mixture (slurry) is used as operating two phase fluid. Four different conditions are taken into consideration with fix sand inlet concentration (20%) and sand particle size (0.1 mm).

The conditions are as below –

- Concentric annuli with stationary inner pipe.
- Concentric annuli with 150 rpm rotating inner pipe.
- 50% eccentric annuli with stationary inner pipe.
- 50% eccentric annuli with 150 rpm inner pipe.

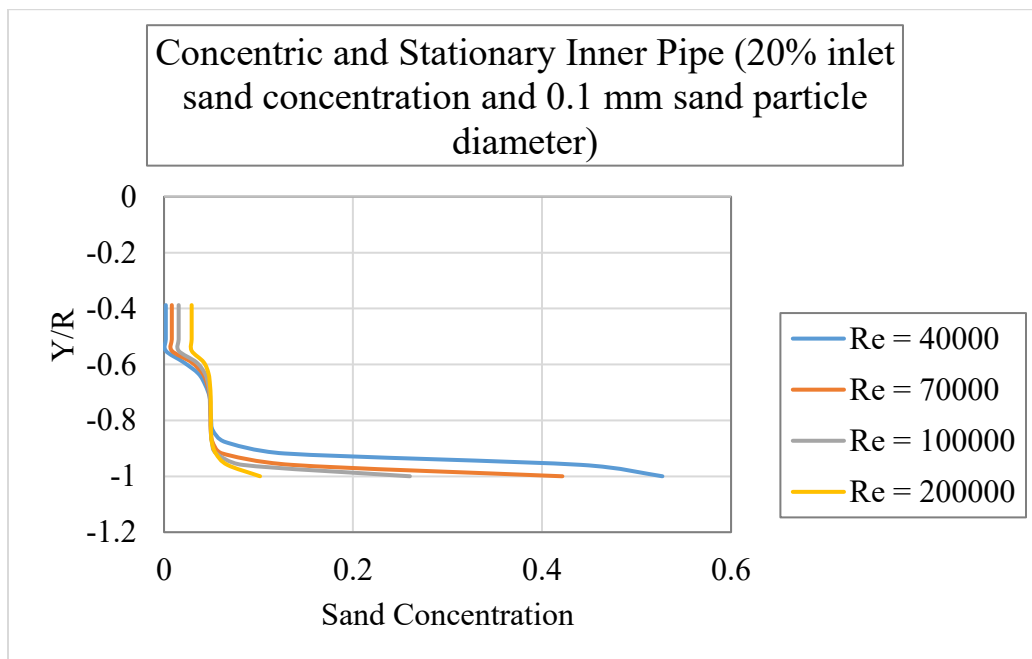


Figure 8. Effect of fluid flow on particle concentration profile (Concentric annuli with stationary inner pipe)

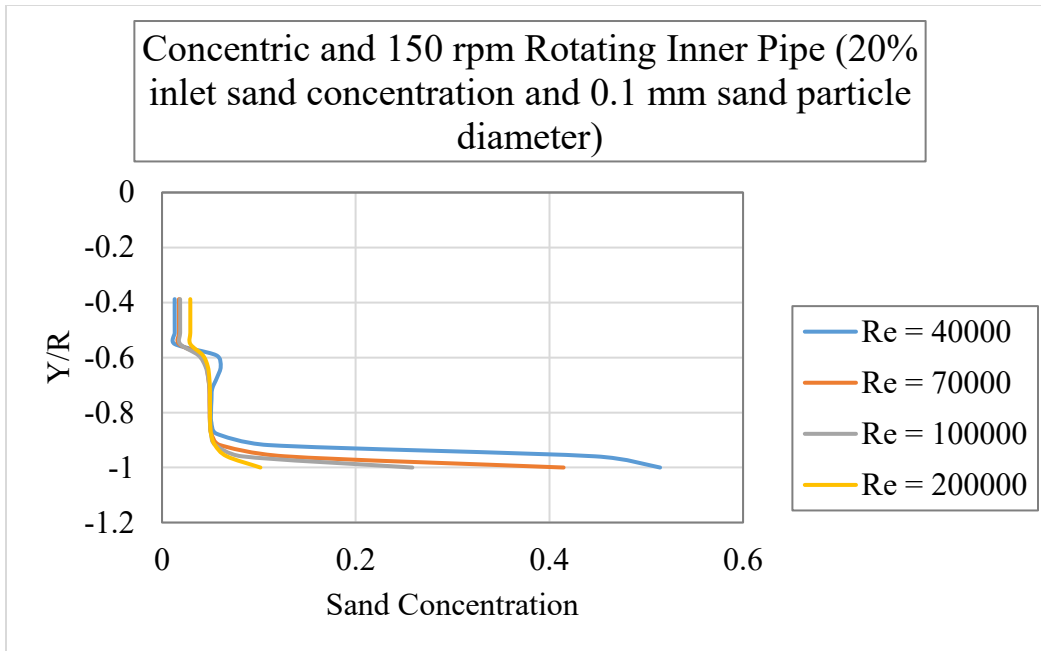


Figure 9. Effect of fluid flow on particle concentration profile (Concentric annuli with 150 rpm rotating inner pipe)

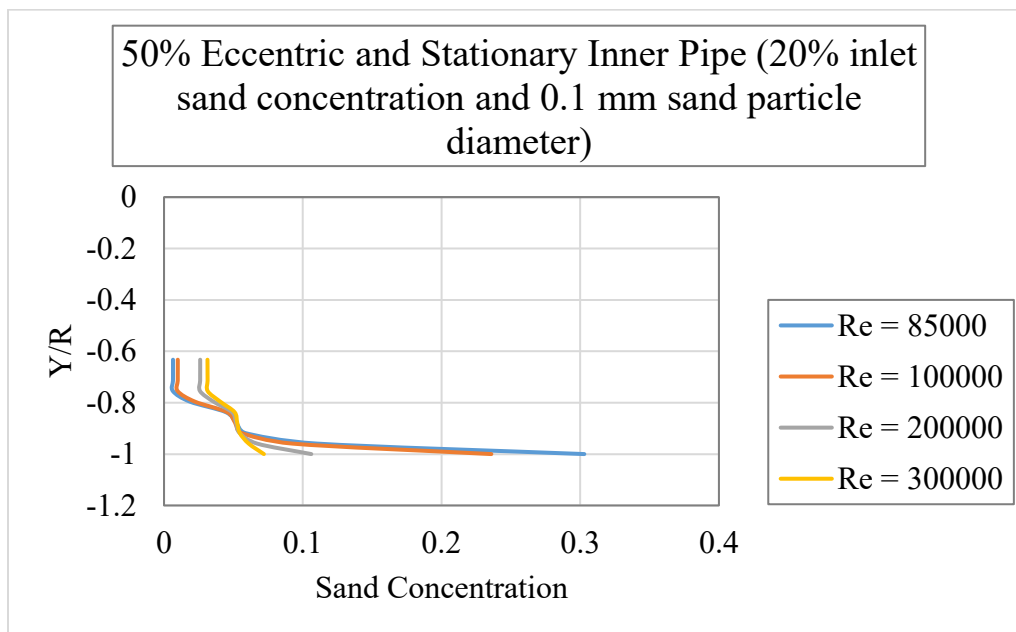


Figure 10. Effect of fluid flow on particle concentration profile (50% eccentric annuli with stationary inner pipe)

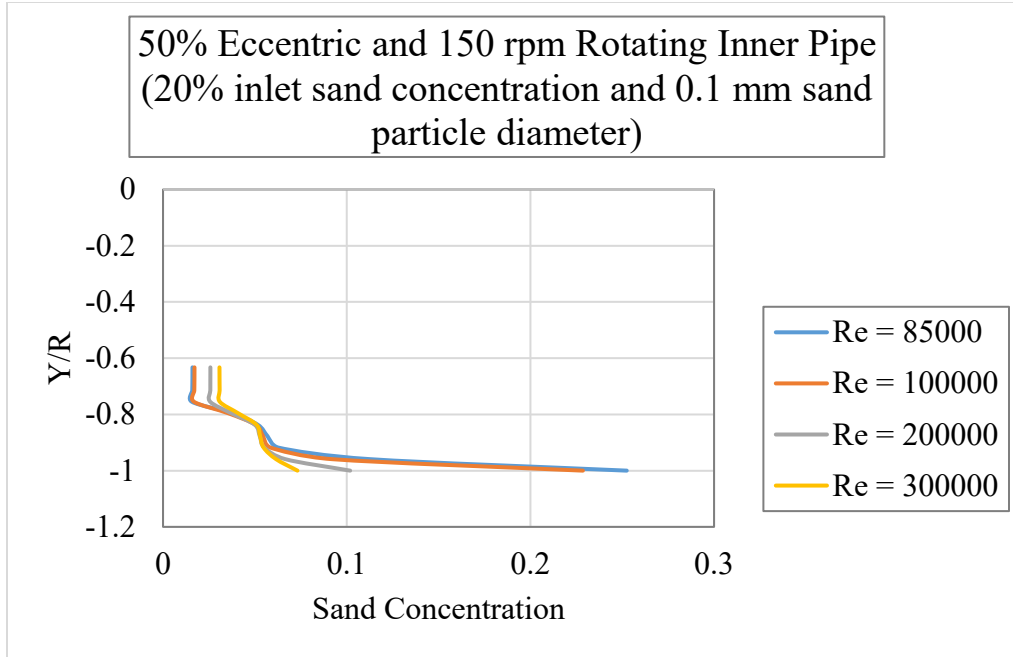
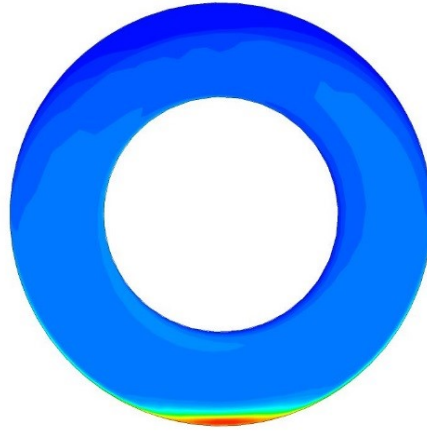
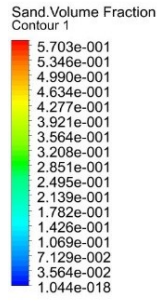


Figure 11. Effect of fluid flow on particle concentration profile (50% eccentric annuli with 150 rpm inner pipe)

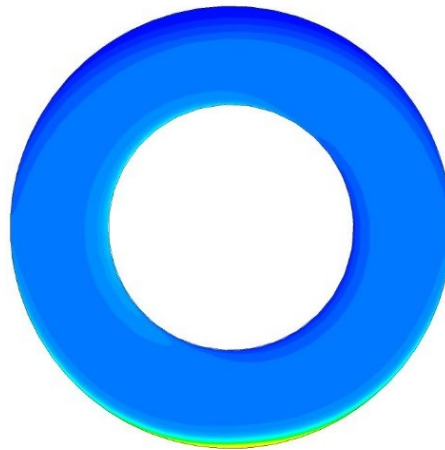
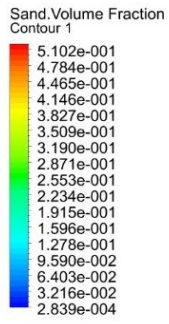
The analysis is done near bottom wall. In each case, with the increase of flow rate bed concentration near wall decrease. Due to gravitational force and horizontal orientation sand particles have the tendency to gather near bottom wall and create a flow blockage. Decreasing flow enhance the process. From the analysis it is found that below 9×10^4 Reynolds number bed concentration near bottom wall is more than 25% in all cases and when it goes down 4×10^4 the percentage is above 50%. In Figure 12, sample contour distribution of sand particles is shown at different flow rate. Operating conditions are taken from Figure 8. Contour distribution of annuli cross section at 3 m distance from inlet, displays the effect of fluid flow and gravitational force on concentration distribution clearly.



ANSYS
R16.2
Academic



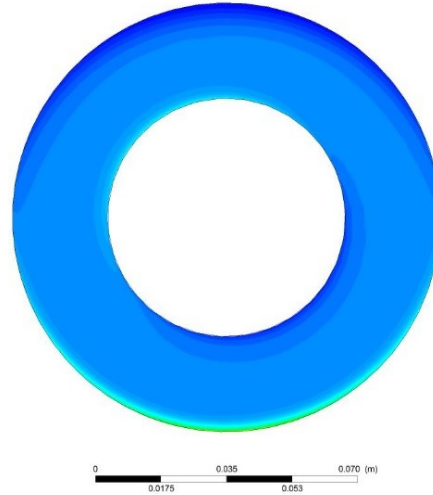
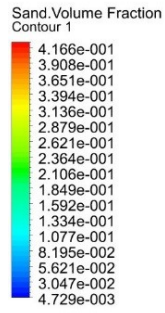
(a)



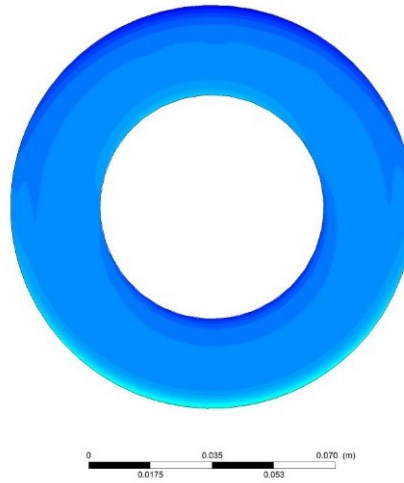
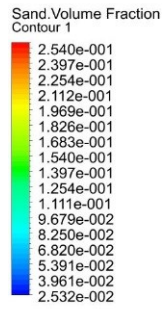
ANSYS
R16.2
Academic



(b)



(c)



(d)

Figure 12. Contour distribution of sand concentration profile: (a) $Re = 4 \cdot 10^4$, (b) $Re = 7 \cdot 10^4$, (c) $Re = 10^5$ and (d) $Re = 2 \cdot 10^5$

Effect of Drill Pipe Rotation and Eccentricity

Inner pipe of annuli can affect pressure loss by changing its eccentricity and rotation. The effect of inner pipe rotation and eccentricity are presented in Figure 13 and 14. Single phase water is used as fluid in this analysis. From Figure 13, it can be visualized that pressure loss increases with the increase of rotational speed and this trend is same at different flow rates. Stationary, 50 rpm, 100 rpm and 150 rpm rotation of inner pipe is taken into consideration. Increasing trend is higher at high flow rates. Due to rotational speed particle – particle and particle – wall collision and rebound increases which results in higher pressure loss.

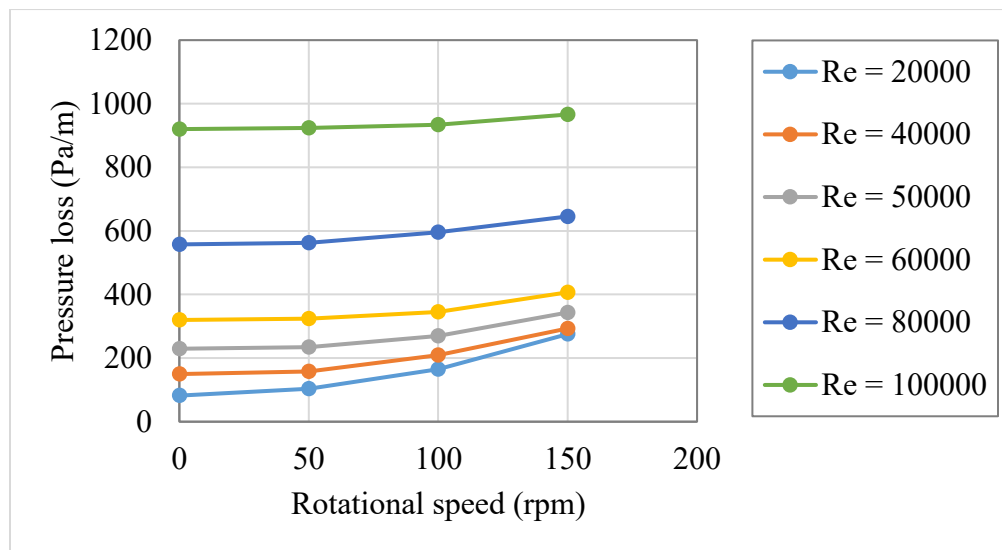


Figure 13. Effect of inner pipe rotation on pressure loss

Figure 14 shows the effect of inner pipe eccentricity on pressure loss. Concentric, 25% eccentricity, 50% eccentricity and 75% eccentricity are analyzed in this figure. At a fixed flow rate (Re = 50000), with the increase of inner pipe eccentricity pressure loss decreases. This trend is applicable during inner pipe stationary condition. With inner pipe rotation, the trend is opposite. Due to extra collision added by pipe rotation this change occurs.

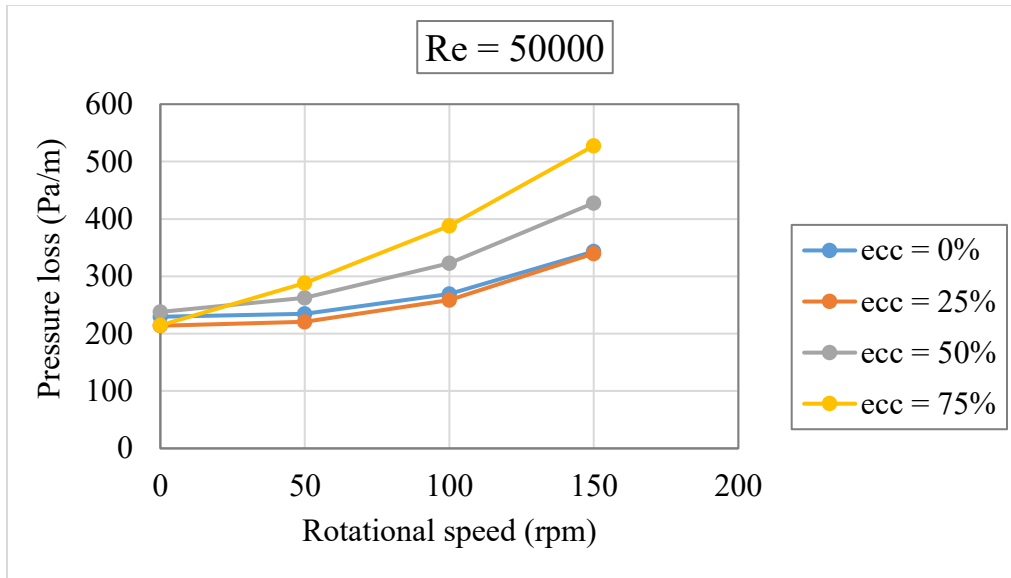


Figure 14. Effect of inner pipe eccentricity on pressure loss at different rotational speed

Effect of Particle Size

In slurry flow, sand particle size has effective role on particle blockage near bottom wall of horizontal annular pipe. Figure 15 analyzes the effect of sand particle size at concentric and stationary inner pipe with 5% inlet sand concentration. With the increase of sand particle size, particle deposition near bottom wall increases. With the increase of size, individual particle weight increases which eventually results this blockage. From previous analysis we have found maximum bed concentration decreases with the increase of flow rate (Figures 7 – 11) but for particle size 0.005 mm, maximum bed concentration near bottom wall is almost constant at different flow rates. That means, for smaller particle size (< 0.01 mm) the effect of flow rate on particle deposition has been reduced to a negligible level.

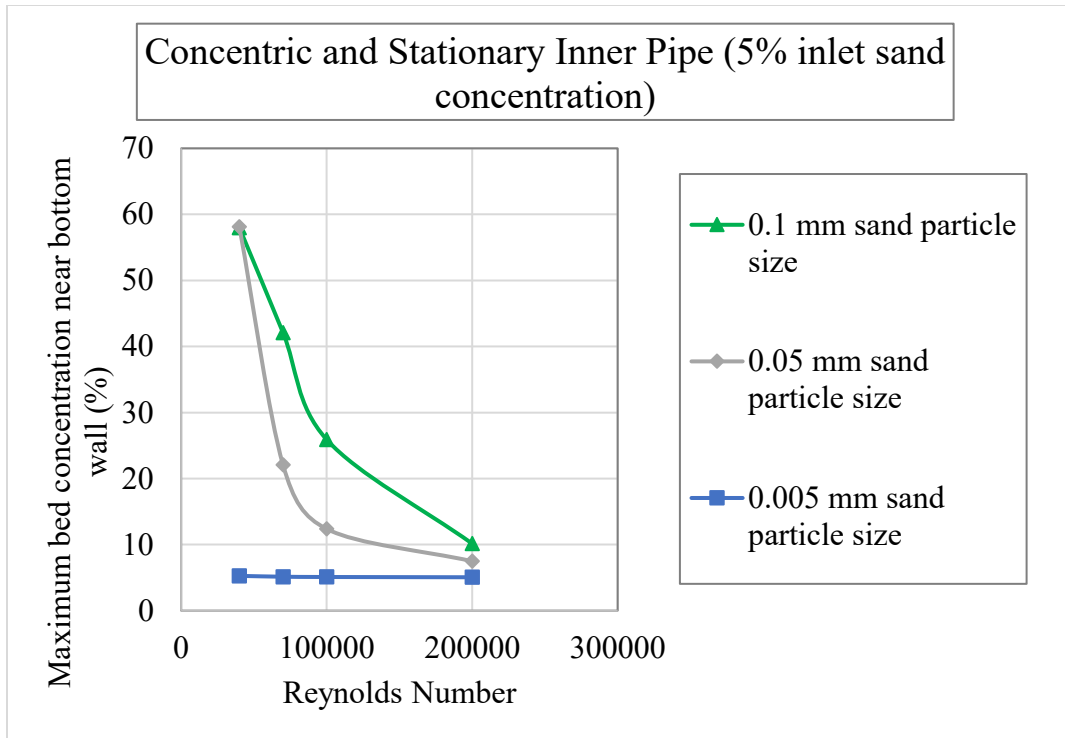


Figure 15. Effect of sand particle size on bed concentration near wall

Conclusions

In an effort to develop a widely accepted CFD model of multiphase flow through drilling annuli, current work relates the overall plan and the initial progress of the project. In summary, this study can be recounted as follows:

- i) A CFD modeling methodology to predict frictional pressure loss and settling conditions is validated. The validation is presented with examples which demonstrates its applicability in complex drilling conditions.
- ii) The effects of following important drilling parameters on pressure loss and settling conditions are tested: fluid flow rate, rotational speed and eccentricity of drill pipe and solid particle size.

- iii) Preliminary results of current research program are presented. The project is expected to produce a comprehensive CFD model capable of considering all important drilling parameters.

References

- [1]. Pilehvari, A. and R. Serth, Generalized hydraulic calculation method for axial flow of non-Newtonian fluids in eccentric annuli. *SPE drilling & completion*, 24(04), (2009). 553-563.
- [2]. Reed, T. and A. Pilehvari, 1993. "A new model for laminar, transitional, and turbulent flow of drilling muds". In *Proceedings of SPE Production Operations Symposium*, Society of Petroleum Engineers.
- [3]. Anifowoshe, O.L. and S.O. Osisanya, 2012. "The Effect of Equivalent Diameter Definitions on Frictional Pressure Loss Estimation in an Annulus with Pipe Rotation". In *Proceedings of SPE Deepwater Drilling and Completions Conference*, Society of Petroleum Engineers.
- [4]. Ahmed, R.M., M.S. Enfis, H.M. El Kheir, M. Laget, and A. Saasen, 2010. "The Effect of Drillstring Rotation on Equivalent Circulation Density: Modeling and Analysis of Field Measurements". In *Proceedings of SPE Annual Technical Conference and Exhibition*, Society of Petroleum Engineers.
- [5]. Dosunmu, I.T. and S.N. Shah, Evaluation of friction factor correlations and equivalent diameter definitions for pipe and annular flow of non-Newtonian fluids. *Journal of Petroleum Science and Engineering*, 109, (2013). 80-86.
- [6]. Erge, O., E.M. Ozbayoglu, S.Z. Miska, M. Yu, N. Takach, A. Saasen, and R. May, Equivalent circulating density modeling of Yield Power Law fluids validated with CFD approach. *Journal of Petroleum Science and Engineering*, 140, (2016). 16-27.

- [7]. Hansen, S.A. and N. Sterri, 1995. "Drill Pipe Rotation Effects on Frictional Pressure Losses in Slim Annuli". In Proceedings of SPE Annual Technical Conference and Exhibition, Society of Petroleum Engineers.
- [8]. Sorgun, M., Computational Fluid Dynamics Modeling of Pipe Eccentricity Effect on Flow Characteristics of Newtonian and Non-Newtonian Fluids. *Energy Sources, Part A: Recovery, Utilization, and Environmental Effects*, 33(12), (2011). 1196-1208.
- [9]. Sorgun, M. and M. Ozbayoglu, Predicting Frictional Pressure Loss During Horizontal Drilling for Non-Newtonian Fluids (vol 33, pg 631, 2011). *Energy Sources Part A-recovery Utilization and Environmental Effects*, 33(11), (2011). 1104-1106.
- [10]. Subramanian, R. and J. Azar, 2000. "Experimental study on friction pressure drop for nonnewtonian drilling fluids in pipe and annular flow". In Proceedings of International Oil and Gas Conference and Exhibition in China, Society of Petroleum Engineers.
- [11]. Camçi, G. and T.A. Özbelge, Determination of dilute slurry densities in a vertical annulus using isokinetic sampling. *Chem. Eng. Comm.*, 193(11), (2006). 1482-1501.
- [12]. Dewangan, S.K. and S.L. Sinha, Exploring the hole cleaning parameters of horizontal wellbore using two-phase Eulerian CFD approach. *The Journal of Computational Multiphase Flows*, 8(1), (2016). 15-39.
- [13]. Özbelge, T.A. and A.N. Eraslan, A computational hydrodynamic and heat transfer study in turbulent up-flows of dilute slurries through a concentric annulus. *Turkish Journal of Engineering and Environmental Sciences*, 30(1), (2006). 1-13.
- [14]. Özbelge, T.A. and G.C. Ünal, A new correlation for two-phase pressure drops in fully developed dilute slurry up-flows through an annulus. *Chemical Engineering Communications*, 196(4), (2008). 491-498.

- [15]. Ofei, T.N., Effect of Yield Power Law Fluid Rheological Properties on Cuttings Transport in Eccentric Horizontal Narrow Annulus. *Journal of Fluids*, 2016, (2016).
- [16]. Sorgun, M. and E. Ulker, Modeling and Experimental Study of Solid-Liquid Two-Phase Pressure Drop in Horizontal Wellbores with Pipe Rotation. *Journal of Energy Resources Technology-Transactions of the Asme*, 138(2), (2016).
- [17]. Sun, X., K. Wang, T. Yan, S. Shao, and J. Jiao, Effect of drillpipe rotation on cuttings transport using computational fluid dynamics (CFD) in complex structure wells. *Journal of Petroleum Exploration and Production Technology*, 4(3), (2014). 255-261.
- [18]. Alder, B. and T. Wainwright, Studies in molecular dynamics. II. Behavior of a small number of elastic spheres. *The Journal of Chemical Physics*, 33(5), (1960). 1439-1451.
- [19]. Chapman, S. and T.G. Cowling, *The mathematical theory of non-uniform gases: an account of the kinetic theory of viscosity, thermal conduction and diffusion in gases*: Cambridge university press, 1970.
- [20]. Syamlal, M., W. Rogers, and T.J. O'Brien, *MFIX documentation: Theory guide*. National Energy Technology Laboratory, Department of Energy, Technical Note DOE/METC-95/1013 and NTIS/DE95000031, (1993).
- [21]. Anderson, T.B. and R. Jackson, Fluid mechanical description of fluidized beds. *Equations of motion. Industrial & Engineering Chemistry Fundamentals*, 6(4), (1967). 527-539.
- [22]. Bowen, R.M., *Theory of mixtures. Continuum physics*, 3(Part I), (1976).
- [23]. Patankar, S., *Numerical heat transfer and fluid flow*: CRC press, 1980.
- [24]. Vasquez, S. and V. Ivanov, 2000. "A phase coupled method for solving multiphase problems on unstructured meshes". In *Proceedings of ASME 2000 Fluids Engineering Division Summer Meeting (ASME FEDSM'00)*, paper FEDSM2000-11281, pp. 1-6.

- [25]. Weiss, J.M., J.P. Maruszewski, and W.A. Smith, Implicit solution of preconditioned Navier-Stokes equations using algebraic multigrid. *AIAA journal*, 37(1), (1999). 29-36.
- [26]. Barth, T. and D. Jespersen, The design and application of upwind schemes on unstructured meshes, 27th Aerospace Sciences Meeting American Institute of Aeronautics and Astronautics 1989.
- [27]. Gibson, M. and B. Launder, Ground effects on pressure fluctuations in the atmospheric boundary layer. *Journal of fluid mechanics*, 86(03), (1978). 491-511.
- [28]. Launder, B., G.J. Reece, and W. Rodi, Progress in the development of a Reynolds-stress turbulence closure. *Journal of fluid mechanics*, 68(03), (1975). 537-566.
- [29]. Launder, B.E., Second-moment closure and its use in modelling turbulent industrial flows. *International Journal for Numerical Methods in Fluids*, 9(8), (1989). 963-985.
- [30]. Chorin, A.J., Numerical solution of the Navier-Stokes equations. *Mathematics of computation*, 22(104), (1968). 745-762.
- [31]. Brown, N.P. and N.I. Heywood, *Slurry Handling: Design of solid-liquid systems*: Springer Science & Business Media, 1991.
- [32]. Wasp, E.J., J.P. Kenny, and R.L. Gandhi, *Solid-liquid flow: slurry pipeline transportation*. [Pumps, valves, mechanical equipment, economics]. Ser. Bulk Mater. Handl.;(United States), 1(4), (1977).
- [33]. Kelessidis, V.C., P. Dalamarinis, and R. Maglione, Experimental study and predictions of pressure losses of fluids modeled as Herschel–Bulkley in concentric and eccentric annuli in laminar, transitional and turbulent flows. *Journal of Petroleum Science and Engineering*, 77(3), (2011). 305-312.

- [34]. Haaland, S.E., Simple and explicit formulas for the friction factor in turbulent pipe flow. *Journal of Fluids Engineering*, 105(1), (1983). 89-90.
- [35]. Özbelge, T. and A. Beyaz, Dilute solid–liquid upward flows through a vertical annulus in a closed loop system. *International Journal of Multiphase Flow*, 27(4), (2001). 737-752.
- [36]. Dyakowski, T., L.F.C. Jeanmeure, and A.J. Jaworski, Applications of electrical tomography for gas–solids and liquid–solids flows — a review. *Powder Technology*, 112(3), (2000). 174-192.
- [37]. Lucas, G., J. Cory, R. Waterfall, W. Loh, and F. Dickin, Measurement of the solids volume fraction and velocity distributions in solids–liquid flows using dual-plane electrical resistance tomography. *Flow Measurement and Instrumentation*, 10(4), (1999). 249-258.
- [38]. Na, W., J.B. Jia, X. Yu, Y. Faraj, Q. Wang, Y.F. Meng, M. Wang, and W.T. Sun, Imaging of gas-liquid annular flows for underbalanced drilling using electrical resistance tomography. *Flow Measurement and Instrumentation*, 46, (2015). 319-326.
- [39]. Tan, C., S.-J. Ren, and F. Dong, Reconstructing the phase distribution within an annular channel by electrical resistance tomography. *Heat Transfer Engineering*, 36(12), (2015). 1053-1064.
- [40]. Kaushal, D. R., Kimihiko Sato, Takeshi Toyota, Katsuya Funatsu, and Yuji Tomita. "Effect of particle size distribution on pressure drop and concentration profile in pipeline flow of highly concentrated slurry." *International Journal of Multiphase Flow* 31, no. 7 (2005): 809-823.
- [41]. Camçı, Gülden. "Application of isokinetic sampling technique for local solid densities in upward liquid-solid flows through an annulus." PhD diss., METU, 2003.

[42]. Skudarnov, P. V., C. X. Lin, and M. A. Ebadian. "Double-species slurry flow in a horizontal pipeline." *Journal of fluids engineering* 126, no. 1 (2004): 125-132.

Chapter 3. CFD Simulation of Three Phase Gas-Liquid-Solid Flow in

Horizontal Pipes

Rasel A Sultan

Memorial University of Newfoundland
Faculty of Engineering and Applied Science
St. John's, NL, Canada
ras380@mun.ca

M. A. Rahman

Memorial University of Newfoundland
Faculty of Engineering and Applied Science
St. John's, NL, Canada
marahman@mun.ca

Sohrab Zendeboudi

Memorial University of Newfoundland
Faculty of Engineering and Applied Science
St. John's, NL, Canada
szendeboudi@mun.ca

Vassilios C. Kelessidis

Petroleum Institute
Department of Petroleum Engineering
Abu Dhabi, UAE
vkelessidis@pi.ac.ae

Abstract

The objective of this work is to analyze fluid flow in horizontal pipes with three phase gas-liquid-solid Newtonian fluid by our developed CFD simulation model and validate the simulation with experimental works. Air as gas, water as liquid and silica sand as solid particle is used for this work. ANSYS fluent version 16.2 is used to do the simulation. Eulerian model with Reynolds Stress Model (RSM) turbulence closure is adopted to analyze multiphase fluid flow. Length of pipe is 2.9 m and diameter is 0.0416 m, which are selected from experimental works to validate the simulation and after a good agreement with experimental data, sensitivity analysis is conducted to observe the three phase fluid flow characteristics through horizontal flow. Pressure gradient (pressure drop per unit length) is used as primary parameter to analyze. Effect of in situ concentration of solid in slurry, diameter of pipeline, roughness of wall material and viscosity of water in slurry are analyzed throughout this paper. This article provides validity of our proposed model. After that we tried to perform some parametric studies, changing variables of three phase

fluid flow through horizontal pipeline with ours validated model. The main approach here is to demonstrate our CFD model in different ways to researchers and industries related to multiphase pipeline flow fields and make it acceptable to them. Also, Fluid Structure Interaction (FSI) is introduced at the end of this study to explain the goal of this project.

Introduction

Gas-liquid-solid three phase flow in pipeline or annuli has great interest in oil and gas industries to recover produced formation fluid [1], mining [2, 3], biomass transportation [4], horizontal petroleum production and transport [5], nuclear waste deposition [6]. The addition of solid particles to two phase air-water flow can reduce drag in pipe flow which can lead to decreasing pressure drop and pumping power [7], and also decreasing the size of pump [8]. The three phase slurry transportation with air and water helps to reduce air pollution, noise, accidents and energy demand. Also adding air or air injection in two phase slurry system reduce pumping cost and enhance bitumen recovery from oil field [9].

There are extensive experimental studies in this field [5-6, 8, 10-29], focusing on pressure gradient, deposition velocity (i.e. minimum superficial velocity of mixture to restrain gathering of solids or wastes in the pipeline), and the in-situ concentration of different phases. But these works are representing with narrow range of operating conditions and incomplete due to having minimum number of measurements. [27]. For example, Gillies et al. only focused on pressure gradients and in situ concentration of fluids [19]; Fukuda and Shoji elaborated pressure gradient only [14].

The CFD simulation of solid-liquid-gas three phase flow are limited to a few [29-33]. Also those studies are limited to small ranges of analysis. For example, Li et al. studied CFD simulation of solid-liquid-gas three phase flow to analyze hydraulic transport process through pipeline but with limited ranges [29].

CFD approach with three phase pipeline flow can be used to find more effective outputs and so it is considered appropriate to use for this study. Eulerian multiphase model for phase mixture behavior along with Reynolds Stress Model (RSM) for turbulence behavior are deliberated in our proposed model. These combination shows optimum and more accurate results. There is few acceptable commercial software available to perform multiphase fluid flow. ANSYS fluid is used to perform the analysis.

In this study, we compare the CFD simulation with experimental studies at different conditions and ranges with horizontal pipe. After verifying our simulation model, parametric study is conducted with a good range of variable. These parametric studies are also verified with available correlations to demonstrate high reliance on this proposed model at different applications and different conditions in present and future works related to pipe flow with multiphase fluids.

Mathematical Model

The Euler-Euler approach is considered for each phase, in contrast to the Eulerian-Lagrangian model that calculate solid phase with individual discrete calculations. The Eulerian model from Euler-Euler approach is used here as multiphase model. In our work, we have solid-liquid-gas fluids where granular (solid-liquid) flow is expected to be in a high range. Due to this high range of solid phase the Eulerian model is selected as optimum and effective in our case.

The volume of phase q , is defined by

$$V_q = \int a_q dV \quad (1)$$

where,

$$\sum_{q=1}^n a_q = 1 \quad (2)$$

Continuity equation for mixture is as below -

$$\frac{\partial}{\partial t} (a_q \rho_q) + \nabla \cdot (a_q \rho_q \vec{v}_q) = 0 \quad (3)$$

where, ρ_q is the phase reference density, or the volume averaged density of the q^{th} phase in the solution domain. \vec{v}_q indicates velocity vector.

The momentum equation for a fluid phase q is -

$$\begin{aligned} \frac{\partial}{\partial t} (a_q \rho_q \vec{v}_q) + \nabla \cdot (a_q \rho_q \vec{v}_q \vec{v}_q) = & -a_q \nabla p + \nabla \cdot \bar{\tau}_q + a_q \rho_q \vec{g} + \sum_{p=1}^n \{K_{pq} (\vec{v}_p - \vec{v}_q) + \\ & \dot{m}_{pq} \vec{v}_{pq} - \dot{m}_{qp} \vec{v}_{qp}\} + (\vec{F}_q + \vec{F}_{lift,q} + \vec{F}_{vm,q}) \end{aligned} \quad (4)$$

Here, \vec{g} is the acceleration due to gravity, $\bar{\tau}_q$ is the q^{th} phase stress-strain tensor, \vec{F}_q is an external body force, $\vec{F}_{lift,q}$ is a lift force and $\vec{F}_{vm,q}$ is a virtual mass force.

Following the work of Alder and Wainwrig (1960) [34], Chapman and Cowling (1970) [35] and Syamlal et al. (1993) [36], a multi-fluid granular model is used to describe the flow behavior of a fluid-solid mixture.

The conservation of momentum for the solid phase is -

$$\begin{aligned} \frac{\partial}{\partial t} (a_s \rho_s \vec{v}_s) + \nabla \cdot (a_s \rho_s \vec{v}_s \vec{v}_s) = & -a_s \nabla p - \nabla p_s + \nabla \cdot \bar{\tau}_s + a_s \rho_s \vec{g} + \sum_{l=1}^N \{K_{ls} (\vec{v}_l - \vec{v}_s) + \\ & \dot{m}_{ls} \vec{v}_{ls} - \dot{m}_{sl} \vec{v}_{sl}\} + (\vec{F}_s + \vec{F}_{lift,s} + \vec{F}_{vm,s}) \end{aligned} \quad (5)$$

where, p_s is the s^{th} solids pressure, $K_{ls} = K_{sl}$ is the momentum exchange coefficient between fluid or solid phase l and solid phase s , N is the total number of phases.

The solids pressure term consists of a kinetic term and a second particle collisions term -

$$p_s = a_s \rho_s \theta_s + 2\rho_s(1 + e_{ss})a_s^2 g_{0,ss} \theta_s \quad (6)$$

where, e_{ss} is the coefficient of restitution for particle collisions, $g_{0,ss}$ is the radial distribution function, and θ_s is the granular temperature. The solids stress viscosity term contains or shear viscosity due to collision ($\mu_{s,col}$), kinetic viscosity ($\mu_{s,kin}$) and frictional viscosity ($\mu_{s,fr}$). So, it can be written as -

$$\mu_s = \mu_{s,col} + \mu_{s,kin} + \mu_{s,fr} \quad (7)$$

where, $\mu_{s,col}$ is shear viscosity due to collision, $\mu_{s,kin}$ is kinetic viscosity and $\mu_{s,fr}$ frictional viscosity.

Previous studies and literatures indicate few comparisons between all the turbulence models like Reynolds-averaged Navier–Stokes (RANS) models: k– ϵ , k– ω and Reynolds stress model, and Large Eddy Simulation (LES) for steady fluid flow through pipeline or annuli [37]. In Vijiapurapu and Cui [37] results obtained with different turbulence models were compared with experimental results from Zagarola and Smits [38] and Nourmohammadi et al. [39]. The k– ϵ and k– ω models can provide acceptable accurate result with low computational cost and least effort. On the other hand, LES model solves large scales of turbulence with smallest scales and so it is more universal and acceptable model, but it takes higher computational cost with higher computational time [37]. Among all these turbulence model Reynolds Stress Model (RSM) is optimum to use for turbulence flow through simple pipe or annuli. RSM needs less computational time or computational cost than LES model and gives more accurate result than k– ϵ and k– ω models [37]. For example, RSM can calculate directional effects of the Reynolds stress field that can not be done by other Reynolds-averaged Navier–Stokes (RANS) models.

An analysis with different turbulence model is conducted using data from Kaushal et al. (2005) [40] to find out optimum model for further investigations. In Fig. 1, single phase water velocity 1 m/s is maintained through horizontal pipeline. The analysis shows RSM as the most optimum model with least error.

Considering above comparisons RSM is considered here as turbulence model for multiphase fluid flow. RSM solves the Reynolds-averaged Navier-Stokes equation by solving transport equations for the Reynolds stresses, together with an equation for the dissipation rate.

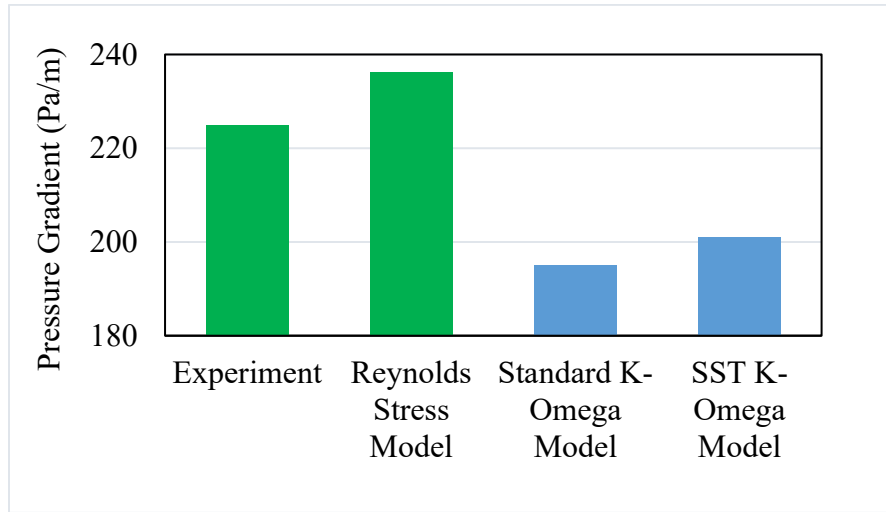


Figure 1. Optimum turbulence model analysis

Modelling approach of RSM is originated in 1975 by Launder et al. [41]. The exact transport equation of Reynolds Stress (R_{ij} or $\overline{u'_i u'_j}$) is as below -

$$\frac{DR_{ij}}{Dt} = P_{ij} + D_{ij} - \varepsilon_{ij} + \phi_{ij} + \theta_{ij} \quad (8)$$

Here,

$\frac{DR_{ij}}{Dt}$ is the summation of changing rate of R_{ij} and transport of R_{ij} by convection.

P_{ij} is production rate of R_{ij} .

D_{ij} is diffusion transport of R_{ij} .

ε_{ij} is rate of dissipation.

Φ_{ij} is pressure strain correlation term.

θ_{ij} is rotation term.

D_{ij} can be modeled assuming rate of transport of Reynolds stresses by diffusion is proportional to gradients of Reynolds stresses. Diffusion term used in simulation is as below -

$$D_{T,ij} = \frac{\partial}{\partial x_k} \left(\frac{\mu_t}{\sigma_k} \frac{\partial R_{ij}}{\partial x_k} \right) \quad (9)$$

where, $\sigma_k = 0.82$ [42], $\mu_t = C_\mu \frac{k^2}{\varepsilon}$ and $C_\mu = 0.09$.

Production rate P_{ij} of R_{ij} or $\overline{u'_i u'_j}$ can be expressed as -

$$P_{ij} = - \left(\overline{u'_i u'_m} \frac{\partial U_j}{\partial x_m} + \overline{u'_j u'_m} \frac{\partial U_i}{\partial x_m} \right) \quad (10)$$

The pressure-strain term, Φ_{ij} on Reynold stresses consists of three major components [43, 44] and those are $\Phi_{ij,1}$ or slow pressure-strain term also known as the return-to-isotropy term, $\Phi_{ij,2}$ or rapid pressure-strain term and $\Phi_{ij,w}$ as wall-reflection term. So, it can be presented as –

$$\Phi_{ij} = \Phi_{ij,1} + \Phi_{ij,2} + \Phi_{ij,w} \quad (11)$$

where,

$$\Phi_{ij,1} = -C_1 \frac{\varepsilon}{k} \left[\overline{u'_i u'_j} - \frac{2}{3} \delta_{ij} k \right] \quad (12)$$

$$\Phi_{ij,2} = -C_2 \left[P_{ij} - \frac{2}{3} \delta_{ij} P \right] \quad (13)$$

With, $C_1 = 1.8$ and $C_2 = 0.6$

The wall-reflection term, $\Phi_{ij,w}$ is responsible for the normal stresses distribution near the wall.

This term is modeled as -

$$\begin{aligned} \Phi_{ij,w} \equiv & C_1' \frac{\epsilon}{k} (\overline{u'_k u'_m} n_k n_m \delta_{ij} - \frac{3}{2} \overline{u'_i u'_k} n_j n_k - \frac{3}{2} \overline{u'_j u'_k} n_i n_k) \frac{C_l k^{\frac{3}{2}}}{\epsilon d} + C_2' (\Phi_{km,2} n_k n_m \delta_{ij} \\ & - \frac{3}{2} \Phi_{ik,2} n_j n_k - \frac{3}{2} \Phi_{jk,2} n_i n_k) \frac{C_l k^{\frac{3}{2}}}{\epsilon d} \end{aligned} \quad (14)$$

where, $C_1' = 0.5$, $C_2' = 0.3$, n_k is the horizontal component of the component normal to the wall,

d is the shortest distance to the wall, and $C_l = \frac{C_\mu^{\frac{3}{4}}}{k}$, where $C_\mu = 0.09$ and k is the von Kármán constant (=0.4187).

The dissipation rate ϵ_{ij} or destruction rate of R_{ij} , is modeled as -

$$\epsilon_{ij} = \frac{2}{3} \delta_{ij} \epsilon \quad (15)$$

where,

$$\epsilon = 2\nu \overline{s'_{ij} \cdot s'_{ij}} \quad (16)$$

and s'_{ij} = fluctuating deformation rate

Rotation term is expressed as –

$$\theta_{ij} = -2\omega_k (R_{jm} e_{ikm} + R_{im} e_{jkm}) \quad (17)$$

Here,

ω_k = rotation vector.

e_{ikm} = alternating symbol, +1, -1 or 0 depending on i, j and k.

Simulation Methodology

In the present study, circular pipe is selected in simulation. The computational grids for the horizontal pipe is generated using ANSYS Fluent. Meshing is finalized by proper mesh independency check. Inflation near the wall is added for a more precise characteristic of different parameters in near wall area. Shear stress between the wall surface and gas molecules are much higher; this inflation helps to create a denser mesh near the wall. Although the use of unsymmetrical meshes is computationally more challenging, but it will produce more realistic results compared to symmetrical meshes. Mesh distribution statistics for sensitivity analysis is listed below in Table 1. The length of the pipe is maintained long enough in this study to achieve a fully developed flow at the outlet; the minimum flow development section or entrance length is around $50D$ (D = inner diameter of the pipe) [45, 46]. Computational grid distribution of the pipe geometry (used in the three-phase model) is shown in Fig. 2.

Table 1. Mesh Distribution Statistics

| Nodes | Elements | Wall Inflation Layers |
|--------|----------|-----------------------|
| 131374 | 293488 | 12 |

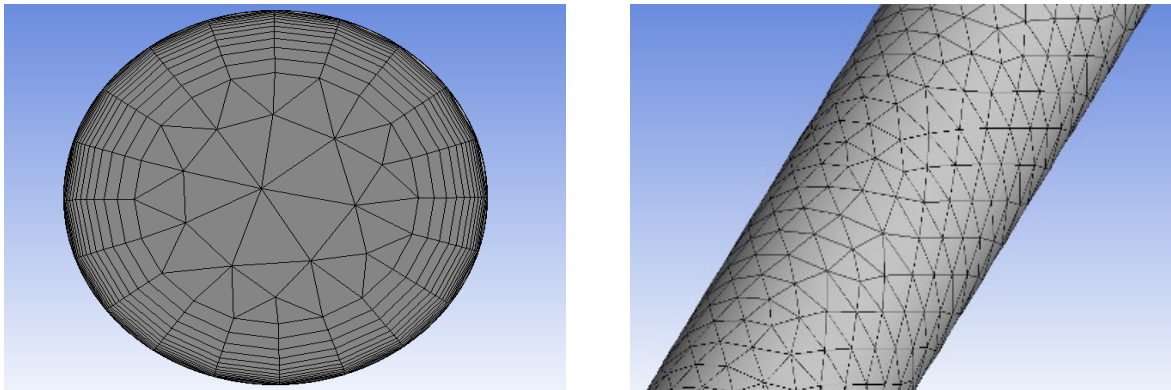


Figure 2. Mesh distribution in the pipe geometry

Fluent, ver. 16.2, ANSYS Inc. is used to build a CFD simulation model of the pipeline flow of air-water-sand slurry. In solution, a convergence value of 10^{-5} is used to terminate the iterations, this threshold value is selected after optimization to ensure a satisfactory accuracy at the lowest computation time. Figure 3. shows an analysis to find out optimum convergence rate (between a range of 10^{-4} to 10^{-6}) using parameters (inlet velocity) from experiment. In average, 20 minutes' computational time was counted for each simulation of this project. SIMPLE algorithm is applied with first and second order upwind discretization method to have stability and confirm convergence in governing equations. Upwind discretization is such a method that simulate numerically the direction of the normal velocity in the flow field. No-slip boundary condition is adopted for interaction between solid or liquid phase and wall.

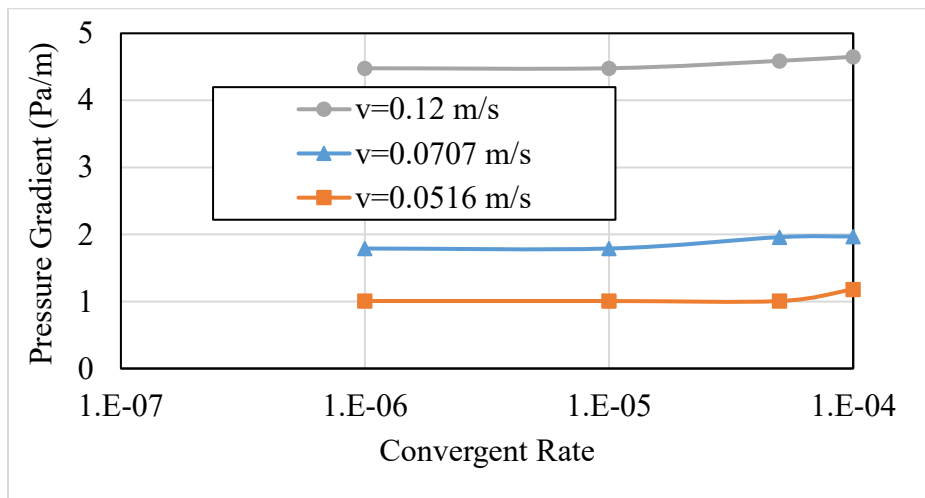


Figure 3. Optimum convergence rate analysis

Simulation Validation

The CFD simulation is first verified using single phase flow of water with experimental data from Skudarnov et al. [47], and the empirical correlation of Wood's [48]. Here, the geometry of pipe, fluid and wall material is taken similar to Skudarnov et al.; we use the pipe length of 17 m, and

internal diameter of 0.023 m, water (with density of 998.2 kg/m³ and viscosity of 0.001003 kg/m.s) as fluid and stainless steel (with density of 8030 kg/m³, and roughness of 32 μm) as the pipe properties.

Fluent meshing is finalized with 2,80,2578 elements and 1,30,165 nodes volume cells. Pressure gradient (pressure drop per unit length) at different fluid flow velocities through the pipe is compared in Fig. 4.

The prediction of Wood’s [48] empirical correlation for the turbulent flow in a pipe with a rough wall is as below:

$$f = a + b.Re^{-c} \quad (18)$$

Where $a = 0.0026\left(\frac{\epsilon}{D}\right)^{0.225} + 0.133\left(\frac{\epsilon}{D}\right)$;

$b = 22\left(\frac{\epsilon}{D}\right)^{0.44}$;

and $c = 1.62\left(\frac{\epsilon}{D}\right)^{0.134}$

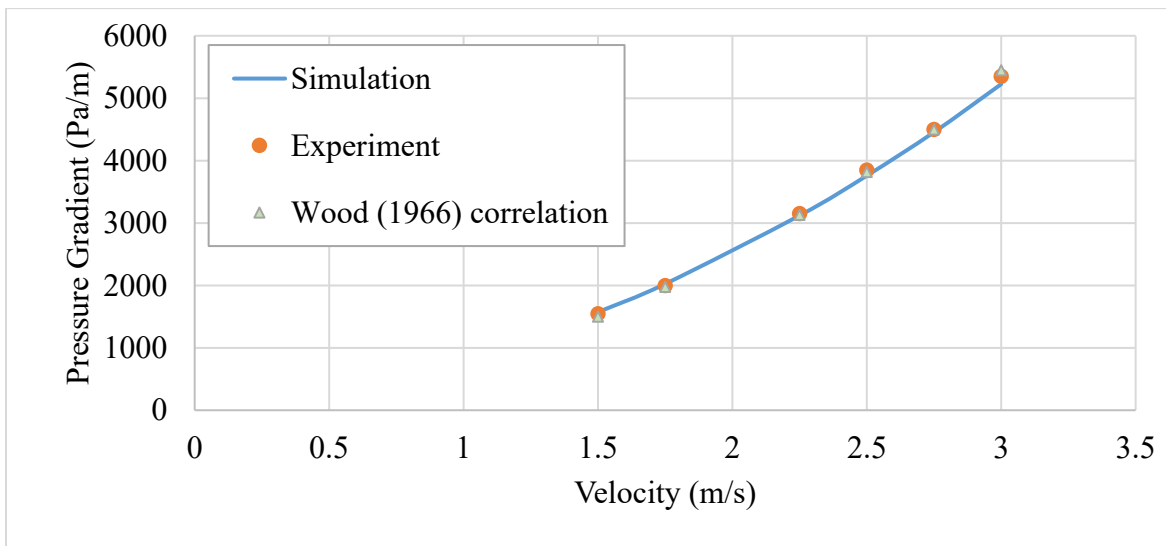


Figure 4. Comparison of simulation data with correlations (Wood, 1966) and experimental data of Skudarnov et al. (2004)

The results shown in Fig. 4 demonstrate an excellent agreement between simulation results, the experimental results and those of the Wood's correlation. Less than 5% error with 1.5% average error with respect to experimental data and 2.34% average difference from the empirical correlation was obtained.

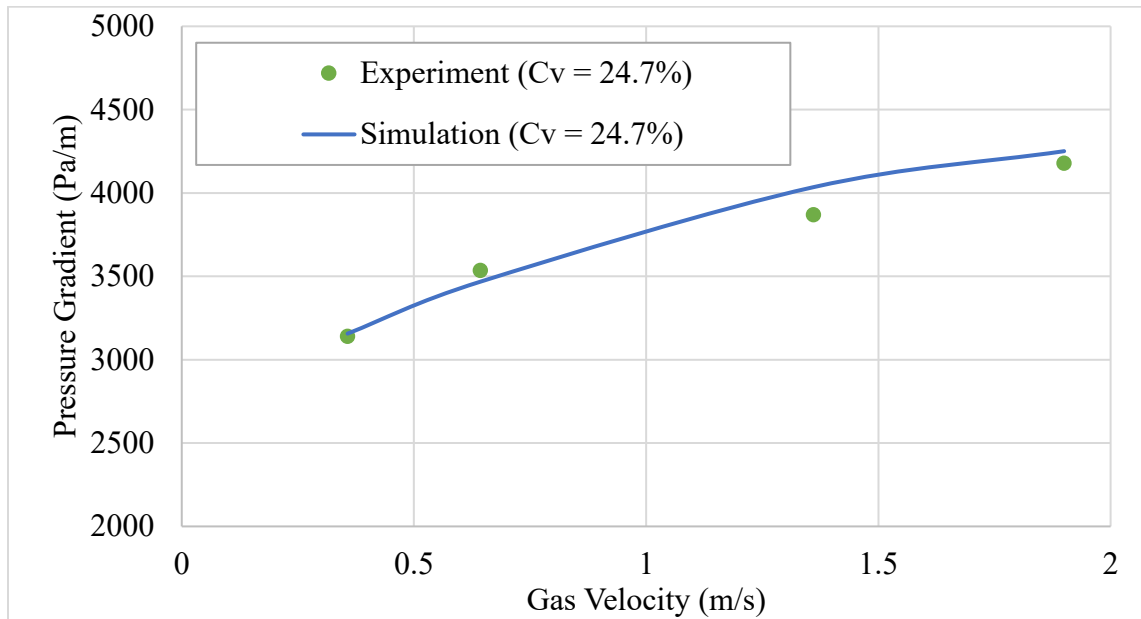


Figure 5. Comparison of pressure gradient as a function of gas velocity with 24.7% solid volume concentration in slurry (C_v) and 3 m/s slurry velocity

Pressure gradient for air-water-sand three phase flow obtained from simulation is compared to the experimental data of Fukuda and Shoji [14]. In their experiment, the length of pipe is 2.9 m, with a diameter of 0.0416 m; water is used as liquid phase (density of 998.2 kg/m³, and viscosity of 0.001 kg/m.s); silica sand particles resemble the solid (density of 2650 kg/m³, mean particle diameter of 74 μ m), and air is used for the gas phase (density 1.225 kg/m³, viscosity 1.789 $\times 10^{-5}$ kg/m.s); and the pipe wall material is smooth polycarbonate [49]. Fig. 5. shows the pressure gradients with solid volume concentration of 24.7% in the slurry and a slurry velocity of 3 m/s at different gas velocity, from simulation and experimental results.

From Fig. 5., the average error in the simulation data is 2.1%, with a maximum error of 4.26% (at gas velocity of 1.36 m/s). This shows very good agreement between experiment and simulation data. One of the parameters that should be fine-tuned in the simulation is the static settlement concentration (or, packing limit) which was chosen 0.63 in this study. The effect of size distribution of solid on this parameter is important.

Parametric Sensitivity Study

After validating the simulation results, we will study the flow behavior at different conditions. The in-situ concentration of solid (in slurry), the pipe inner diameter, pipe surface roughness, and the viscosity of water in the slurry are studied. Geometry is similar to the work by Fukuda and Shoji [14].

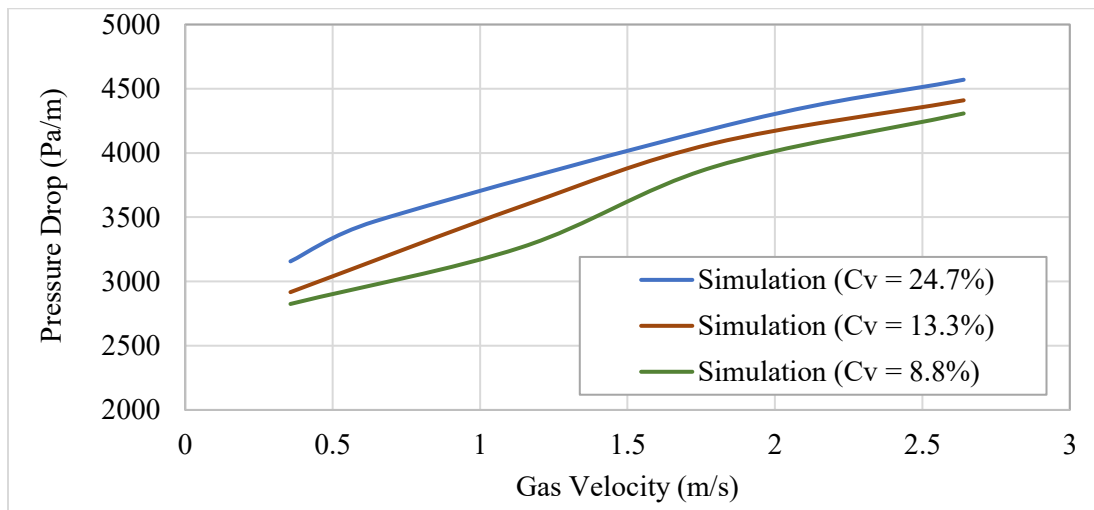


Figure 6. Pressure Gradient at different gas velocity and solid volume concentration in slurry with other variables constant

Figure 6. shows the pressure gradient of three phase flow in pipeline at different gas velocity and solid volume concentration in slurry (C_v), having other parameters fixed. The pressure gradient in the pipe increases with the of gas velocity, and with the in-situ concentration of sand in slurry.

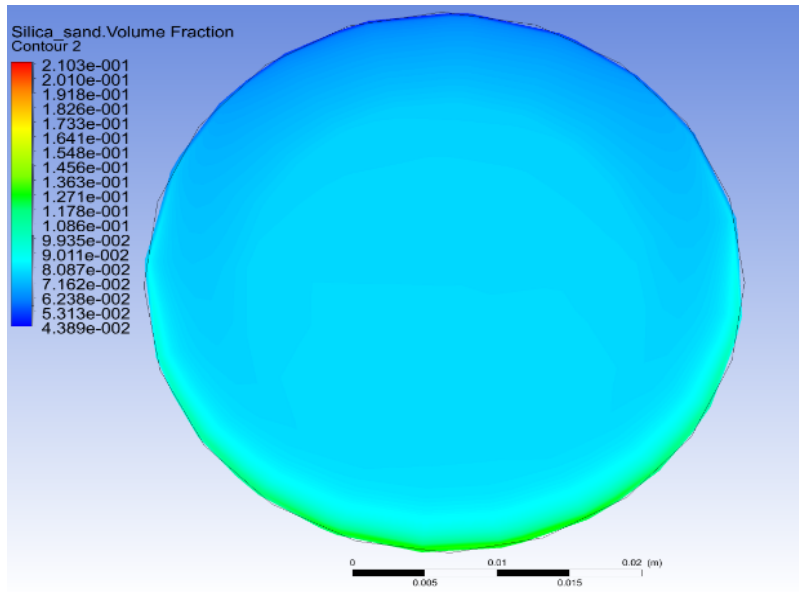
According to Darcy-Weisbach equation [50]:

$$\Delta P = \frac{fL}{D} \frac{\rho v^2}{2} \quad (19)$$

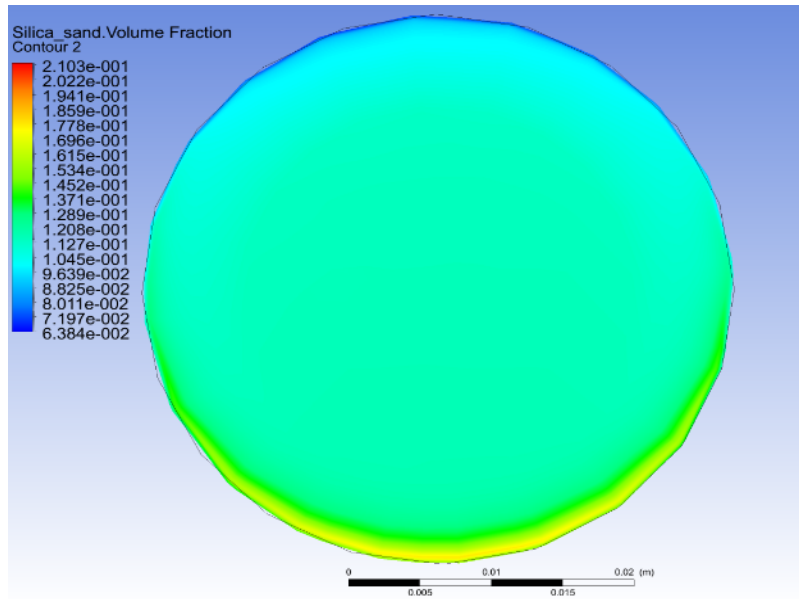
where, ΔP is pressure drop, f is friction factor, L is the pipe length, D is the inner pipe diameter, ρ is fluid density and v is the fluid velocity.

From Eq. (19), the pressure gradient is directly proportional to the square of fluid velocity if other parameters are kept constant. Considering three phase flow and slurry mixture velocity to be constant, the change in fluid velocity can be represented by that of the gas velocity. The three-phase fluid mixture density increases with sand volumetric concentration in slurry and that causes the pressure gradient to increase. The sand concentration and the gas velocity should be kept at a minimum level (minimum requirement in a specific work) to maintain a low pressure drop in pipeline.

Figure 7. shows concentration distribution of sand in vertical plane at outlet for two different in-situ volumetric concentration of sand in slurry. Air volumetric concentration is maintained constant (27.54%) with constant air inlet velocity (1.14 m/s). Here, sand concentration distribution at outlet vertical plane has noticeable difference for two different sand concentration input. Figure 8. demonstrate sand concentration distribution by changing air input velocity and air injection with same sand in-situ concentration (24.7%). This comparison shows the effect of air injection with slurry flow. Here, increasing of air injection with same sand concentration in slurry decreases sand volumetric concentration in total volume of fluid flow through pipeline. From Fig. 7 and 8 it can be seen that sand concentration is much higher in lower part of horizontal pipeline which is the effect of gravitational force that works downward in horizontal orientation. Also this analysis shows usage of appropriate air injection in slurry flow to reduce pipeline blockage by stationary slurry near bottom wall. Analysis of sand concentration distribution can also lead to find out ‘deposition velocity’.

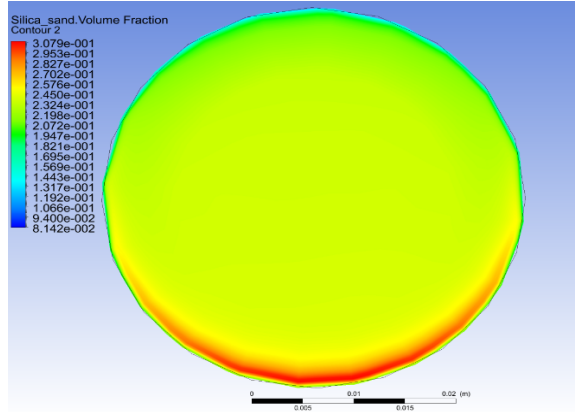


(a)

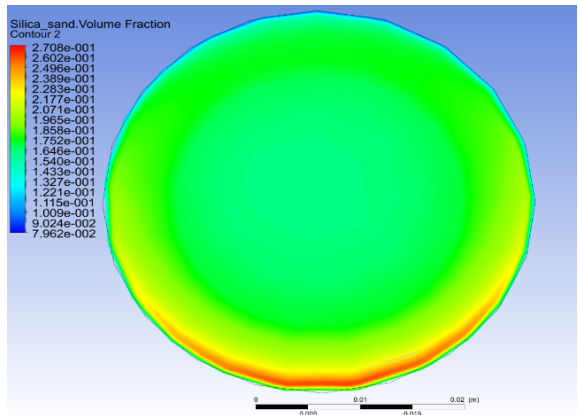


(b)

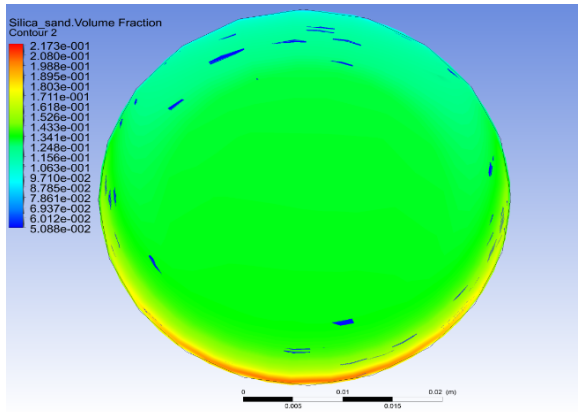
Figure 7. Sand concentration distribution in vertical plane at outlet with 1.14 m/s air inlet. (a) $C_v = 8.8\%$ and (b) $C_v = 13.3\%$



(a)



(b)



(c)

Figure 8. Sand concentration distribution in vertical plane at outlet with $C_v = 24.7\%$. (a) 0.643 m/s air inlet, (b) 1.36 m/s air inlet and (c) 1.9 m/s air inlet

Keeping the sand in-situ concentration in slurry, fluid viscosity and pipe wall roughness constant, Fig. 9. describes the change in pressure gradient with the pipe inner diameter (D) and by the gas velocity. According to Eq. (19), the pressure gradient decreases with the increase in the pipe internal diameter and decreases with the increase in gas velocity. The rate of change in the pressure gradient with gas velocity is lower for smaller pipes. This higher-pressure gradient condition controls the lower limit of pipes to be used for three phase flow.

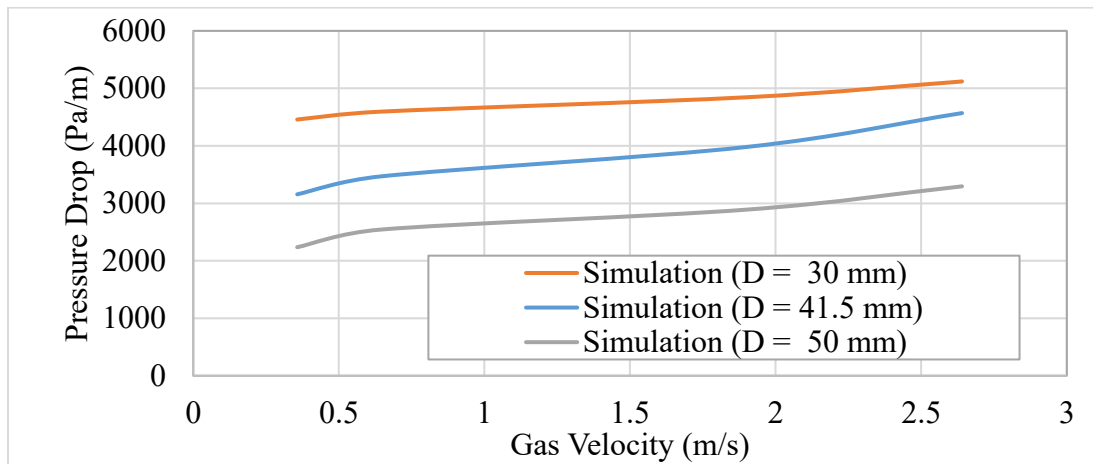


Figure 9. Pressure Gradient at different gas velocity and pipe diameter with other variables constant

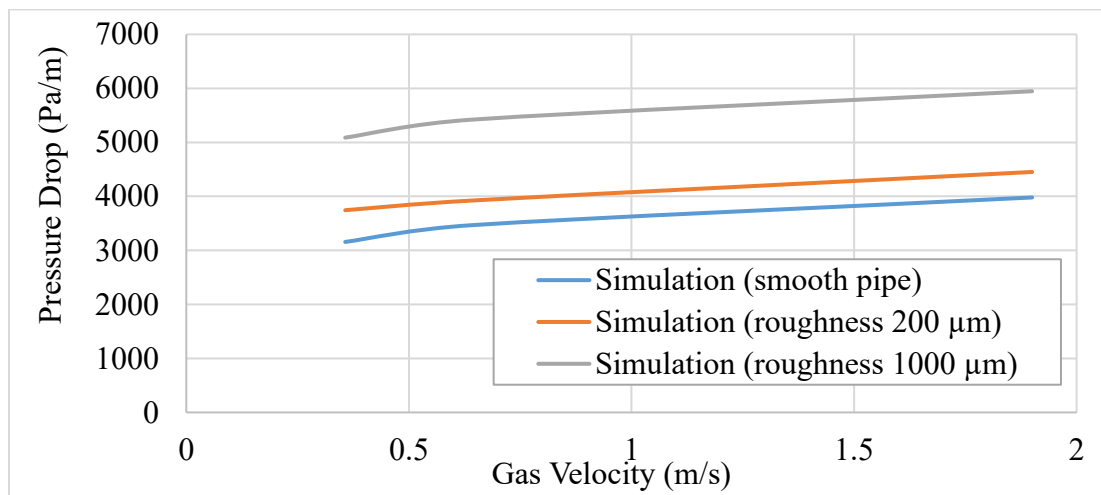


Figure 10. Pressure Gradient at different gas velocity and pipe wall roughness with other variables constant

Changing the pipe roughness effect on gas-liquid-solid three phase flow pressure drop is shown in Fig. 10. According to the correlation by Colebrook [51], the pipe wall roughness is proportional to the square root of friction factor which is proportional to the pressure drop. So, the pressure drop increases with surface roughness. The implicit correlation of Colebrook is as below:

$$\frac{1}{f} = -0.869 \ln \left(\frac{\varepsilon/D}{3.7} + \frac{2.523}{Re\sqrt{f}} \right) \quad (20)$$

where, ε wall roughness, Re Reynolds Number.

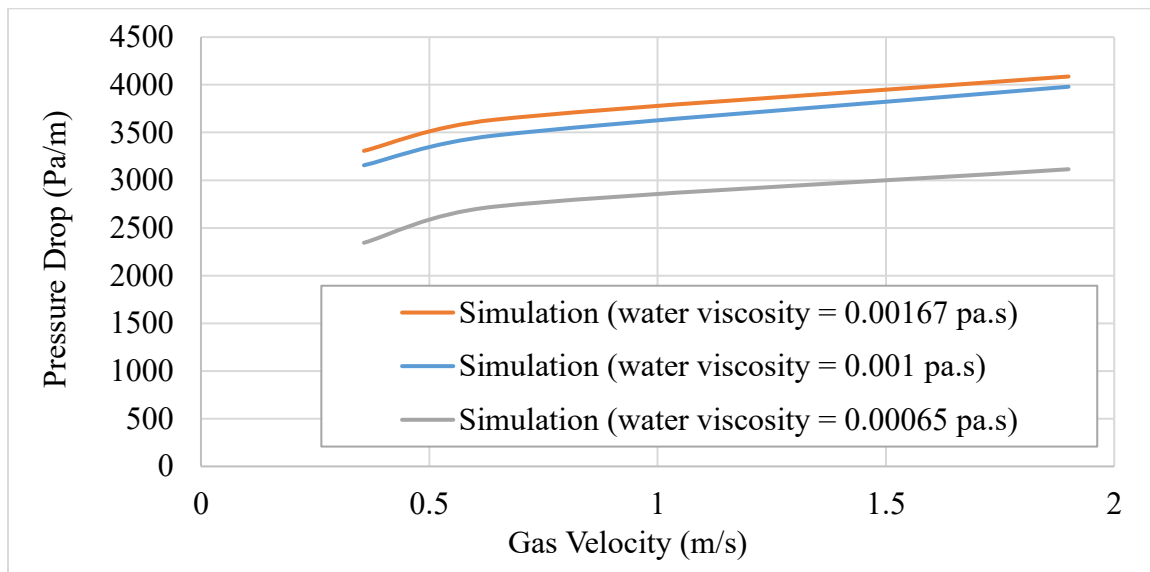


Figure 11. Pressure Gradient at different gas velocity and water viscosity with other variables constant

Also, increasing wall roughness increases friction near wall that creates more turbulence in flow and thus increases pressure drop. With time wall roughness increases due to sand particle deposition, moisture and wall material damage.

Due to temperature effects, the water viscosity can change. We show the effect of viscosity of water on the pressure gradient in gas-liquid-solid three phase flow in Fig. 11. The water viscosity at room temperature (20° C) is about 0.001 Pa.s but it decreases with temperature [52]. From Fig. 11, it is seen that pressure gradient increase with the increase of water viscosity, at the same gas

velocity. The viscosity value of 0.00065 Pa.s corresponds to water temperature of about 40° C. In Eq. (20), the friction factor is inversely proportional to the square of Reynolds number. The Reynolds number itself decreases with the increase in fluid viscosity; that means, the fluid viscosity has proportional relation with friction factor and eventually with pressure drop. Figure 11. also shows parallel pressure gradient trends with change in water viscosity.

Conclusion

The above analysis on three phase fluid flow through horizontal pipeline helps to understand a number of important points. Our selected Eulerian multiphase model with RSM turbulence closure is verified with other model combinations numerically and analytically. After finalizing this model combination, we verified our model with available experimental data. The combinations show acceptable errors with explainable reasons. Simulation process is conducted with optimum and acceptable conditions with numerical explanations. To establish this model, in next approach we perform some parametric sensitivity analysis changing major parameters that effects multiphase fluid flow. The results are compared with some available correlations and indicate its acceptancy. From sensitivity analysis some points are drawn as below -

- Sand concentration has proportional relation with pressure gradient.
- Pipeline diameter is inversely proportional to pressure gradient i.e. with the increase of pipe inner diameter pressure gradient decreases and vice versa.
- Pipe material should be inspected and reinstalled by routine to maintain a minimum wall roughness as with the increase of wall roughness pressure gradient or energy loss increases.
- Surrounding temperature of pipe should be kept in a minimum limit to maintain a minimum pressure loss and also for safety issue.

Another important conclusion can be drawn from sand concentration distribution analysis. Importance of air injection in slurry flow and finding ‘depositing velocity’ are the main outputs from this analysis.

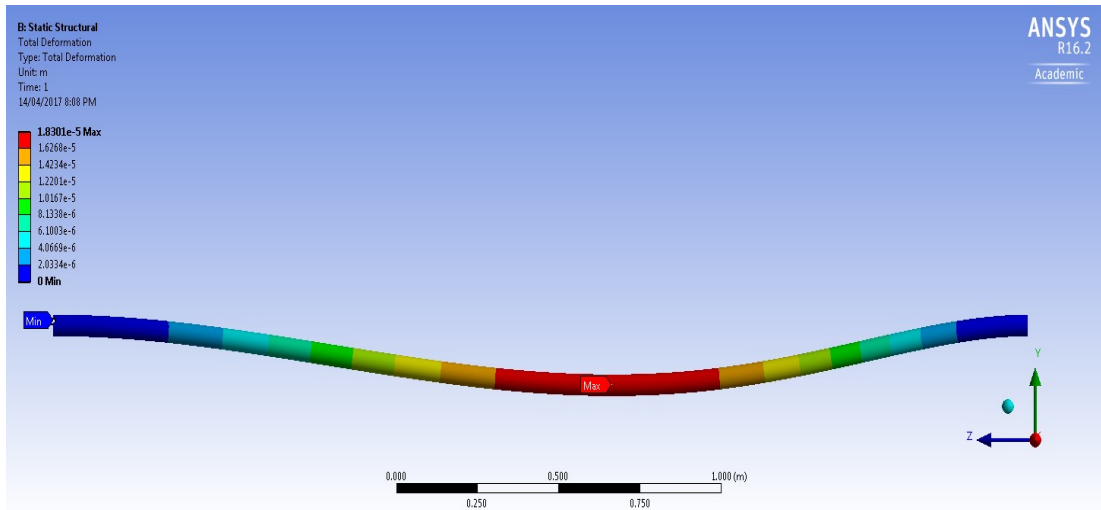


Figure 12. Contour of pipeline deformation

Considering pipe flow safety, our future work is to analyze Fluid Structure Interaction (FSI). Due to multiphase flow through pipeline in different conditions of pipe, pressure stresses is created and as a result pipe deforms. Figure 12. shows the deformation of pipe due to three phase air-water-sand flow through horizontal pipeline. The geometry and other parameters are taken from Fukuda and Shoji [14]. Considering two fixed support at two end (inlet, outlet) the maximum deformation is found near the midway of the pipeline which follows solid structure theory for deformation. This study will eventually minimize pipeline flow hazards and economical losses.

References

- [1]. Geilikman, M. B., & Dusseault, M. B. (1997). Fluid rate enhancement from massive sand production in heavy-oil reservoirs. *Journal of Petroleum Science and Engineering*, 17(1), 5-18.

- [2]. Rajnauth, J., & Barrufet, M. (2012). Monetizing Gas: Focusing on Developments in Gas Hydrate as a Mode of Transportation. *Energy Science and Technology*, 4(2), 61-68.
- [3]. Xu, H. L., Zhou, G., Wu, B., & Wu, W. R. (2012). Influence of wave and current on deep-sea mining transporting system. *Journal of Central South University*, 19, 144-149.
- [4]. Miao, Z., Shastri, Y., Grift, T., Hansen, A., & Ting, K. (2012). Lignocellulosic biomass feedstock transportation alternatives, logistics, equipment configurations, and modeling. *Biofuels, Bioproducts and Biorefining*, 6(3), 351-362.
- [5]. Bello, O., Reinicke, K., & Teodoriu, C. (2005). Particle Holdup Profiles in Horizontal Gas-liquid-solid Multiphase Flow Pipeline. *Chemical Engineering & Technology*, 28(12), 1546-1553.
- [6]. Mao, F., Desir, F. K., & Ebadian, M. A. (1997). Pressure drop measurement and correlation for three-phase flow of simulated nuclear waste in a horizontal pipe. *International journal of multiphase flow*, 23(2), 397-402.
- [7]. Orell, A. (2007). The effect of gas injection on the hydraulic transport of slurries in horizontal pipes. *Chemical Engineering Science*, 62(23), 6659-6676.
- [8]. Pouranfard, A. R., Mowla, D., & Esmaeilzadeh, F. (2015). An experimental study of drag reduction by nanofluids in slug two-phase flow of air and water through horizontal pipes. *Chinese Journal of Chemical Engineering*, 23(3), 471-475.
- [9]. Sanders, R., Schaan, J., & McKibben, M. (2007). Oil Sand Slurry Conditioning Tests in a 100 mm Pipeline Loop. *Canadian Journal of Chemical Engineering*, 85(5), 756-764.
- [10]. Scott, D. S., & Rao, P. K. (1971). Transport of solids by gas-liquid mixtures in horizontal pipes. *The Canadian Journal of Chemical Engineering*, 49(3), 302-309.

- [11]. Toda, M., Shimazaki, K., & Maeda, S. (1978). Pressure drop of three-phase flow in horizontal pipes. *Kagaku Kogaku Ronbunshu*, 4, 56-62.
- [12]. Barnea, D., Shoham, O., Taitel, Y., & Dukler, A. E. (1985). Gas-liquid flow in inclined tubes: flow pattern transitions for upward flow. *Chemical Engineering Science*, 40(1), 131-136.
- [13]. Hatate, Y., Nomura, H., Fujita, T., Tajiri, S., & Ikari, A. (1986). Gas holdup and pressure drop in three-phase horizontal flows of gas-liquid-fine solid particles system. *Journal of chemical engineering of Japan*, 19(4), 330-335.
- [14]. Fukuda, T., & Shoji, Y. (1986). Pressure Drop and Heat Transfer for Tree Phase Flow: 1st Report, Flow in Horizontal Pipes. *Bulletin of JSME*, 29(256), 3421-3426.
- [15]. Kago, T., Saruwatari, T., Kashima, M., Morooka, S., & Kato, Y. (1986). Heat transfer in horizontal plug and slug flow for gas-liquid and gas-slurry systems. *Journal of chemical engineering of Japan*, 19(2), 125-131.
- [16]. Toda, M., & Konno, H. (1987). Fundamentals of Gas-Liquid-Solid Three Phase Flow. *JAPANESE JOURNAL OF MULTIPHASE FLOW*, 1(2), 139-156.
- [17]. Angelsen, S., Kvernfold, O., Lingelem, M., & Olsen, S. (1989). Long-Distance Transport of Unprocess HC Sand Settling in Multiphase Pipelines. In *The Fourth International Conference on Multiphase Flow*, Nice, France (pp. 19-21).
- [18]. Pieter Oudeman, S. P. E. (1994). Sand Transport and Deposition in Horizontal Multiphase Trunklines off Subsea Satellite Developments. *Transactions*, 295, 34.
- [19]. Gillies, R. G., McKibben, M. J., & Shook, C. A. (1997). Pipeline flow of gas, liquid and sand mixtures at low velocities. *Journal of Canadian Petroleum Technology*, 36(09).

- [20]. Pironti, F., Pellegrino, G., Meza, G., & Ramírez, N. (1997). Pressure drop of three-phase suspension flows (water-air-sand) in horizontal pipelines. *Revista Técnica de la Facultad de Ingeniería. Universidad del Zulia*, 20(2).
- [21]. Salama, M. M. (2000). Sand production management. *Journal of energy resources technology*, 122(1), 29-33.
- [22]. Stevenson, P., Thorpe, R. B., Kennedy, J. E., & McDermott, C. (2001). The transport of particles at low loading in near-horizontal pipes by intermittent flow. *Chemical Engineering Science*, 56(6), 2149-2159.
- [23]. King, M. J., Fairhurst, C. P., & Hill, T. J. (2001). Solids Transport in Multiphase Flows—Application to High-Viscosity Systems. *Journal of energy resources technology*, 123(3), 200-204.
- [24]. Danielson, T. J. (2007, January). Sand transport modeling in multiphase pipelines. In *Offshore Technology Conference. Offshore Technology Conference*.
- [25]. Bello, O. O., Udong, I. N., Falcone, G., & Teodoriu, C. (2010, January). Hydraulic analysis of gas/oil/sand flow in horizontal wells. In *SPE Latin American and Caribbean Petroleum Engineering Conference. Society of Petroleum Engineers*.
- [26]. Goharzadeh, A., Rodgers, P., & Touati, C. (2010). Influence of Gas-Liquid Two-Phase Intermittent Flow on Hydraulic Sand Dune Migration in Horizontal Pipelines. *Journal of Fluids Engineering*, 132(7), 071301.
- [27]. Rahman, M. A., Adane, K. F., & Sanders, R. S. (2013). An improved method for applying the lockhart–martinelli correlation to three-phase gas–liquid–solid horizontal pipeline flows. *The Canadian Journal of Chemical Engineering*, 91(8), 1372-1382.

- [28]. Al-Hadhrami, L. M., Shaahid, S. M., Tunde, L. O., & Al-Sarkhi, A. (2014). Experimental study on the flow regimes and pressure gradients of air-oil-water three-phase flow in horizontal pipes. *The Scientific World Journal*, 2014.
- [29]. Li, L., Xu, H. L., & Yang, F. Q. (2015). Three-phase flow of submarine gas hydrate pipe transport. *Journal of Central South University*, 22, 3650-3656.
- [30]. Annaland, M., Deen, N. G., & Kuipers, J. A. M. (2005). Numerical simulation of gas–liquid–solid flows using a combined front tracking and discrete particle method. *Chemical engineering science*, 60(22), 6188-6198.
- [31]. Washino, Tan, Salman, & Hounslow. (2011). Direct numerical simulation of solid–liquid–gas three-phase flow: Fluid–solid interaction. *Powder Technology*, 206(1), 161-169.
- [32]. Baltussen, M. W., Seelen, L. J. H., Kuipers, J. A. M., & Deen, N. G. (2013). Direct Numerical Simulations of gas–liquid–solid three phase flows. *Chemical Engineering Science*, 100, 293-299.
- [33]. Liu, X., Aramaki, Y., Guo, L., & Morita, K. (2015). Numerical simulation of gas–liquid–solid three-phase flow using particle methods. *Journal of Nuclear Science and Technology*, 52(12), 1480-1489.
- [34]. Alder, B. J., & Wainwright, T. E. (1960). Studies in molecular dynamics. II. Behavior of a small number of elastic spheres. *The Journal of Chemical Physics*, 33(5), 1439-1451.
- [35]. Chapman, S., & Cowling, T. G. (1970). *The mathematical theory of non-uniform gases: an account of the kinetic theory of viscosity, thermal conduction and diffusion in gases.* Cambridge university press.

- [36]. Syamlal, M., Rogers, W., & O'Brien, T. J. (1993). MFIIX documentation: Theory guide. National Energy Technology Laboratory, Department of Energy, Technical Note DOE/METC-95/1013 and NTIS/DE95000031.
- [37]. Vijiapurapu, S., & Cui, J. (2010). Performance of turbulence models for flows through rough pipes. *Applied Mathematical Modelling*, 34(6), 1458-1466.
- [38]. Zagarola, M. V., & Smits, A. J. (1997). Scaling of the mean velocity profile for turbulent pipe flow. *Physical review letters*, 78(2), 239.
- [39]. Nourmohammadi, K., Hopke, P. K., & Stukel, J. J. (1985). Turbulent air flow over rough surfaces: II. turbulent flow parameters. *Journal of Fluids Engineering*, 107(1), 55-60.
- [40]. Kaushal, D. R., Sato, K., Toyota, T., Funatsu, K., & Tomita, Y. (2005). Effect of particle size distribution on pressure drop and concentration profile in pipeline flow of highly concentrated slurry. *International Journal of Multiphase Flow*, 31(7), 809-823.
- [41]. Launder, B. E., Reece, G. J., & Rodi, W. (1975). Progress in the development of a Reynolds-stress turbulence closure. *Journal of fluid mechanics*, 68(03), 537-566.
- [42]. Lien, F. S., & Leschziner, M. A. (1994). Assessment of turbulence-transport models including non-linear RNG eddy-viscosity formulation and second-moment closure for flow over a backward-facing step. *Computers & Fluids*, 23(8), 983-1004.
- [43]. Daly, B. J., & Harlow, F. H. (1970). Transport equations in turbulence. *Physics of Fluids* (1958-1988), 13(11), 2634-2649.
- [44]. Launder, B. E. (1989). Second-moment closure: present... and future?. *International Journal of Heat and Fluid Flow*, 10(4), 282-300.

- [45]. Wasp, E. J., Kenny, J. P., & Gandhi, R. L. (1977). Solid-liquid flow: slurry pipeline transportation. [Pumps, valves, mechanical equipment, economics]. Ser. Bulk Mater. Handl; (United States), 1(4).
- [46]. Brown, N. P., & Heywood, N. I. (Eds.). (1991). Slurry Handling: Design of solid-liquid systems. Springer Science & Business Media.
- [47]. Skudarnov, P., Lin, C., & Ebadian, M. (2004). Double-species slurry flow in a horizontal pipeline. *Journal of Fluids Engineering, Transactions of the ASME*, 126(1), 125-132.
- [48]. Wood, D. J., 1966, *Civil Eng.-A.S.C.E.* 36 (12), 60. Cited in Govier, G. W., & Aziz, K. (1977). *The flow of complex mixtures in pipes*. Krieger Pub Co.
- [49]. Bhagwat, S. M., & Ghajar, A. J. (2016). Experimental investigation of non-boiling gas-liquid two phase flow in upward inclined pipes. *Experimental Thermal and Fluid Science*, 79, 301-318.
- [50]. Brown, G. O. (2003). The history of the Darcy-Weisbach equation for pipe flow resistance. In *Environmental and Water Resources History* (pp. 34-43).
- [51]. Colebrook, C. F., Blench, T., Chatley, H., Essex, E., Finnicome, J., Lacey, G., ... & Macdonald, G. (1939). Correspondence. *Turbulent Flow in Pipes, with Particular Reference to The Transition Region Between the Smooth and Rough Pipe Laws. (Includes Plates)*. *Journal of the Institution of Civil engineers*, 12(8), 393-422.
- [52]. Wagner, W., & Kretschmar, H. J. (2008). IAPWS industrial formulation 1997 for the thermodynamic properties of water and steam. *International Steam Tables: Properties of Water and Steam Based on the Industrial Formulation IAPWS-IF97*, 7-150.

Summary

This analysis proposed a multiphase fluid flow model which can be applicable for different applications specially related to petroleum industry. Our selected model is verified with other empirical models and available experimental data. It demonstrated very good and acceptable agreement from single phase to three phase flow. Parametric analysis with two phase and three phase flow provide some important information about the effects of hydrodynamic parameters on pressure loss and settling conditions.

Chapter 1 proposed a CFD model with detailed literature analysis and validation of the model with twelve different experimental sources. Mesh analysis, length independent analysis and turbulent model selection are done elaborately with several comparisons. As a result, proposed CFD model showed good agreement with experimental data (maximum error < 30% and average error < 15%). These indicate validity of our model inside the given ranges.

Chapter 2 tested the effects of fluid flow rate, rotational speed and eccentricity of drill pipe and solid particle size on pressure loss and settling conditions inside annular pipe using the proposed CFD model. Preliminary results are presented with proper explanations. Two phase slurry (water and sand) flow is used to run the parametric analysis changing parameters (fluid velocity, fluid type, particle size, particle concentration, drill pipe rotation speed and drill pipe eccentricity) inside annuli. Related two phase flow parametric analysis is represented in Appendix 1 and Appendix 2 using slurry and slug (water and air) flow through pipeline.

Chapter 3 analyzed three phase fluid flow through horizontal pipeline. Air-water-sand flow through pipeline is used to conduct the analysis changing few major parameters (pipe diameter, pipe wall roughness, fluid viscosity and sand concentration). Three phase flow analysis is very

rare and this preliminary approach in chapter 3 provided the proper guidance for further research. Related experimental approach with our proposed model is discussed in Appendix 3. Considering pipe flow safety, Fluid Structure Interaction (FSI) is introduced in this chapter. Because of fluid flow pressure on wall surface, deformation occurs. This can cause unexpected hazard. FSI analysis can detect the proper reason of pipe deformations and reduce the risk at work place.

Recommendations for future work:

- Further analysis is required with more accuracy which can include choosing different coefficients and constants such as coefficient of lift, coefficient of drag, restitution coefficient and wall boundary conditions to minimize small errors and increase acceptance of this model at versatile conditions of operation.
- It is expected to find out numerical correlations between different parameters by conducting further parametric study at distinct phases of fluid flow through pipeline and annuli.
- Complex geometry of pipeline and annuli can be introduced (e.g. bending, inclination etc.).
- Experimental study along with the proposed CFD model will add better scope to study comprehensively the multiphase flow system through pipeline and annuli. Experimental facilities are developed in Memorial University of Newfoundland (MUN) and Texas A&M University at Qatar (TAMUQ) which can be used for further analysis with our findings.
- Elaborate work on Fluid Structure Interaction (FSI) is required focusing the safety and risk of multiphase flow through pipeline and annuli at different conditions.

Appendix 1. Sensitivity Analysis of A CFD Model for Simulating Slurry

Flow Through Pipeline

Rasel A Sultan^{*,a}, M. A. Rahman^a, Sohrab Zendehboudi^a, Vandad Talimi^b, Vassilios C. Kelessidis^c

^aFaculty of Engineering and Applied Science, Memorial University of Newfoundland, St. John's, NL, Canada

^bC-CORE, St. John's, NL, Canada

^cFaculty of Petroleum Engineering, Texas A&M University at Qatar, Doha, Qatar

Abstract

Three-dimensional CFD modeling of two-phase slurry flows is shown in this paper through 26mm diameter horizontal pipe for mixture velocity range of 3.5–4.7m/s and overall volumetric concentration range of 9.95%–34% with three grain sizes viz. 0.165, 0.29 and 0.55 mm. Eulerian model with Reynolds Stress Model (RSM) turbulence closure is adopted to analyze the monodispersed sand particles of varying granular diameters and density 2650 kg/m³. The objective of this work is to analyze the sensitivity slurry flow using CFD simulation and validating the simulation with experimental studies available in the literature. The simulated local solid concentration values and pressure gradients are found to be in good agreement with experimental results at different conditions. Pressure drop per meter or pressure gradient increases with flow velocity of mixture. Effects of grain size on various slurry flow parameters especially on local solid concentration distribution is also studied.

Keywords: CFD; Slurry flow; Pressure gradient; Solid concentration; Pipeline.

Introduction

Liquid-solid and liquid-gas two-phase flow in pipeline or annuli are of great importance in different industries with transport requirement. In recent years, solid transportation in liquid

through pipelines or annuli has become increasingly popular due to its numerous application in different industries and enormous focus of society on reduction in environmental pollution. Usually slurry flow has been applied to transport raw materials, wastes and sludges which are in solid form (Soliman and Collier, 1990), beneficiation in extractive metallurgy and mining plants (Roco and Shook, 1983), coal processing plants (Choi et al., 2001), fluidized beds (Huilin et al., 2002), food and chemical plants, petroleum industries and many more. Slurry transportation system helps to reduce traffic, air pollution, noise, accidents along with saving on energy consumption and lesser ecological disturbance.

Two-phase slurry flow through pipeline is researched from the beginning of third decade of 20th century, aiming towards developing general solutions based on available experimental data for solid volumetric or mass concentration profiles, pressure gradient and slurry velocity profile, which are primarily required for better understanding of whole slurry flow process. Among the initial researches, O'Brien (1933) and Rouse (1937) contributed their work of slurry flow in open channel with low solid concentration, they use diffusion model to predicted the concentration distribution. Also Durand (1951), Durand and Condolios (1952), Newitt et al. (1955) are considered as the pioneers to describe friction pressure losses in slurry flow. Correlations established by Einstein (1906), Thomas (1965) and Krieger (1972) for homogeneous distribution of slurry and model by Ling et al. (2003) for heterogeneous slurry distribution gave a new dimension in the study of predicting pressure gradient of slurry flow. Some other works on empirical correlations for slurry pressure gradient are Govier and Aziz (1972), Vocadlo and Charles (1972). Aude et al. (1974), Aude et al. (1975), Seshadri (1982) and Seshadri et al. (1982) studied on long distance slurry flow in pipeline and showed this can be used as a reliable mode of transportation of solid. Many researches took place aiming at predicting concentration distribution

for slurry flow in pipelines. A few notables of them are Shook and Daniel (1965), Shook et al. (1968), Karabelas (1977), Seshadri et al. (1982), Roco and Shook (1983), Roco and Shook (1984), Gillies et al. (1991), Gillies and Shook (1994), Gillies et al. (1999), Kaushal and Tomita (2002), Kaushal and Tomita (2003), Kumar et al. (2003), Kaushal et al. (2005). Apart from this, several studies for predicting pressure drop over the length also took place for slurry flows. A few notables of them are Wasp et al. (1970), Wilson (1976), Wasp et al. (1977), Doron et al. (1987), Gillies et al. (1991), Sundqvist et al. (1996), Mishra et al. (1998), Ghanta and Purohit (1999), Wilson et al. (2002), Kaushal and Tomita (2002), Kumar (2002), Kaushal and Tomita (2003), Skudarnov et al. (2004), Kaushal et al. (2005), Kumar et al. (2008), Vlasak et al. (2012), Pouranfard (2014). These empirical correlations and experimental studies are based on limited scope, data and application range (Lahiri and Ghanta, 2007). CFD simulation models have been utilized to minimize these limitations. CFD studies by Hernández et al. (2008), Chen et al. (2009), Kumar and Kaushal (2015), Kumar and Kaushal (2016) on slurry flow in pipeline have provided a new dimension in this field.

The approach of this study is to perform several comparisons of CFD simulation with experimental and empirical studies at different conditions and ranges for different industrial purposes. A parametric study is conducted using CFD simulation with versatile range of variables to minimize limitation in applications. Furthermore, different variables like modelling pressure loss, measuring/modeling concentration profile, analyzing the physics that control the hydrodynamics of fluid flow in annuli or pipeline is studied.

Mathematical Models

The Eulerian model of granular version has been adopted as multiphase model for present study. The selection of appropriate multiphase model depends mainly on the range of volume fraction

(α) of solid phase under consideration. Since high value of volume fraction is used in this study this model is taken into account. Granular version helps in capturing the effects of friction and collisions between particles which is especially important in higher concentration slurries having varying grain sizes.

Multiphase Model

The Eulerian multiphase model allows for the modeling of multiple separate, yet interacting phases. The phases can be liquids, gases, or solids in nearly any combination. The Eulerian treatment is used for each phase, in contrast to the Eulerian-Lagrangian treatment that is used for the discrete phase model.

Volume Fractions

The description of multiphase flow as interpenetrating continua incorporates the concept of phasic volume fractions, denoted here by a_q . Volume fractions represent the space occupied by each phase, and the laws of conservation of mass and momentum are satisfied by each phase individually. The derivation of the conservation equations can be done by ensemble averaging the local instantaneous balance for each of the phases (Anderson and Jackson, 1967) or by using the mixture theory approach (Bowen, 1976).

The volume of phase q , V_q , is defined by

$$V_q = \int a_q dV \quad (1)$$

where,

$$\sum_{q=1}^n a_q = 1 \quad (2)$$

The effective density of phase q is,

$$\hat{\rho}_q = a_q \rho_q \quad (3)$$

where ρ_q is the physical density of phase q .

Conservation Equations

The equations for fluid-fluid and granular multiphase flows, are presented here for the general case of an n -phase flow.

Continuity Equation

The volume fraction of each phase is calculated from a continuity equation as below –

$$\frac{1}{\rho_{rq}} \left\{ \frac{\partial}{\partial t} (a_q \rho_q) + \nabla \cdot (a_q \rho_q \vec{\vartheta}_q) \right\} = \sum_{p=1}^n (\dot{m}_{pq} - \dot{m}_{qp}) \quad (4)$$

where ρ_{rq} is the phase reference density, or the volume averaged density of the q^{th} phase in the solution domain, \dot{m}_{pq} characterizes the mass transfer from the p^{th} to q^{th} phase and \dot{m}_{qp} characterizes the mass transfer from the q^{th} to p^{th} phase.

Fluid-Fluid Momentum Equations

The conservation of momentum for a fluid phase q is –

$$\begin{aligned} \frac{\partial}{\partial t} (a_q \rho_q \vec{\vartheta}_q) + \nabla \cdot (a_q \rho_q \vec{\vartheta}_q \vec{\vartheta}_q) = & -a_q \nabla p + \nabla \cdot \bar{\tau}_q + a_q \rho_q \vec{g} + \sum_{p=1}^n \{ K_{pq} (\vec{\vartheta}_p - \vec{\vartheta}_q) + \\ & \dot{m}_{pq} \vec{\vartheta}_{pq} - \dot{m}_{qp} \vec{\vartheta}_{qp} \} + (\vec{F}_q + \vec{F}_{lift,q} + \vec{F}_{vm,q}) \end{aligned} \quad (5)$$

Here \vec{g} is the acceleration due to gravity, $\bar{\tau}_q$ is the q^{th} phase stress-strain tensor, \vec{F}_q is an external body force, $\vec{F}_{lift,q}$ is a lift force and $\vec{F}_{vm,q}$ is a virtual mass force.

Fluid-Solid Momentum Equations

Following the work of Alder and Wainwrigth (1960), Chapman and Cowling (1970) and Syamlal et al. (1993), a multi-fluid granular model is used to describe the flow behavior of a fluid-solid mixture.

The conservation of momentum for the fluid phases is similar to Equation (5), and that for the s^{th} solid phase is –

$$\begin{aligned} \frac{\partial}{\partial t} (a_s \rho_s \overline{\vartheta}_s) + \nabla \cdot (a_s \rho_s \overline{\vartheta}_s \overline{\vartheta}_s) = & -a_s \nabla p - \nabla p_s + \nabla \cdot \bar{\tau}_s + a_s \rho_s \vec{g} + \sum_{l=1}^N \{K_{ls} (\overline{\vartheta}_l - \overline{\vartheta}_s) + \\ & \dot{m}_{ls} \overline{\vartheta}_{ls} - \dot{m}_{sl} \overline{\vartheta}_{sl}\} + (\overline{F}_s + \vec{F}_{lift,s} + \vec{F}_{vm,s}) \end{aligned} \quad (6)$$

where p_s is the s^{th} solids pressure, $K_{ls} = K_{sl}$ is the momentum exchange coefficient between fluid or solid phase l and solid phase s , N is the total number of phases.

Solids Pressure

For granular flows in the compressible regime (i.e., where the solids volume fraction is less than its maximum allowed value), a solids pressure is calculated independently and used for the pressure gradient term, ∇p_s in the granular-phase momentum equation. Because a Maxwellian velocity distribution is used for the particles, a granular temperature is introduced into the model, and appears in the expression for the solids pressure and viscosities. The solids pressure is composed of a kinetic term and a second term due to particle collisions –

$$p_s = a_s \rho_s \theta_s + 2\rho_s (1 + e_{ss}) a_s^2 g_{0,ss} \theta_s \quad (7)$$

where, e_{ss} is the coefficient of restitution for particle collisions, $g_{0,ss}$ is the radial distribution function, and θ_s is the granular temperature. Here a default value of 0.9 for e_{ss} is used, but the

value can be adjusted to suit the particle type. The granular temperature θ_s is proportional to the kinetic energy of the fluctuating particle motion. The function $g_{0,ss}$ is a distribution function that governs the transition from the "compressible" condition with $a < a_{s,max}$, where the spacing between the solid particles can continue to decrease, to the "incompressible" condition with $a = a_{s,max}$, where no further decrease in the spacing can occur. A value of 0.63 is the default for $a_{s,max}$, but it can be modify during the problem setup.

Solids Shear Stresses

The solids stress tensor contains shear and bulk viscosities arising from particle momentum exchange due to translation and collision. A frictional component of viscosity can also be included to account for the viscous-plastic transition that occurs when particles of a solid phase reach the maximum solid volume fraction.

The collisional and kinetic parts, and the optional frictional part, are added to give the solids shear viscosity-

$$\mu_s = \mu_{s,col} + \mu_{s,kin} + \mu_{s,fr} \quad (8)$$

where, $\mu_{s,col}$ is shear viscosity due to collision, $\mu_{s,kin}$ is kinetic viscosity and $\mu_{s,fr}$ frictional viscosity.

The collisional part of the shear viscosity is modeled as Gidaspow et al. (1991) and Syamlal et al. (1993) –

$$\mu_{s,col} = \frac{4}{5} a_s \rho_s d_s g_{0,ss} (1 + e_{ss}) \left(\frac{\theta_s}{\pi} \right)^{1/2} \quad (9)$$

The default expression of kinetic viscosity is from Syamlal et al. (1993):

$$\mu_{s,kin} = \frac{a_s d_s \rho_s \sqrt{\theta_s \pi}}{6(3 - e_{ss})} \left[1 + \frac{2}{5} (1 + e_{ss}) (3e_{ss} - 1) a_s g_{0,ss} \right] \quad (10)$$

The frictional viscosity is included using Schaeffer's (1987) expression –

$$\mu_{s,fr} = \frac{p_s \sin \phi}{2\sqrt{I_{2D}}} \quad (11)$$

Turbulence Model

Turbulent quantity for fluid flow are assumed using Reynolds Stress Model (RSM) (Launder et al., 1975, Gibson and Launder, 1978 and Launder, 1989). This is the most elaborate turbulence model. Abandoning the isotropic eddy-viscosity hypothesis, the RSM closes the Reynolds-averaged Navier-Stokes equations (Chorin, 1968) by solving transport equations for the Reynolds stresses, together with an equation for the dissipation rate. Here five additional transport equations are required in 2D flows and seven additional transport equations must be solved in 3D.

The exact transport equation for the Reynolds Stress Model (RSM) is as below –

$$\begin{aligned} & \underbrace{\frac{\partial}{\partial t} (\rho \overline{u'_i u'_j})}_{\text{Local Time Derivative}} + \underbrace{\frac{\partial}{\partial x_k} (\rho u_k \overline{u'_i u'_j})}_{\text{Convection } (C_{ij})} = - \underbrace{\frac{\partial}{\partial x_k} \left[\rho \overline{u'_i u'_j u'_k} + p (\delta_{kj} u'_i + \delta_{ik} u'_j) \right]}_{\text{Turbulent Diffusion } (D_{T,ij})} \\ & + \underbrace{\frac{\partial}{\partial x_k} \left[u \frac{\partial y}{\partial x_k} (\overline{u'_i u'_j}) \right]}_{\text{Molecular Diffusion } (D_{L,ij})} - \underbrace{\rho \left(\overline{u'_i u'_k} \frac{\partial u_j}{\partial x_k} + \overline{u'_j u'_k} \frac{\partial u_i}{\partial x_k} \right)}_{\text{Stress Production } (P_{ij})} - \underbrace{\rho \beta (\overline{g_i u'_j \theta} + \overline{g_j u'_i \theta})}_{\text{Buoyancy Production } (G_{ij})} \\ & + \underbrace{p \left(\frac{\partial u'_i}{\partial x_j} + \frac{\partial u'_j}{\partial x_i} \right)}_{\text{Pressure Strain } (\Phi_{ij})} - \underbrace{2\mu \frac{\partial u'_i}{\partial x_k} \frac{\partial u'_j}{\partial x_k}}_{\text{Dissipation } (\epsilon_{ij})} \\ & - \underbrace{2\rho \Omega_k (\overline{u'_j u'_m} \epsilon_{ikm} + \overline{u'_i u'_m} \epsilon_{jkm})}_{\text{Production by system Rotation } (F_{ij})} + \underbrace{S_{user}}_{\text{User-Defined Source}} \end{aligned} \quad (12)$$

Of the various terms in these exact equations, C_{ij} , $D_{L,ij}$, P_{ij} and F_{ij} do not require any modeling. However, $D_{T,ij}$, G_{ij} , Φ_{ij} and ϵ_{ij} need to be modeled to close the equations $D_{T,ij}$ can be modeled by the generalized gradient-diffusion model of Daly and Harlow (1970), which is –

$$D_{T,ij} = C_s \frac{\partial}{\partial x_k} \left(\rho \frac{\overline{k u'_k u'_l} \overline{\partial u'_l u'_j}}{\epsilon} \right) \quad (13)$$

However, this equation can result in numerical instabilities (Launder, 1989), so it has been simplified in this study to use a scalar turbulent diffusivity as follows (Launder, 1989) –

$$D_{T,ij} = \frac{\partial}{\partial x_k} \left(\frac{\mu_t}{\sigma_k} \frac{\overline{\partial u'_l u'_j}}{\partial x_k} \right) \quad (14)$$

Lien and Leschziner (Lien and Leschziner, 1987) derived a value of adjustable constant $\sigma_k = 0.82$.

where, turbulent viscosity (μ_t) is computed as –

$$\mu_t = \rho C_\mu \frac{k^2}{\epsilon} \text{ and } C_\mu = 0.09 \quad (15)$$

where, C_μ is an adjustable constant.

Expression for G_{ij} for ideal gases is as follows –

$$G_{ij} = -\frac{\mu_t}{\rho Pr_t} \left(g_i \frac{\partial \rho}{\partial x_j} + g_j \frac{\partial \rho}{\partial x_i} \right) \quad (16)$$

where Pr_t is the turbulent Prandtl number for energy, with a default value of 0.85 used in simulation.

The pressure-strain term, Φ_{ij} is modeled according to the proposal by Gibson and Launder (1978), Fu et al. (1987), and Launder (1989).

The classical approach to modeling Φ_{ij} uses the following decomposition –

$$\Phi_{ij} = \Phi_{ij,1} + \Phi_{ij,2} + \Phi_{ij,w} \quad (17)$$

where, $\Phi_{ij,1}$ is the slow pressure-strain term, also known as the return-to-isotropy term, $\Phi_{ij,2}$ is called the rapid pressure-strain term, and $\Phi_{ij,w}$ is the wall-reflection term.

The slow pressure-strain term, $\Phi_{ij,1}$, is modeled as -

$$\Phi_{ij,1} \equiv -C_1 \rho \frac{\epsilon}{k} \left[\overline{u'_i u'_j} - \frac{2}{3} \delta_{ij} k \right] \quad (18)$$

with, $C_1 = 1.8$.

The rapid pressure-strain term, $\Phi_{ij,2}$, is modeled as –

$$\Phi_{ij,2} \equiv C_2 \left[(P_{ij} + F_{ij} + G_{ij} - C_{ij}) - \frac{2}{3} \delta_{ij} (P + G - C) \right] \quad (19)$$

where $C_2 = 0.60$, P_{ij} , F_{ij} , G_{ij} and C_{ij} are defined as in Equation (12), $P = \frac{1}{2} P_{kk}$, $G = \frac{1}{2} G_{kk}$, $C = \frac{1}{2} C_{kk}$.

The wall-reflection term, $\Phi_{ij,w}$ is responsible for the redistribution of normal stresses near the wall.

It tends to damp the normal stress perpendicular to the wall, while enhancing the stresses parallel to the wall. This term is modeled as –

$$\begin{aligned} \Phi_{ij,w} \equiv & C'_1 \frac{\epsilon}{k} \left(\overline{u'_k u'_m n_k n_m} \delta_{ij} - \frac{3}{2} \overline{u'_i u'_k n_j n_k} - \frac{3}{2} \overline{u'_j u'_k n_i n_k} \right) \frac{C_l k^{\frac{3}{2}}}{\epsilon d} \\ & + C'_2 \left(\Phi_{km,2} n_k n_m \delta_{ij} - \frac{3}{2} \Phi_{ik,2} n_j n_k - \frac{3}{2} \Phi_{jk,2} n_i n_k \right) \frac{C_l k^{\frac{3}{2}}}{\epsilon d} \end{aligned} \quad (20)$$

where $C'_1 = 0.5$, $C'_2 = 0.3$, n_k is the x_k component of the unit normal to the wall, d is the normal distance to the wall, and $C_l = \frac{C_\mu^{\frac{3}{4}}}{k}$, where $C_\mu = 0.09$ and k is the von Kármán constant (= 0.4187) (Karman, 1937).

The dissipation tensor, ϵ_{ij} , is modeled as –

$$\epsilon_{ij} = \frac{2}{3} \delta_{ij} (\rho\epsilon + Y_M) \quad (21)$$

where $Y_M = 2\rho\epsilon M_t^2$ is an additional "dilatation dissipation" term according to the model by Sarkar (1991). The turbulent Mach number in this term is defined as –

$$M_t = \sqrt{\frac{k}{a^2}} \quad (22)$$

Solution Method

For Eulerian multiphase calculations, the phase coupled SIMPLE (PC-SIMPLE) algorithm (Vasquez and Ivanov, 2000) is used for the pressure-velocity coupling. PC-SIMPLE is an extension of the SIMPLE algorithm (Patankar, 1980) to multiphase flows. The velocities are solved coupled by phases, but in a segregated fashion. The block algebraic multigrid scheme used by the density-based solver described in (Weiss et al., 1999) is used to solve a vector equation formed by the velocity components of all phases simultaneously. Then, a pressure correction equation is built based on total volume continuity rather than mass continuity. Pressure and velocities are then corrected so as to satisfy the continuity constraint.

Pressure-Correction Equation

For incompressible multiphase flow, the pressure-correction equation takes the form of –

$$\sum_{k=1}^n \frac{1}{\rho_{rk}} \left\{ \frac{\partial}{\partial t} a_k \rho_k + \nabla \cdot a_k \rho_k \vec{v}'_k + \nabla \cdot a_k \rho_k \vec{v}^*_k - (\sum_{l=1}^n (\dot{m}_{lk} - \dot{m}_{kl})) \right\} = 0 \quad (23)$$

where ρ_{rk} is the phase reference density for the k^{th} phase (defined as the total volume average density of phase k), \vec{v}'_k is the velocity correction for the k^{th} phase, and \vec{v}^*_k is the value of \vec{v}_k at the current iteration.

Volume Fractions

The volume fractions are obtained from the phase continuity equations. In discretized form, the equation of the k^{th} volume fraction is –

$$a_{p,k} a_k = \sum_{nb} (a_{nb,k} a_{nb,k}) + b_k = R_k \quad (24)$$

In order to satisfy the condition that all the volume fractions sum to one,

$$\sum_{k=1}^n a_k = 1 \quad (25)$$

Simulation Methodology

Geometry and mesh generation

In the present study, a 13.15m long and 26.0mm internal diameter pipe is selected for the sensitivity analysis. The computational grids for this horizontal pipe is generated using ANSYS Fluent meshing with 1,86,767 elements with 82,827 nodes volume cells finalized conducting proper mesh independency check. Ten layers of Inflation near wall is added to observe more precisely the characteristics of different parameters near wall. Shear stress between wall surface and gas molecules are much higher and this inflation helps to create denser meshing near wall. Also it is more time consuming and reliable to use unsymmetrical meshing rather symmetrical meshing. The length of the pipe is sufficient enough to achieve a fully developed

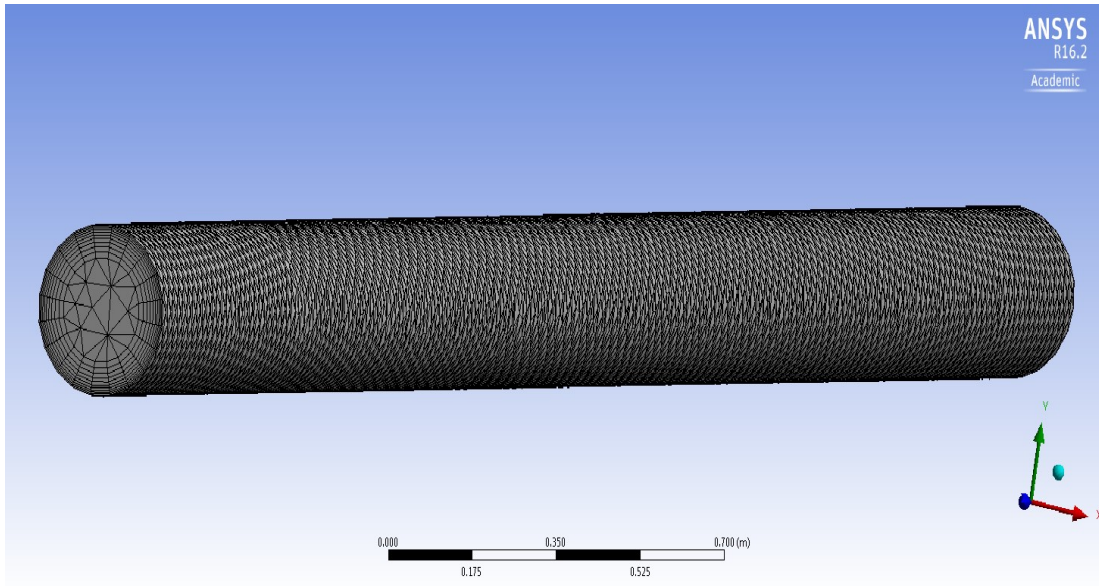


Fig.1. Mesh distribution in the pipe geometry

flow at the outlet as minimum flow development section should be at least $50D$ (D = internal diameter of pipe) (Wasp et al., 1977, Brown and Heywood, 1991) and here this length is maintained. Computational grid distribution of geometry is shown in Figure 1.

Boundary conditions

There are three boundaries available in the given flow domain namely the inlet boundary, the wall boundary and the outlet boundary. Here, inlet velocity range of $3.5\text{--}4.7\text{m/s}$ and overall volumetric concentration range of $9\%\text{--}34\%$ with three grain sizes viz. 0.165 , 0.29 and 0.55 mm have been considered as boundary input. A 0.2 mm of pipe wall roughness is adopted during simulation. As the nature of wall-particle collisions influences the shear stress and turbulent energy flux at the walls, a specular coefficient is defined for solid phase at the walls. a value of 0.5 is selected which corresponds to wall quality between smooth frictionless walls and very rough walls. No slip for liquid phase has been adopted at walls. Inlet and outlet pressure are assumed same.

Solution process and convergence criteria

Fluent, ver. 16.2, ANSYS Inc. is used to build a CFD simulation model of pipeline flow of water-sand slurry. A convergence value of 10^{-5} has been adopted for termination of iteration, this value is selected with optimizing analysis to have most satisfactory accuracy with less time. A second order upwind discretization for momentum equation and first upwind discretization for volume fraction, turbulent kinetic energy and its dissipation are adopted to ensure stability and convergence of iterative process.

Validation of Simulation

Comparison of pressure gradient

Pressure gradient of water-sand slurry flow from simulation is compared with Skudarnov et al. (2004) experimental data. In the experiment, length of pipe is 17m, diameter of pipe is 0.023m, fluid taken water (density 9982 Kg/m^3 , viscosity 0.001003 Kg/m-s) and slurry taken glass spheres slurry (double-species slurry with densities of 2490 kg/m^3 and 4200 kg/m^3 , 50% by 50% by volume mixtures), wall material is stainless steel (density 8030 kg/m^3 , roughness $32 \text{ }\mu\text{m}$). Figure 2 shows the comparison of pressure gradient with $d_m = 140 \text{ }\mu\text{m}$ and $C_v = 15\%$. Where, d_m = mean particle diameter (μm) C_v = volume concentration (%).

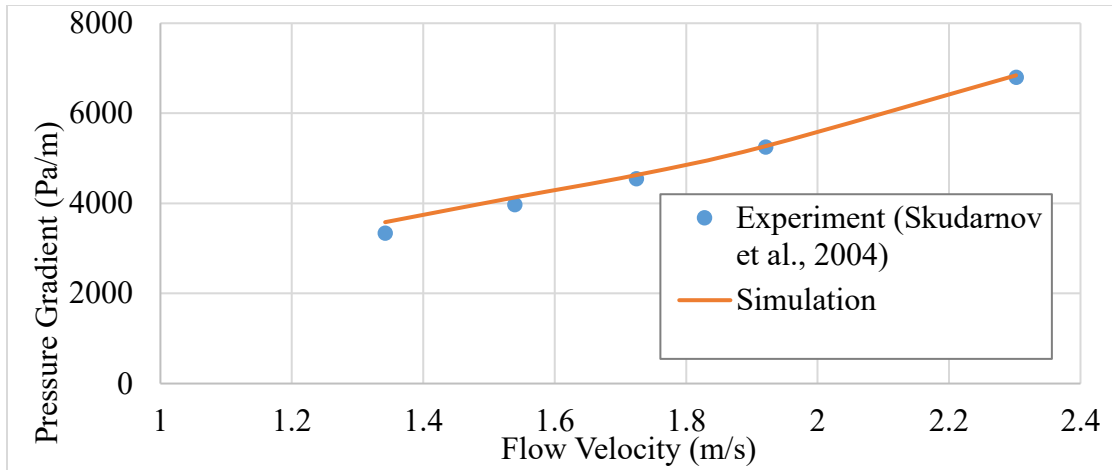


Fig.2. Comparison of pressure gradient from simulation with experimental data of Skudarnov et al. (2004) for double-species slurry with $d_m = 140 \mu\text{m}$ and $C_v = 15\%$.

The result shows very good agreement with experimental values with less than 10% error at each point. The small errors that are arising may be due to experimental errors (it was estimated in the reference paper that the accuracy of the pressure gradient is $\pm 50 \text{ Pa/m}$.) and numerical error of mathematical equations while applying simulation.

Comparison of local solid concentration profile

Local solid concentration profile of water-sand slurry flow from simulation is compared with Gillies and Shook, (1994) experimental data. In the experiment, length of pipe is 2.7m, diameter of pipe is 53.2mm, fluid taken water (density 9982 Kg/m^3 , viscosity 0.001003 Kg/m-s) and slurry taken Silica (chemical formula SiO_2 , density 2650 Kg/m^3 , wall material is aluminum (density 2800 kg/m^3 , roughness 0.2mm). Here, grain size or mean particle diameter is 0.18 mm , mixture velocity 3.1 m/s and three different solid volumetric concentration 14%, 29% and 45% is considered from experiment. Figure 3 shows the comparison of volumetric concentration of solid particles with particle sizes 0.18 mm .

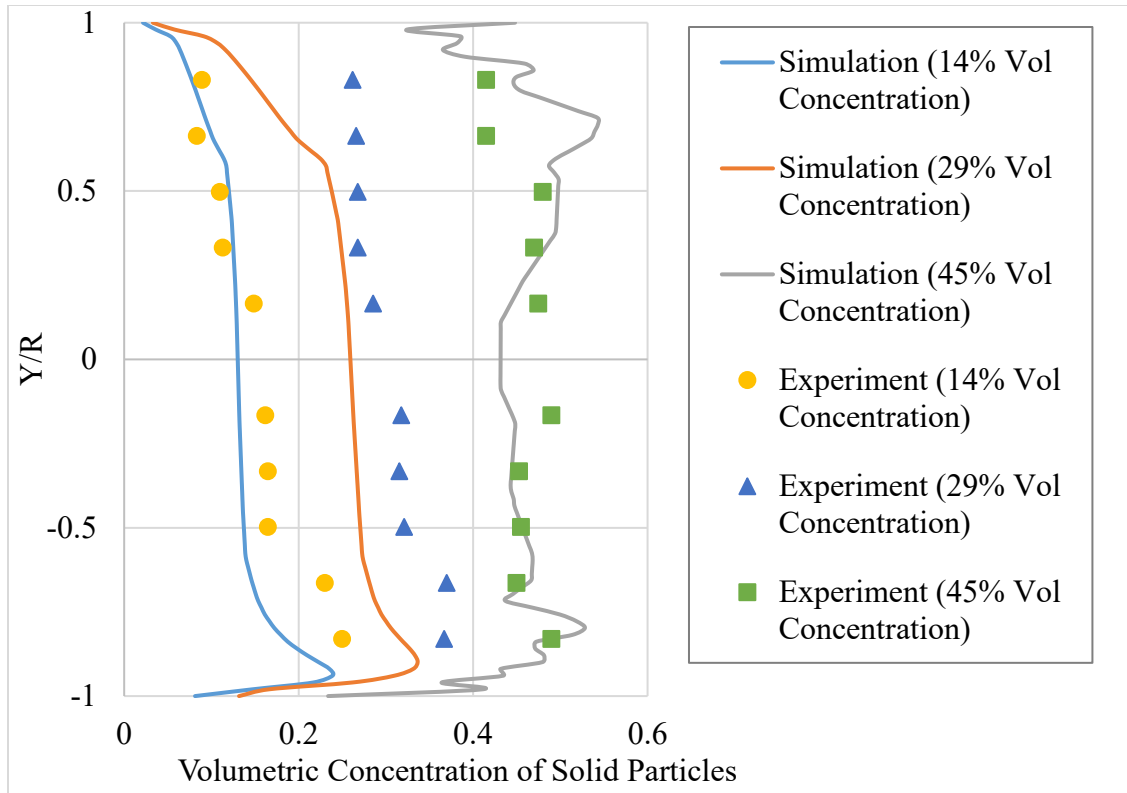


Fig. 3. Comparison of simulated and measured values of local volumetric concentration of solid across vertical centerline for particle sizes 0.18 mm.

Simulated results are in good agreement with experimental values for grain sizes 0.18mm. However, simulated values deviate from experimental values near the wall especially in the lower half of the cross-section. One of the possible reasons could be abrasive rounding of these large size particles by repeated passages during experiment, resulting significant quantities of fines were generated which were distributed uniformly within the pipe. This would have led to possible increase in carrier density. Since information of this aspect was not available in the reference research, the same is not incorporated while doing simulations.

Apart from this, another possible reason for these deviations could be approximate value of static settled concentration (packing limit) used during simulations, as the value of 0.63 used is best suited for finer grain sizes only.

However, it is also necessary to analyze newer boundary conditions at the wall for slurry pipeline flows with larger grain sizes to minimize deviations with experimental results.

Sensitivity Analysis

Solid Concentration Profile Analysis

Figures 4–7 shows simulated local volumetric concentration distribution of solid phase along vertical centerline at outlet cross-section. Geometry, mesh and boundary condition details are discussed in simulation methodology chapter. Both length and diameter of this analysis are taken within range of two validated work geometry. These figures indicate that lower portion of pipe cross section contain more solid particles than upper portion. This happens due to gravity effect and more dense solid particle than water. It means slurry flow in horizontal pipe is not uniform and there is a probability to have particle deposition at a certain mixture velocity and solid volumetric concentration which can create blockage of smooth flow. Figure 8 shows contours of local volumetric concentration distribution of solid phase in the vertical plane at outlet cross-section for particle size of 0.165 mm and mixture velocity of 3.5 m/s at different

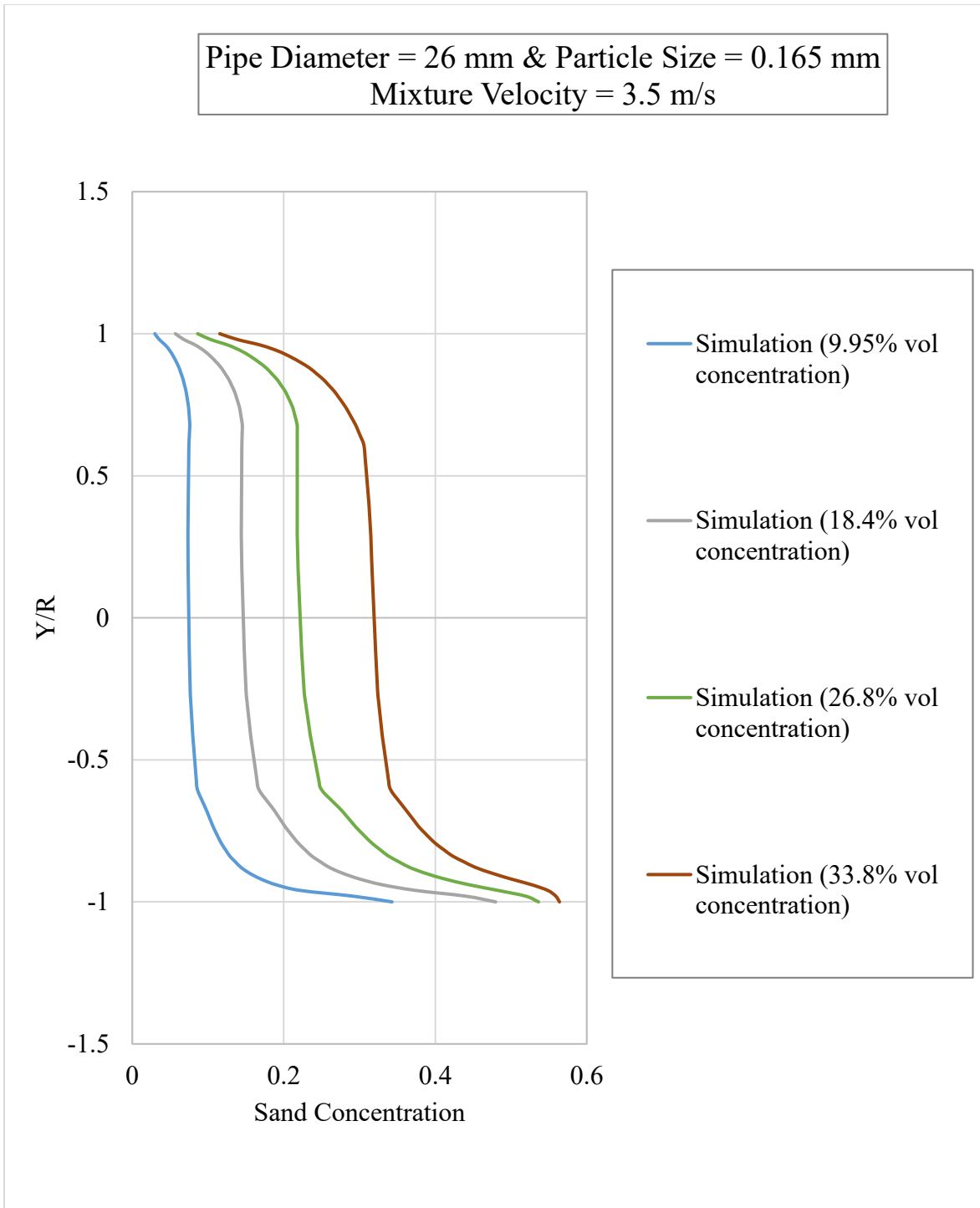


Fig.4. Simulated local volumetric sand concentration across vertical centre line of pipe outlet for particle size of 0.165 mm and mixture velocity of 3.5 m/s at different efflux concentrations.

Pipe Diameter = 26 mm & Particle Size = 0.29 mm
Mixture Velocity = 4.0 m/s

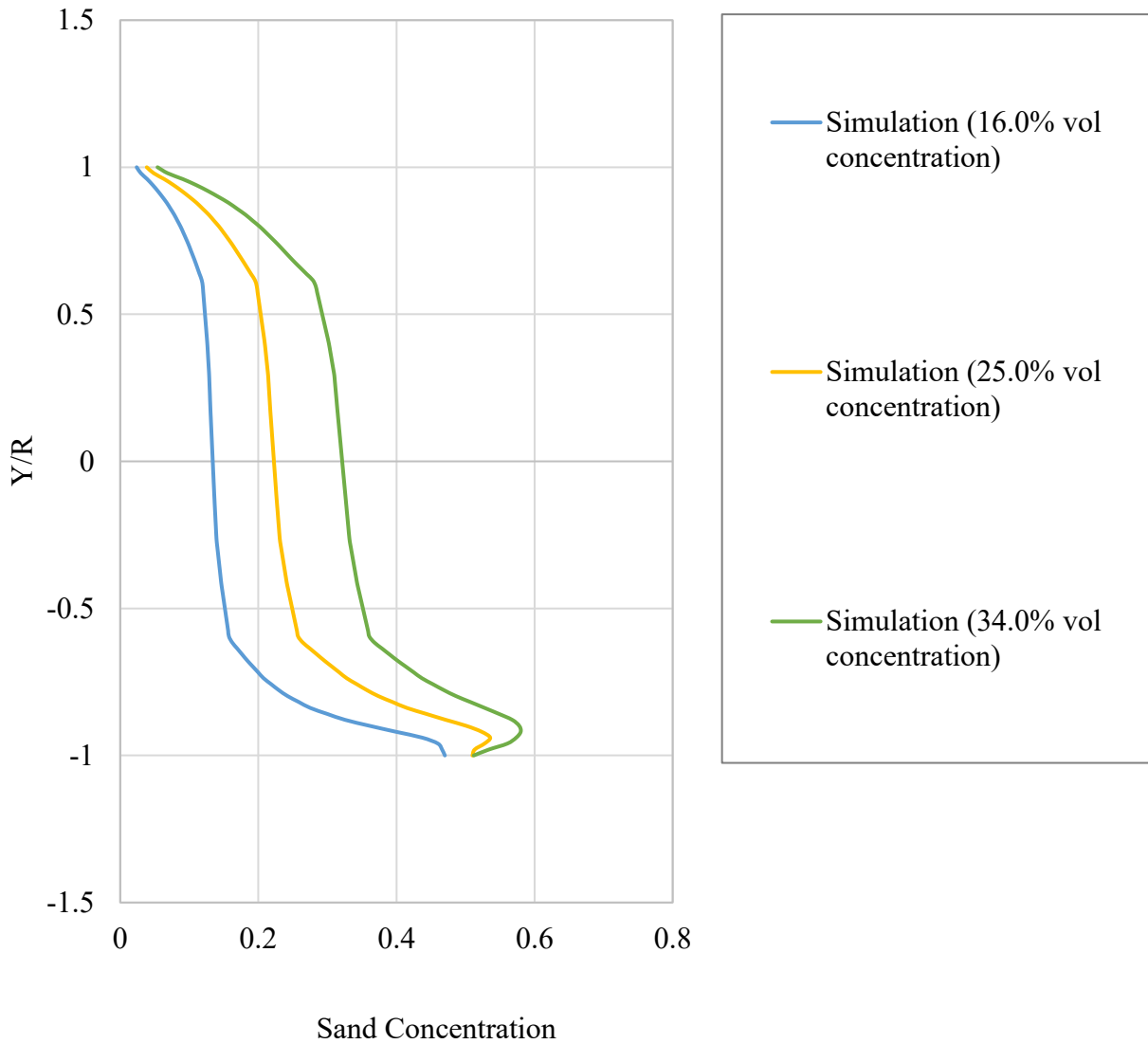


Fig.5. Simulated local volumetric sand concentration across vertical centre line of pipe outlet for particle size of 0.29 mm and mixture velocity of 4.0 m/s at different efflux concentrations.

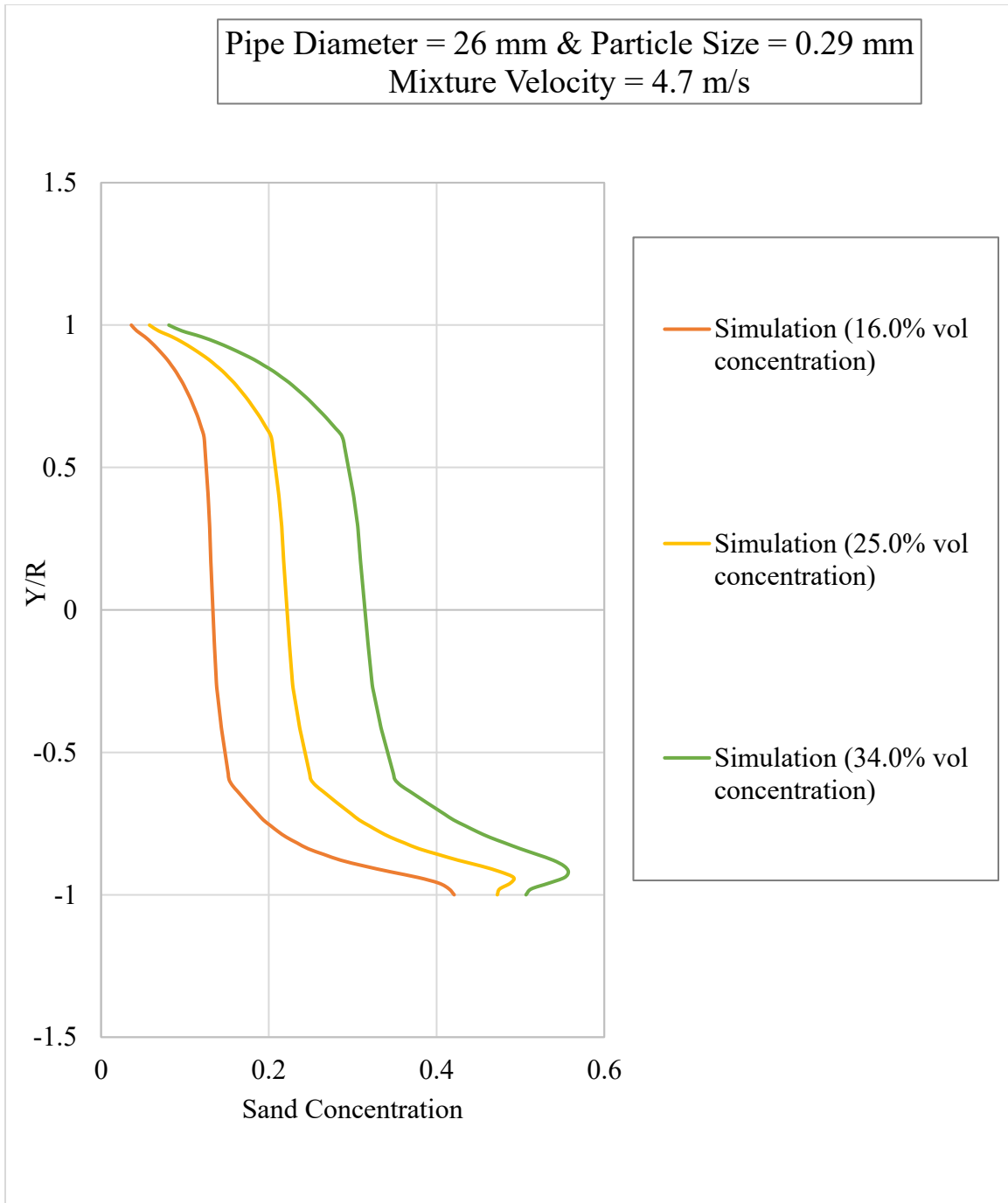


Fig.6. Simulated local volumetric sand concentration across vertical centre line of pipe outlet for particle size of 0.29 mm and mixture velocity of 4.7 m/s at different efflux concentrations.

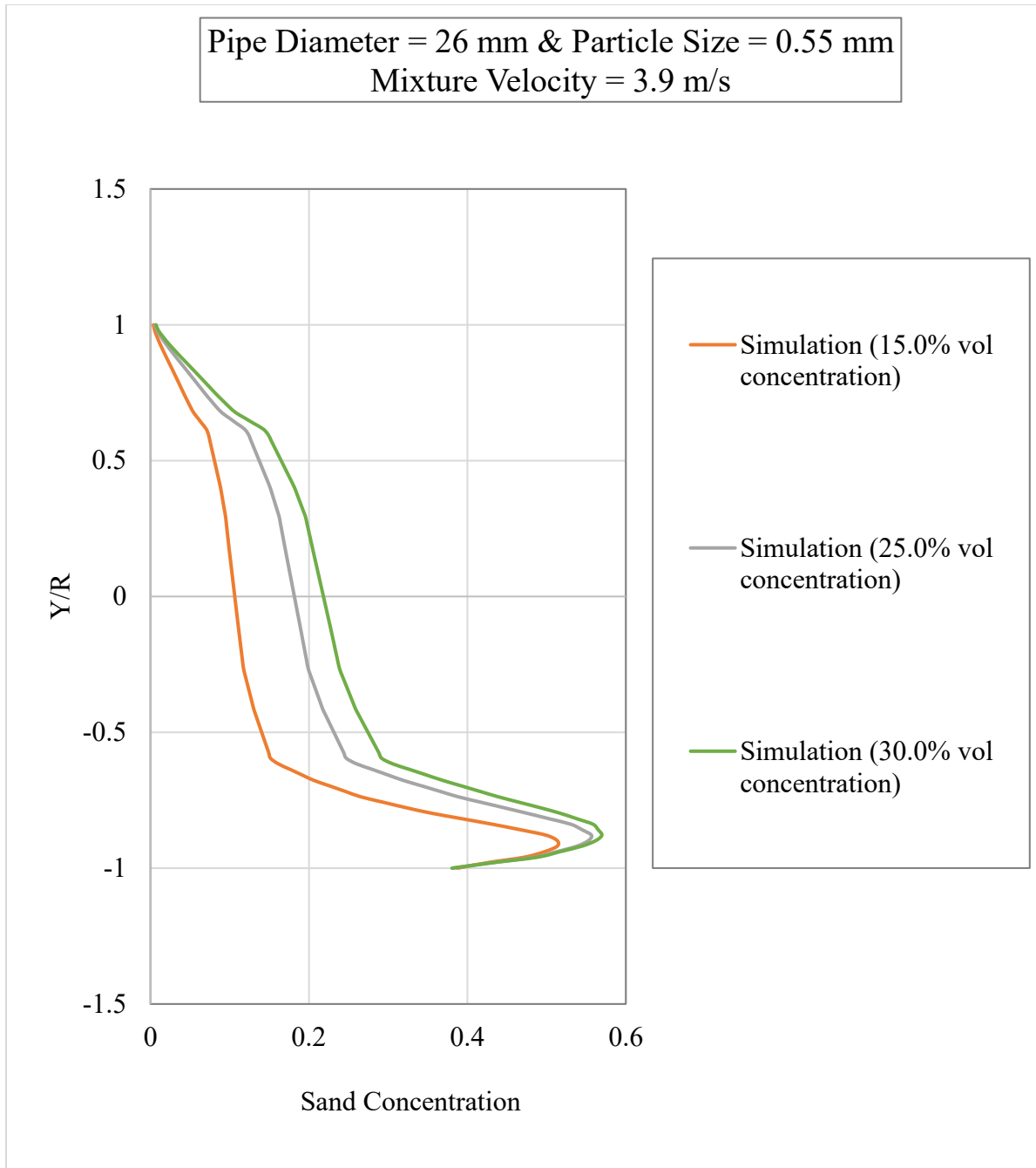
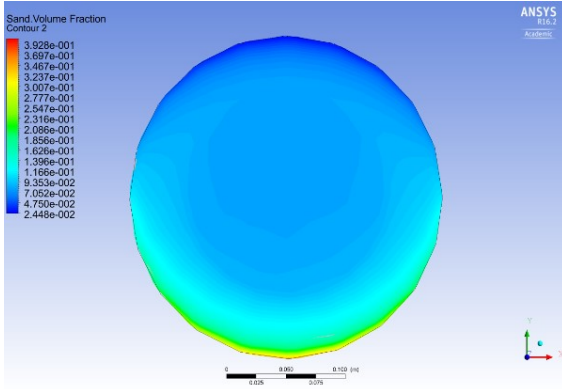
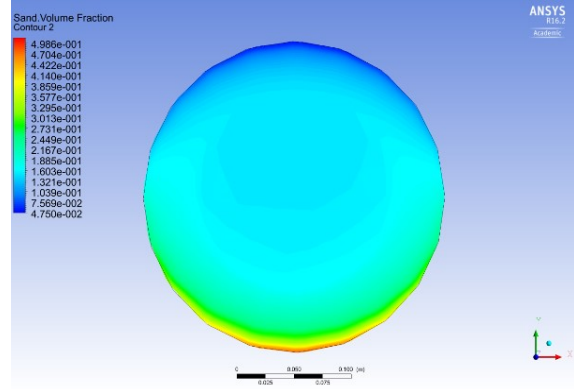


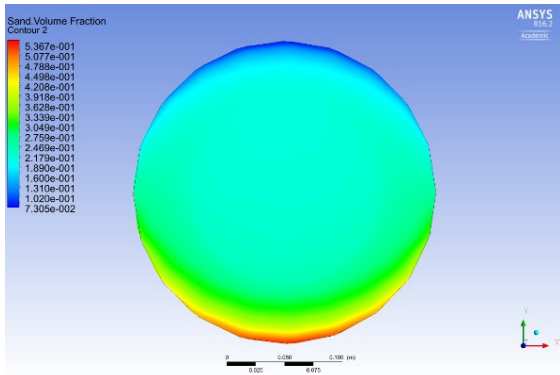
Fig.7. Simulated local volumetric sand concentration across vertical centre line of pipe outlet for particle size of 0.55 mm and mixture velocity of 3.9 m/s at different efflux concentrations.



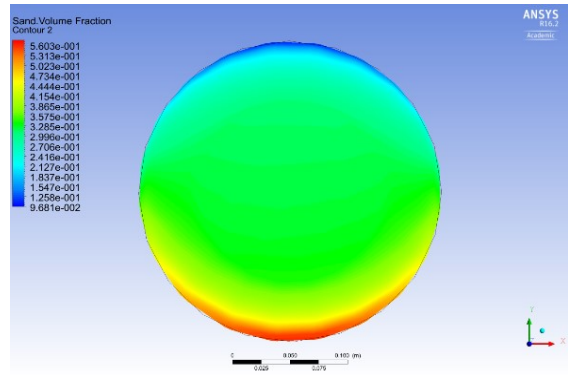
(a) solid volumetric concentration 9.95%



(b) solid volumetric concentration 18.4%



(c) solid volumetric concentration 26.8%



(d) solid volumetric concentration 33.8%

Fig.8. Solid concentration distribution in the vertical plane at outlet for particle size 0.165mm and at 3.5 m/s of mixture velocity.

efflux concentrations. From contour analysis it is clear that the region of highest solid concentration locates very near to the wall in the lower half of pipe cross section.

It is also observed that the spread of highest solid concentration region increases with increase in efflux concentration, particle grain size and mixture velocity but with reduced intensity. Due to similar trends, contours at other velocities and particle sizes have not been shown.

Conclusion

Keeping in mind to develop a widely accepted, reliable, efficient CFD model this paper analyze CFD simulation of two phase (sand-water) slurry flows through 26 mm diameter pipe in horizontal orientation for flow velocity range of 3.5-4.7 m/s and efflux concentration range of 9.95-34% with three particle sizes viz. 0.165 mm, 0.29 mm and 0.55 mm with density 2650 kg/m³. Local volumetric concentration of solid particle at pipe outlet is very well simulated for different combinations of particle size, mixture velocity and efflux concentrations under consideration. Before these analysis, this simulation model is validated with two different experimental results having different boundary conditions from available literatures. This comparison process shows very good agreement with experimental result and validate our model over certain range of operating condition. Mathematical equations of multiphase flow and turbulence models is also added to explain our simulation process with its acceptancy at certain operating conditions.

This study helps to understand two phase slurry flows for different applications. The analysis of local solid concentration can give idea of selecting optimizing range of particle size, volumetric concentration of slurry and mixture velocity during operation. This study can lead to find out 'deposition velocity' in slurry flow. However, scatter in simulation data of various flow parameters especially with bigger particle sizes of slurry indicates that the model used in the present study needs further development. Also it can be seen from figures 3, 6 and 7 that sudden reduction of solid concentration is occurring near wall with higher efflux concentration and particle size, which is not expected practically. This indicates simulation instability near lower wall over a range of efflux concentration and particle size, this needs to be solved. The choice of different coefficients and constants such as coefficient of lift, coefficient of drag, restitution coefficient and wall

boundary conditions needs to be further researched. Also introducing three phase flow adding gas can lead to new findings and benefits with this two phase slurry flow.

References

Alder, B. J., & Wainwright, T. E. (1960). Studies in molecular dynamics. II. Behavior of a small number of elastic spheres. *The Journal of Chemical Physics*, 33(5), 1439-1451.

Anderson, T. B., & Jackson, R. (1967). Fluid mechanical description of fluidized beds. Equations of motion. *Industrial & Engineering Chemistry Fundamentals*, 6(4), 527-539.

Aude, T. C., Thompson, T. L., & Wasp, E. J. (1974). Economics of slurry pipeline systems. *Publication of: Cross (Richard B) Company*, 15(Proc Paper).

Aude, T. C., Thompson, T. L., & Wasp, E. J. (1975). Slurry-pipeline systems for coal; other solids come of age. *Oil Gas J.; (United States)*, 73(29).

Bowen, R. M. (1976). Theory of mixtures. *Continuum physics*, 3(Pt I).

Brown, N. P., & Heywood, N. I. (Eds.). (1991). *Slurry Handling: Design of solid-liquid systems*. Springer Science & Business Media.

Chapman, S., & Cowling, T. G. (1970). *The mathematical theory of non-uniform gases: an account of the kinetic theory of viscosity, thermal conduction and diffusion in gases*. Cambridge university press.

Chen, L., Duan, Y., Pu, W., & Zhao, C. (2009). CFD simulation of coal-water slurry flowing in horizontal pipelines. *Korean journal of chemical engineering*, 26(4), 1144-1154.

Choi, Young-Chan, Park, Tae-Jun, Kim, Jae-Ho, Lee, Jae-Goo, Hong, Jae-Chang, & Kim, Yong-Goo. (2001). Experimental studies of 1 ton/day coal slurry feed type oxygen blown, entrained flow gasifier. *Korean Journal of Chemical Engineering*, 18(4), 493-498.

- Chorin, A. J. (1968). Numerical solution of the Navier-Stokes equations. *Mathematics of computation*, 22(104), 745-762.
- Daly, B. J., & Harlow, F. H. (1970). Transport equations in turbulence. *Physics of Fluids (1958-1988)*, 13(11), 2634-2649.
- Doron, P., Granica, D., & Barnea, D. (1987). Slurry flow in horizontal pipes—experimental and modeling. *International Journal of Multiphase Flow*, 13(4), 535-547.
- Durand, R. (1951). Transport hydraulique de graviers et galets en conduite. *La Houille Blanche*, 609-619.
- Durand, R., & Condolios, E. (1952, November). The hydraulic transport of coal and solid material in pipes. In *Proceedings of Colloquium on Hydraulic Transportation, France*.
- Durand, R., & Condolios, E. (1952). Experimental study on conveying solids in pipes, 2^{eme} journees de l'hydraulique. *Soc. Hydrotech. Fr*, 29.
- Einstein, A. (1906). Zur theorie der brownschen bewegung. *Annalen der physik*, 324(2), 371-381.
- Fu, S., Launder, B. E., & Leschziner, M. A. (1987). Modelling strongly swirling recirculating jet flow with Reynolds-stress transport closures. In *6th Symposium on Turbulent Shear Flows* (pp. 17-6).
- Ghanta, K. C., & Purohit, N. K. (1999). Pressure drop prediction in hydraulic transport of bi-dispersed particles of coal and copper ore in pipeline. *The Canadian Journal of Chemical Engineering*, 77(1), 127-131.
- Gibson, M. M., & Launder, B. E. (1978). Ground effects on pressure fluctuations in the atmospheric boundary layer. *Journal of Fluid Mechanics*, 86(03), 491-511.

- Gidaspow, D., Bezburuah, R., & Ding, J. (1991). *Hydrodynamics of circulating fluidized beds: kinetic theory approach* (No. CONF-920502-1). Illinois Inst. of Tech., Chicago, IL (United States). Dept. of Chemical Engineering.
- Gillies, R. G., Shook, C. A., & Wilson, K. C. (1991). An improved two layer model for horizontal slurry pipeline flow. *The Canadian Journal of Chemical Engineering*, 69(1), 173-178.
- Gillies, R. G., & Shook, C. A. (1994). Concentration distributions of sand slurries in horizontal pipe flow. *Particulate science and technology*, 12(1), 45-69.
- Gillies, R. G., Hill, K. B., Mckibben, M. J., & Shook, C. A. (1999). Solids transport by laminar Newtonian flows. *Powder Technology*, 104(3), 269-277.
- Gopaliya, M. K., & Kaushal, D. R. (2015). Analysis of Effect of Grain Size on Various Parameters of Slurry Flow through Pipeline Using CFD. *Particulate Science and Technology*, 33(4), 369-384.
- Govier, G., & Aziz, K. (1972). *The flow of complex mixtures in pipes*. New York: Van Nostrand Reinhold.
- Hernández, F. H., Blanco, A. J., & Rojas-Solórzano, L. (2008, January). CFD modeling of slurry flows in horizontal pipes. In *ASME 2008 Fluids Engineering Division Summer Meeting collocated with the Heat Transfer, Energy Sustainability, and 3rd Energy Nanotechnology Conferences* (pp. 857-863). American Society of Mechanical Engineers.
- Huilin, Gidaspow, & Bouillard. (2002). Chaotic behavior of local temperature fluctuations in a laboratory-scale circulating fluidized bed. *Powder Technology*, 123(1), 59-68.
- Karabelas, A. J. (1977). Vertical distribution of dilute suspensions in turbulent pipe flow. *AIChE Journal*, 23(4), 426-434.

- Karman, T. V. (1937). The fundamentals of the statistical theory of turbulence. *Journal of the Aeronautical Sciences*, 4(4), 131-138.
- Kaushal, D. R., & Tomita, Y. (2002). Solids concentration profiles and pressure drop in pipeline flow of multisized particulate slurries. *International journal of multiphase flow*, 28(10), 1697-1717.
- Kaushal, D. R., & Tomita, Y. (2003). Comparative study of pressure drop in multisized particulate slurry flow through pipe and rectangular duct. *International Journal of Multiphase Flow*, 29(9), 1473-1487.
- Kaushal, D. R., Sato, K., Toyota, T., Funatsu, K., & Tomita, Y. (2005). Effect of particle size distribution on pressure drop and concentration profile in pipeline flow of highly concentrated slurry. *International Journal of Multiphase Flow*, 31(7), 809-823.
- Krieger, I. M. (1972). Rheology of monodisperse latices. *Advances in Colloid and Interface Science*, 3(2), 111-136.
- Kumar, U. (2002). *Studies on the flow of non-uniform particulate slurries through straight pipes and bends* (Doctoral dissertation).
- Kumar, U., Mishra, R., Singh, S. N., & Seshadri, V. (2003). Effect of particle gradation on flow characteristics of ash disposal pipelines. *Powder technology*, 132(1), 39-51.
- Kumar, U., Singh, S. N., & Seshadri, V. (2008). Prediction of flow characteristics of bimodal slurry in horizontal pipe flow. *Particulate Science and Technology*, 26(4), 361-379.
- Kumar Gopaliya, M., & Kaushal, D. R. (2016). Modeling of sand-water slurry flow through horizontal pipe using CFD. *Journal of Hydrology and Hydromechanics*, 64(3), 261-272.
- Lahiri, S. K., & Ghanta, K. C. (2007). Computational technique to predict the velocity and concentration profile for solid-liquid slurry flow in pipelines. In *The 17th International Conference on the Hydraulic Transport of Solids, Capetown, Southern African*.

- Launder, B. E., Reece, G. J., & Rodi, W. (1975). Progress in the development of a Reynolds-stress turbulence closure. *Journal of fluid mechanics*, 68(03), 537-566.
- Launder, B. E. (1989). Second-moment closure: present... and future?. *International Journal of Heat and Fluid Flow*, 10(4), 282-300.
- Launder, B. E. (1989). Second-moment closure and its use in modelling turbulent industrial flows. *International Journal for Numerical Methods in Fluids*, 9(8), 963-985.
- Lien, F. S., & Leschziner, M. A. (1994). Assessment of turbulence-transport models including non-linear RNG eddy-viscosity formulation and second-moment closure for flow over a backward-facing step. *Computers & Fluids*, 23(8), 983-1004.
- Ling, J., Skudarnov, P. V., Lin, C. X., & Ebadian, M. A. (2003). Numerical investigations of liquid–solid slurry flows in a fully developed turbulent flow region. *International Journal of Heat and Fluid Flow*, 24(3), 389-398.
- Mishra, R., Singh, S. N., & Seshadri, V. (1998). Hydraulic Conveying-Improved Model for the Prediction of Pressure Drop and Velocity Field in Multi-Sized Particulate Slurry Flow through Horizontal Pipes. *Powder Handling and Processing*, 10(3), 279-288.
- Newitt, D. M., Richardson, J. F., Abbott, M., & Turtle, R. B. (1955). Hydraulic conveying of solids in horizontal pipes. *Transactions of the institution of Chemical Engineers*, 33, 93-110.
- O'Brien, M. P. (1933). Review of the theory of turbulent flow and its relation to sediment-transportation. *Eos, Transactions American Geophysical Union*, 14(1), 487-491.
- Patankar, S. (1980). *Numerical heat transfer and fluid flow*. CRC press.

- Pouranfard, A. R., Mowla, D., & Esmailzadeh, F. (2014). An experimental study of drag reduction by nanofluids through horizontal pipe turbulent flow of a Newtonian liquid. *Journal of Industrial and Engineering Chemistry*, 20(2), 633-637.
- Roco, M. C., & Shook, C. A. (1983). Modeling of slurry flow: the effect of particle size. *The Canadian Journal of Chemical Engineering*, 61(4), 494-503.
- Roco, M. C., & Shook, C. A. (1984). Computational method for coal slurry pipelines with heterogeneous size distribution. *Powder Technology*, 39(2), 159-176.
- Rouse, H. (1937). Modern conceptions of the mechanics of fluid turbulence. *Transactions of the American Society of Civil Engineers*, 102(1), 463-505.
- Sarkar, S., & Lakshmanan, B. (1991). Application of a Reynolds stress turbulence model to the compressible shear layer. *AIAA journal*, 29(5), 743-749.
- Schaeffer, D. G. (1987). Instability in the evolution equations describing incompressible granular flow. *Journal of differential equations*, 66(1), 19-50.
- Seshadri, V. (1982). Basic process design for a slurry pipeline. *Proceedings of The Short Term Course on Design of Pipelines for Transporting Liquid and Solid Materials*.
- Seshadri, V., Malhotra, R. C., & Sundar, K. S. (1982). Concentration and size distribution of solids in a slurry pipeline. In *Proc. 11th Natl. Conf. on FMFP, BHEL Hyderabad, India*.
- Shook, C. A., & Daniel, S. M. (1965). Flow of suspensions of solids in pipelines: Part I. Flow with a stable stationary deposit. *The Canadian Journal of Chemical Engineering*, 43(2), 56-61.
- Shook, C. A., & Daniel, S. M. (1965). Flow of suspensions of solids in pipelines: Part I. Flow with a stable stationary deposit. *The Canadian Journal of Chemical Engineering*, 43(2), 56-61.

- Skudarnov, P. V., Lin, C. X., & Ebadian, M. A. (2004). Double-species slurry flow in a horizontal pipeline. *Journal of fluids engineering*, 126(1), 125-132.
- Soliman, R., & Collier, P. (1990). Pressure drop in slurry lines. *Hydrocarbon Processing*, 69(11), Hydrocarbon Processing, 1990, Vol.69 (11).
- Sundqvist, Å., Sellgren, A., & Addie, G. (1996). Slurry pipeline friction losses for coarse and high density industrial products. *Powder technology*, 89(1), 19-28.
- Syamlal, M., Rogers, W., & O'Brien, T. J. (1993). MFIx documentation: Theory guide. *National Energy Technology Laboratory, Department of Energy, Technical Note DOE/METC-95/1013 and NTIS/DE95000031*.
- Thomas, D. G. (1965). Transport characteristics of suspension: VIII. A note on the viscosity of Newtonian suspensions of uniform spherical particles. *Journal of Colloid Science*, 20(3), 267-277.
- Vasquez, S. A., & Ivanov, V. A. (2000, June). A phase coupled method for solving multiphase problems on unstructured meshes. In *Proceedings of ASME FEDSM'00: ASME 2000 fluids engineering division summer meeting, Boston* (pp. 1-6).
- Vlasak, P., Kysela, B., & Chara, Z. (2012). Flow structure of coarse-grained slurry in a horizontal pipe. *Journal of Hydrology and Hydromechanics*, 60(2), 115-124.
- Vocaldo, J. J., & Charles, M. E. (1972, September). Prediction of pressure gradient for the horizontal turbulent flow of slurries. In *2nd International Conference on the Hydraulic Transport of Solids in Pipes, Coventry, UK, Paper* (No. C1, pp. 1-12).
- Wasp, E. J., & Aude, T. C. (1970). Deposition velocities, transition velocities, and spatial distribution of solids in slurry pipelines. In *Presented at the 1st International British*

Hydromechanics Research Association Hydraulic Transport of Solids in Pipes Conference, War Wickshire Univ, Coventry, England, Sept. 1-4, 1970. (No. H4 Proceeding).

Wasp, E. J., Kenny, J. P., & Gandhi, R. L. (1977). Solid-liquid flow: slurry pipeline transportation. [Pumps, valves, mechanical equipment, economics]. *Ser. Bulk Mater. Handl; (United States), 1(4)*.

Weiss, J. M., Maruszewski, J. P., & Smith, W. A. (1999). Implicit solution of preconditioned Navier-Stokes equations using algebraic multigrid. *AIAA journal, 37(1)*, 29-36.

Wilson, K. C. (1976, May). A unified physically-based analysis of solid-liquid pipeline flow. *In Proc. Hydrotransport (Vol. 4, pp. A1-1)*.

Wilson, K. C., Clift, R., & Sellgren, A. (2002). Operating points for pipelines carrying concentrated heterogeneous slurries. *Powder technology, 123(1)*, 19-24.

Appendix 2. A Computational Fluid Dynamics Study of Two-Phase Slurry and Slug Flow in Horizontal Pipelines

Hassn Hadia¹

Rasel A. Sultan¹, M. A. Rahman², John Shirokoff¹, Sohrab Zendehboudi¹

Abstract

This paper presents a Computational Fluid Dynamics (CFD) model to simulate two-phase slurry (water/sand) and slug (water/air) flow systems through utilizing the ANSYS Fluent simulation package. The CFD model is used to forecast the start and growth of the slug phase as well as its effect on horizontal vibrations. Eulerian model with Reynolds Stress Model (RSM) turbulence closure is considered to numerically analyze the slug and slurry flow of mono-dispersed fine particles at high concentrations. The Eulerian model provides fairly acceptable predictions while determining the pressure drop and concentration profile for various effluent concentrations and flow velocities. Furthermore, the optical observations made at the horizontal pipeline flow are used for validation of 3D simulation results for both air/water and water/sand horizontal flow systems where the slug and slurry flow conditions are established. The vibration characteristics of gas/liquid/ solid particles flow patterns in pipelines are also investigated in this work. The outcome of this study can assist engineers and researchers in making better decisions in terms of operation, design, and sizing of two-phase flow systems which have broad applications in subsea oil and gas pipelines.

Keywords: CFD, FLUENT, Pipeline, Slug, Slurry, Vibrations.

INTRODUCTION

The flow in pipeline or annuli are of great importance and widely applied in different industries, such as chemical process and petroleum industries, pipe line engineering, power plants, biomedical

engineering applications, micro-scale fluid dynamics studies, food processing industries, geothermal flows and extrusion of molten plastics [1]. Among all other types of flow, water-solid slurry flow and water-air slug flow have become increasingly popular due to its numerous applications in different industries and enormous focus of society on reduction in environmental pollution. This type of multiphase flow frequently occurs in horizontal pipelines and channels [1].

Liquid-Solid two phase slurry flow has been applied to transport raw materials, waste and sludge which are in solid form [2], beneficiation in extractive metallurgy and mining plants [3], coal processing plants [4], fluidized beds [5], food and chemical plants, petroleum industries and many more. Slurry transportation system helps to reduce traffic, air pollution, noise, accidents along with saving on energy consumption and lesser ecological disturbance. On the other hand, slug flow is caused by aerated slugs of liquid that flow down a pipeline at the same velocity as the gas. Many different operations in an oil field can be at the root of slugging, such as pigging, start-up, blow-down and general transient effects [6]. These problems can occur in the chemical and process industries or in thermo-hydraulic engineering for nuclear power plants [7], but our focus here is on oil and gas production. In these pipelines, multiphase slug flows can develop across a broad range of gas and liquid flow rates and pipe inclinations. Slug initiation, including slug initiation prediction, has been studied by several researchers. In one study, slug initiation prediction is determined by analyzing the stability of a stratified flow in a pipeline [8]. At the same time, computational fluid dynamics (CFD), which is a programming and computation method, is also being applied to investigate the behavior of two-phase flows [9]. Another study looked into slug initiation and growth using a turbulence $k-\epsilon$ model [10]. Unfortunately, however, the modeling of two-phase flows for studying liquid and gas phases is not only time- and labor-intensive, but also intensely difficult due to the involvement of advanced physics and mathematics computations.

Typical issues related to slugging are equipment damage, reduced production, facilities damage, and operational problems with equipment such as pipelines and separator vessels. Given the wide array of these and other potential problems, it is crucial to have a firm grasp not only of the slugging operation itself but also of the mechanisms underlying it.

Phase distribution is a key component when designing engineering structures, mainly due to its impact on the values of parameters like thermal load and pressure drop. It is thus important to know both the system's distribution and flow regime. To that end, dual-phase flow maps can aid in the defining of flow patterns that may occur under different boundary conditions [11]. The main benefit of these mapping tools is that they do not require the user to carry out extensive and complex numerical calculations. Instead, slug movement can be determined by alterations in the liquid slugs and gas bubbles flowing at the top of the liquid films, which combine to form slug units. Slugs moving at a greater velocity than that of average liquid can initiate strong vibrations, causing damage to equipment in the direction and assemblage centers [12]. Slug frequency, which is defined as the number of slugs flowing past a certain point in a pipeline within a certain period of time, is an important factor in determining potential operational difficulties such as pipe vibration and instability, fluctuations in wellhead pressure, and flooding of downstream facilities. Moreover, high slug frequency can cause pipe corrosion [13].

Our study will focus on pipeline vibration caused by unsteady flow, flow directional changes, pipe diameter, etc., in the petroleum, natural gas and chemical industries. Severe pipeline vibrations can impact the operation of pipelines and lead to unsafe and even hazardous conditions. Although pipe vibration is catching the attention of increased numbers of people in the industry, the majority of investigations into the phenomenon thus far have been on pipe vibration due to mechanical vibration sources. The cause of fluid vibration in pipelines has been studied with the help of various

theoretical methods. For the sake of simplification and assumption, some results from some these approaches will be used here as references. Fluid vibration may present in several different forms, such as gas-liquid flow vibration, high-speed flow vibration, fluid pulsation, and flow vibration outside the pipeline [14]. Most existing studies focus on flow-induced vibrations (FIV) (impacts on internal flow from external current), whereas less attention has been allotted to internal flow, slug surge, and external current.

The main aim of the current investigation into issues related to fluid structure interaction (FSI) is to develop a methodology that explains the basic physics of (FSI), along with the impact of the phenomenon on subsea piping parts. The accumulated data from this study (as well as studies in the future) will help to reformulate and revise the FSI model and its capabilities. Potential areas of improvement are to include Reynolds numbers and to show how free stream turbulent intensity levels impact subsea piping [15].

Numerical Method

Conservation Equations in Solid Mechanics

Solid mechanics is a field of physics that investigates how solids react when impacted by external loads.

Elasticity Equations

Fluid structure interactions typically lead to elastic or plastic deformations of solid structures, which is caused by flow-induced forces. Ideally, the material should have an elastic behavior that enables it to regain its original shape (or arrangement) following the application of the load. Although stress can vary linearly, according to strain amount, an elastic deformable solid must

adhere to continuum mechanics. In other words, it must abide by the conservation law that states: the sum of the forces must equal zero [16].

The forces cause a distribution of stress throughout the surface area. So, when a large force is applied, the material might surpass the limitations of the elastic region and thus could fail through fracturing or assuming plastic behavior. The type of stress to which a material is subjected can change according to the location where the force is applied. To resolve the issue of stress components, the most common approach is to apportion the elastic material into smaller elements [16]. The following calculations are intended for normal and shear stresses:

$$\frac{\partial \sigma_x}{\partial x} + \frac{\partial \tau_{xy}}{\partial y} + \frac{\partial \tau_{xz}}{\partial z} + x_b = 0 \quad (1)$$

where ∂ denotes normal stress, τ indicates shear stress, and x_b represents body forces per unit of volume.

Fluid Structure Interaction

Fluid Structure Interaction (FSI) is a multi-physics area that studies the impacts of a flow's pressure fluctuations on a structure in terms of deformation and stress. It also investigates whether a solid structure deformation is too big to change the flow's behavior [16].

Flow-Induced Vibration

If pressure fluctuations against the pipe wall are sufficiently large, fluids being transported through subsea pipes can lead to a phenomenon known as flow-induced vibration (FIV). When dealing with FIV, the pipe's instability is heavily dependent on the pipe's end condition. The type of pipe most susceptible to FIV damage and failure is a straight pipe with fixed ends. If there is breaching of the critical velocity, FIV can cause the pipe to buckle, as shown in the following equation:

$$V_c = \frac{\pi}{L} \left(\frac{EI}{\rho A} \right)^{\frac{1}{2}} \quad (2)$$

where, EI denotes constant flexural rigidity, ρ indicates fluid density, A represents the pipe's internal area, and L and is pipe length [16].

Methodology

Geometry and Mesh.

In this study, numerical simulations were done using a horizontal pipe (3m in length and 0.05m in diameter). Given the importance of the mesh to the numerical solution, the material required specific and exacting characteristics in order to provide a solution that was both feasible and accurate. The Directed Mesh technique in Star-CCM+ was used to develop the material and demonstrated appropriateness for simulating a two-phase flow in the horizontal pipe. More specifically, the Directed Mesh technique was chosen because of its ability to decrease both the computational time and the number of cells in comparison to alternative meshing techniques, as well as its ability to form grids parametrically in a multi-block structure. By employing the path mesh, the user can control and specify the number of divisions in the inlet cross-section, enabling the creation of quadrilateral faces. Furthermore, by applying a novel type of volume distribution, users can specify how many layers they want to have on the pipe. To generate volume mesh, hexahedral grid cells were created through the extrusion of quadrilateral faces along the length of the pipe at each layer as shown in Figure 1. It was determined that a structured hexahedral grid was most appropriate in the present case, as such a grid enabled a fine cross-sectional mesh to be created without also requiring an equivalent longitudinal one. This approach was considered superior, as it offered a faster process convergence. Additionally, as the fluid domains were asymmetrical, a grid independency study was carried out based on the water's superficial velocity

at the outlet. In a multiphase flow, superficial velocity is the ratio of the velocity and the volume fraction of the considered phase. Hence, actual velocity of phase = (Superficial velocity of phase)/(volume fraction of phase).

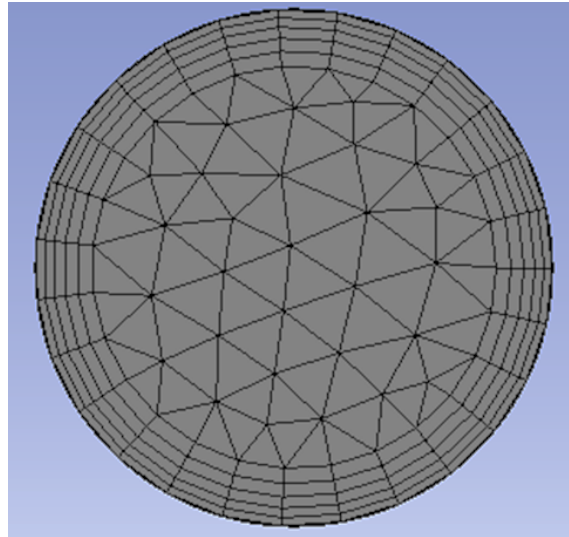


Fig 1. Computational mesh used for simulation

Boundary Conditions

At the gas and liquid inlets, uniform velocity inlets were used as boundary conditions. As well, an atmospheric pressure outlet condition was determined for the outlet to prevent any issues related to backflow at the tube's outlet, and a no-slip boundary condition was applied at the tube walls. The effect of the gravitational force on the flow was also taken into consideration. Overall, the initial volume fraction of gas was altered according to changes in the pipeline's gas velocity.

Convergence criteria

FLUENT is software for simulating flow utilizing pre-stated boundary conditions and a turbulence model. In order to terminate the A iteration, we use a convergence criterion of 10^{-6} . Furthermore, to guarantee the desired degree of accuracy as well as stability and convergence of the iterative

process, we use second-order upwind discretization for the momentum equation, along with a first upwind discretization for volume fraction, turbulent kinetic energy and dissipation.

Results and Simulation

Profiles of Local Solid Concentration

Experimental data from Gillies and Shook (1994) [17] are compared with a local solid concentration profile of water-sand slurry flow from a simulation. The length of the pipe used in the experiment is 2.7 m and the diameter is 53.2 mm. The fluid (water) density is 9982 kg/m^3 , viscosity 0.001003 kg/m-s , while the slurry of Silica has a chemical formula of SiO_2 and a density of 2650 Kg/m^3 . The wall material is aluminum and features a density of 2800 kg/m^3 and a roughness of 0.2 mm . Furthermore, the grain size or mean particle diameter is 0.18 mm , the mixture velocity is 3.1 m/s , and there are three distinct solid volumetric concentrations of 14%, 29% and 45%.

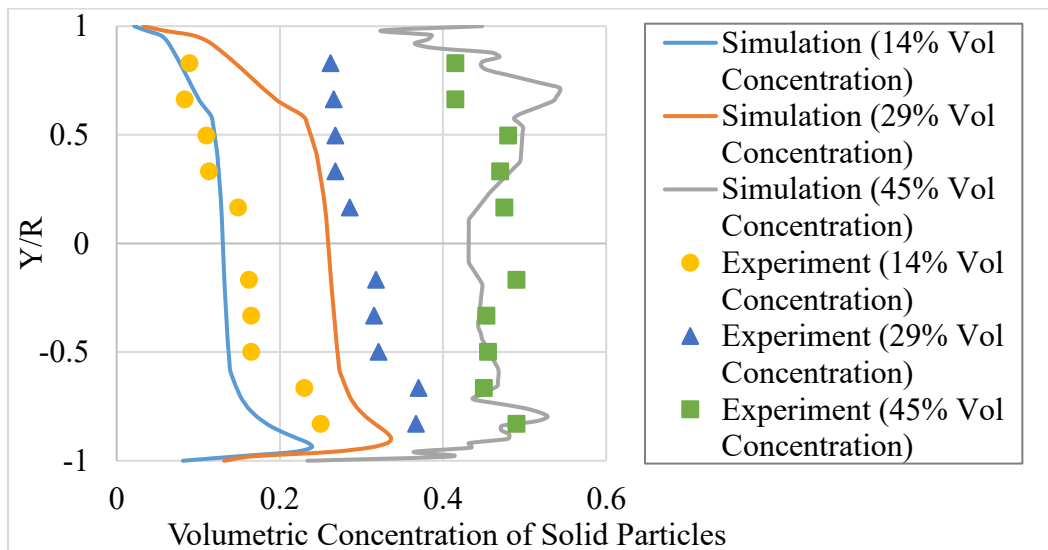


Fig 2. Comparison of simulated and measured values of local volumetric concentration of solid across vertical centerline for particle sizes 0.18 mm.

Figure 2, illustrates a comparison of particle sizes and volumetric concentrations of solid particles. As can be seen, the simulated results show good agreement with the experimental values of grain sizes measuring 0.18 mm, but the simulated values differ somewhat from the experimental values when in close proximity to the wall, particularly in the bottom portion of the cross-section. A potential explanation for this occurrence is abrasive rounding of the large particles due to repeated passages. This could cause fines to be created and uniformly distributed within the pipe, leading to an increase in carrier density. However, because data related to this aspect of the experiment were not available in the reference research, the appropriate adjustments to reflect these data were not made during the simulations.

The deviations might also have resulted from the value of the static settled concentration (packing limit) applied in the simulations. Specifically, the 0.63 value used is most suited to calculations pertaining to very fine grain sizes. To minimize deviations with experimental results, analysis of newer boundary conditions at the wall for slurry pipeline flows should therefore consider larger grain sizes.

Stresses and Deformations

Based on the structural analysis, the horizontal pipe's stresses and deformations were entered into ANSYS. Figure 3 and Figure 4 are showing before and after how the two-phase flow led to a metal pipe displacement of 0.05 m (in diameter) and 3 m (in length).

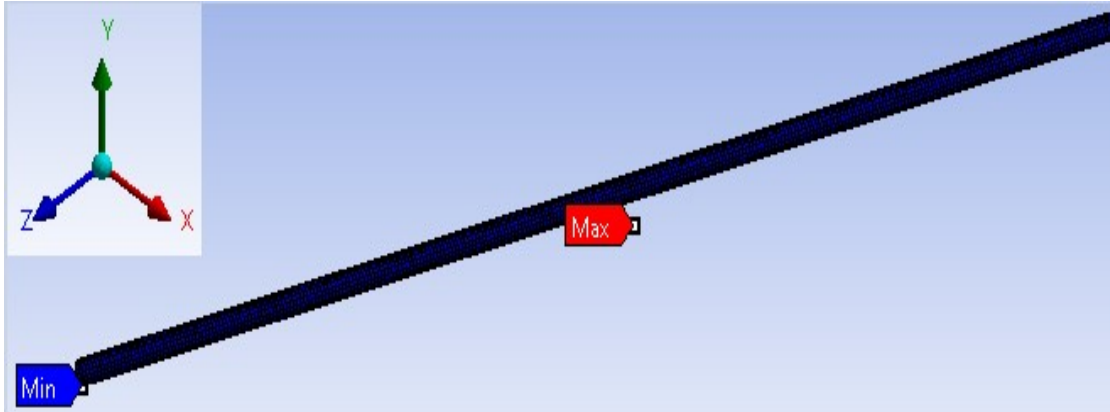


Fig 3. Contour before displacements of the pipe model all view

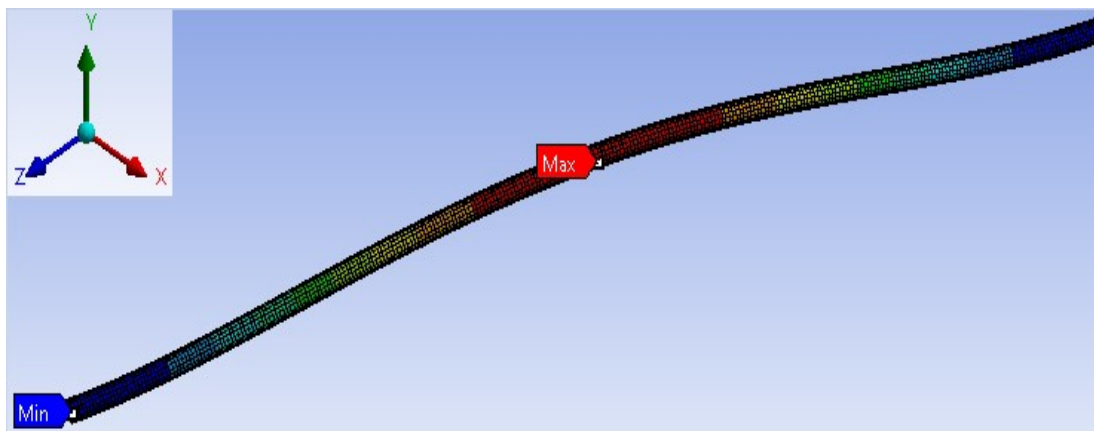


Fig 4. Contour after displacement of the pipe model all view

Conclusion

This work presented a numerical model aimed at achieving the qualitative study of a horizontal pipe's two-phase slug and slurry flows. FLUENT software (computational fluid dynamics [CFD] package) was used in the investigation. Given the large amount of computational operations that would have been required, three-dimensional simulation was simply too costly, so a model simulation was developed based on a Eulerian model and Reynolds stress model (RSM) turbulence. The results demonstrated all of the phenomena related to slug flow in a 3-D model. Overall, the comparison of pressure drops in pressure gradient measurements for both single-and

two-phase flows in horizontal pipes indicate good agreement with the experimental data. Hence, this work adds to the knowledge base around two-phase slurry flows that feature various sized particles.

However, due to some data scatter related to flow parameters (particularly in slurry flows with larger particle sizes), the model applied here requires some revisions. High levels of vibration can be caused by instability arising from two-phase flows (i.e., slug flow), which can then shorten the pipe's fatigue life. Because of the complexity of slug flow behavior, engineers have had difficulty over the years trying to develop a methodology that can anticipate the impact of slugs. Furthermore, the present work demonstrated that the approach has application in problems related to fluid structure interaction in the oil and gas industry. Flow-induced vibration (FIV) is a common occurrence in this industry as a result of the strong coupling of structure and flow. However, assessing hydraulic characteristics and quantitatively investigating pipeline slug flow can benefit from more accurate simulations.

References

- [1]. Dewangan, S. K., & Sinha, S. L. (2016). Exploring the hole cleaning parameters of horizontal wellbore using two-phase Eulerian CFD approach. *The Journal of Computational Multiphase Flows*, 8(1), 15-39.
- [2]. Soliman, R., & Collier, P. (1990). Pressure drop in slurry lines. *Hydrocarbon Processing*, 69(11), *Hydrocarbon Processing*, 1990, Vol.69 (11).
- [3]. Roco, M. C., & Shook, C. A. (1983). Modeling of slurry flow: the effect of particle size. *The Canadian Journal of Chemical Engineering*, 61(4), 494-503.

- [4]. Choi, Young-Chan, Park, Tae-Jun, Kim, Jae-Ho, Lee, Jae-Goo, Hong, Jae-Chang, & Kim, Yong-Goo. (2001). Experimental studies of 1 ton/day coal slurry feed type oxygen blown, entrained flow gasifier. *Korean Journal of Chemical Engineering*, 18(4), 493-498.
- [5]. Huilin, Gidaspow, & Bouillard. (2002). Chaotic behavior of local temperature fluctuations in a laboratory-scale circulating fluidized bed. *Powder Technology*, 123(1), 59-68. Gjgvjgvj
- [6]. Brandstaetter, W., Ragab, A., & Shalaby, S. (2007). Modeling of Two-Phase Flow, and Slug Flow Characteristics in Horizontal/Inclined Pipelines using CFD. Vk
- [7]. Frank, T. (2005, October). Numerical simulation of slug flow regime for an air-water two-phase flow in horizontal pipes. In *Proceedings of the 11th International Topical Meeting on Nuclear Reactor Thermal-Hydraulics (NURETH-11)*, Avignon, France, October (pp. 2-6).
- [8]. Al-Lababidi, S., Addali, A., Yeung, H., Mba, D., & Khan, F. (2009). Gas void fraction measurement in two-phase gas/liquid slug flow using acoustic emission technology. *Journal of Vibration and Acoustics*, 131(6), 064501.
- [9]. Czapp, M., Utschick, M., Rutzmoser, J., & Sattelmayer, T. (2012, July). Investigations on slug flow in a horizontal pipe using stereoscopic particle image velocimetry and CFD simulation with volume of fluid method. In *2012 20th International Conference on Nuclear Engineering and the ASME 2012 Power Conference* (pp. 477-486). American Society of Mechanical Engineers.
- [10]. Razavi, S. Y., & Namin, M. M. (2011). Numerical model of slug development on horizontal two-phase flow. In *Proceedings of the International Conference on Recent Trends in Transportation, Environmental and Civil Engineering* (pp. 14-15).

- [11]. Al-Hashimy, Z. I., Al-Kayiem, H. H., Time, R. W., & Kadhim, Z. K. (2016). Numerical Characterisation of Slug Flow in Horizontal Air/water Pipe Flow. *International Journal of Computational Methods and Experimental Measurements*, 4(2), 114-130.
- [12]. Taitel, Y., & Dukler, A. E. (1976). A model for predicting flow regime transitions in horizontal and near horizontal gas-liquid flow. *AIChE Journal*, 22(1), 47-55.
- [13]. Ghorai, S., & Nigam, K. D. P. (2006). CFD modeling of flow profiles and interfacial phenomena in two-phase flow in pipes. *Chemical Engineering and Processing: Process Intensification*, 45(1), 55-65.
- [14]. Tan ping, Fu Xingjun et al. Study on Vibration of Conveying Water Piping System in Power Plant, *Turbine technology*, Vol .46, No.2, 2004.
- [15]. Chica, L., Pascali, R., Jukes, P., Ozturk, B., Gamino, M., & Smith, K. (2012, July). Detailed FSI Analysis Methodology for Subsea Piping Components. In *ASME 2012 31st International Conference on Ocean, Offshore and Arctic Engineering* (pp. 829-839). American Society of Mechanical Engineers.
- [16]. Chica, L. (2014). FSI study of internal multiphase flow in subsea piping components (Doctoral dissertation, University of Houston).

Appendix 3. CFD and Experimental Approach on Three Phase Gas-Liquid-Solid Newtonian Fluid flow in Horizontal Pipes

Rasel A Sultan ¹, Serag Alfarek ¹, M. A. Rahman ², Sohrab Zendehboudi ¹

¹ Faculty of Engineering and Applied Science, Memorial University of Newfoundland, Canada

² Petroleum Engineering Program, Texas A&M University at Qatar, Qatar

Abstract

This study analyses three-dimensional fluid flow through horizontal pipelines with three-phase gas-liquid-solid Newtonian fluids by Computational Fluid Dynamics (CFD) simulation. Validating the simulation with experimental data, the study aims to develop a versatile acceptable simulation model that can be used further for different applied cases. An experimental setup is developed in our laboratory to determine slug flow (air-water) through a horizontal pipeline. Air as gas, water as liquid and silica as solid particle is used in this work. ANSYS Fluent version 16.2 is employed to perform the simulation. The Eulerian multiphase model with the Reynolds Stress Model (RSM) turbulence closure is adopted to analyse multiphase fluid flow. Parameters are selected from experimental works to validate the simulation. After a good agreement with experimental data, sensitivity analysis is conducted to observe the three phase fluid flow characteristics through horizontal flow. Pressure gradient (pressure drop per unit length) and in situ concentration profile are used as primary parameters. This article provides a clear relationship between the different parameters of three-phase fluid flow through a horizontal pipeline.

Keywords: CFD; Three Phase Flow; Slurry Flow; Slug Flow; Experimental Setup; Pressure Gradient; Pipeline.

Introduction

Flow through pipelines or annuli has a great impact and is widely applied in the oil and gas industry to recover produced formation from deep water or core [1]. Multiphase phase gas-liquid-solid flow has been applied from the beginning.

Liquid-solid two-phase slurry flow has been applied to the transport of raw materials, waste and sludge which are in solid form, coal processing plants, fluidized beds, food and chemical plants, the petroleum industry and many more. The slurry transportation system helps to reduce traffic, air pollution, noise and accidents along with providing savings on energy consumption and lesser ecological disturbance.

On the other hand, slug flow is caused by aerated slugs of liquid that flow down a pipeline at the same velocity as the gas. Many different operations in an oil field can be at the root of slugging, such as pigging, start-up, blow-down and general transient effects. These problems can occur in the chemical and process industries or in thermo-hydraulic engineering for nuclear power plants, but our focus here is on oil and gas production. Slug initiation, including slug initiation prediction, has been studied by several researchers. In one study, slug initiation prediction is determined by analysing the stability of a stratified flow in a pipeline [3]. At the same time, the computational fluid dynamics (CFD) method, is also being applied to investigate the behaviour of two-phase flows [4].

Adding solid particles in the two-phase air-water flow reduces drag, that helps the pipeline system by saving pumping power, increasing flow rate or decreasing size of the pump and has a cost-saving effect [5]. Adding air or air injection in the two-phase slurry system also reduces the pumping cost in oil-fields [6]. There are very few studies and limited research in this field with

three phase air-water-gas flow. Some of those studies are by Scott and Rao (1971) [7], Toda et al. (1978) [8], Fukuda and Shoji (1986) [9], Kago et al. (1986) [10], Toda and Konno (1987) [11] Gillies et al. (1997) [12], Mao et al. (1997) [2], Bello et al. (2010) [13], Rahman et al. (2013) [14] and Pouranfard et al. (2015) [5]. These are all experimental studies, mainly focused on measuring pressure gradient, deposition velocity, in situ concentration of each phase for a wide range of operating conditions. CFD simulation related works are very rare and constitute a new addition in this field. For numerical simulation studies with solid-liquid-gas three phase flow, see Annaland et al. (2005) [15], Washino et al. (2011) [16] and Liu et al. (2015) [17].

The literature of three-phase flow in pipeline or annuli shows meager interest among researchers. Very few experimental and empirical studies of three-phase flow are available [18]. Those few works represent a narrow range of operating conditions and are incomplete due to having the minimum number of measurements. In some studies, pressure drop and velocity profile are measured but there is no flow regime information, while other studies have an in situ gas solid concentration profile but no pressure loss information.

In this study, comparisons of CFD simulation with experimental studies are performed in different conditions and ranges with horizontal pipes. A few experiments are conducted in a flow loop installed in the fluid mechanics facility at Memorial University. Pressure readings at the inlet and outlet of certain geometry are obtained via a sensor, which transmits the signal to software capable of monitoring pressure as well as other parameters like temperature and flow rate. After verifying our simulation model, sensitivity analysis is conducted with a wide range of variables to minimize the limitation of applications in real life.

The Eulerian granular model has been adopted as a multiphase model for the present study. The selection of an appropriate multiphase model depends mainly on the range of the volume fraction (α) of the solid phase under consideration. Since high value of volume fractions is used in this study this model is considered.

The description of multiphase flow as interpenetrating continua incorporates the concept of phasic volume fractions, denoted here by a_q .

The volume of phase q , V_q , is defined by:

$$V_q = \int a_q dV \quad (1)$$

Where,

$$\sum_{q=1}^n a_q = 1 \quad (2)$$

The effective density of phase q is:

$$\hat{\rho}_q = a_q \rho_q \quad (3)$$

Where, ρ_q is the physical density of phase q .

The equations for fluid-fluid and granular multiphase flows, are presented here for the general case of an n -phase flow.

The volume fraction of each phase is calculated from a continuity equation as below:

$$\frac{1}{\rho_{r,q}} \left\{ \frac{\partial}{\partial t} (a_q \rho_q) + \nabla \cdot (a_q \rho_q \vec{v}_q) \right\} = \sum_{p=1}^n (\dot{m}_{pq} - \dot{m}_{qp}) \quad (4)$$

Where, ρ_{rq} is the phase reference density, or the volume averaged density of the q^{th} phase in the solution domain, \dot{m}_{pq} characterizes the mass transfer from the p^{th} to q^{th} phase and \dot{m}_{qp} characterizes the mass transfer from the q^{th} to p^{th} phase.

The conservation of momentum for a fluid phase q is:

$$\begin{aligned} \frac{\partial}{\partial t}(a_q \rho_q \overrightarrow{\vartheta}_q) + \nabla \cdot (a_q \rho_q \overrightarrow{\vartheta}_q \overrightarrow{\vartheta}_q) &= -a_q \nabla p + \nabla \cdot \overline{\overline{\tau}}_q + a_q \rho_q \overrightarrow{g} \\ &+ \sum_{p=1}^n \{K_{pq}(\overrightarrow{\vartheta}_p - \overrightarrow{\vartheta}_q) + \dot{m}_{pq} \overrightarrow{\vartheta}_{pq} - \dot{m}_{qp} \overrightarrow{\vartheta}_{qp}\} \\ &+ (\overline{\overline{F}}_q + \overrightarrow{F}_{lift,q} + \overrightarrow{F}_{vm,q}) \end{aligned} \quad (5)$$

Here, \overrightarrow{g} is the acceleration due to gravity, $\overline{\overline{\tau}}_q$ is the q^{th} phase stress-strain tensor, $\overline{\overline{F}}_q$ is an external body force, $\overrightarrow{F}_{lift,q}$ is a lift force, and $\overrightarrow{F}_{vm,q}$ is a virtual mass force.

Following the work of Alder and Wainwright (1960) [22] and Syamlal et al. (1993) [23], a multi-fluid granular model is used to describe the flow behaviour of a fluid-solid mixture.

The conservation of momentum for the solid phases is:

$$\begin{aligned} \frac{\partial}{\partial t}(a_s \rho_s \overrightarrow{\vartheta}_s) + \nabla \cdot (a_s \rho_s \overrightarrow{\vartheta}_s \overrightarrow{\vartheta}_s) &= -a_s \nabla p - \nabla p_s + \nabla \cdot \overline{\overline{\tau}}_s \\ &+ \sum_{l=1}^N \{K_{ls}(\overrightarrow{\vartheta}_l - \overrightarrow{\vartheta}_s) + \dot{m}_{ls} \overrightarrow{\vartheta}_{ls} - \dot{m}_{sl} \overrightarrow{\vartheta}_{sl}\} + (\overline{\overline{F}}_s + \overrightarrow{F}_{lift,s} + \overrightarrow{F}_{vm,s}) \\ &+ (\overline{\overline{F}}_s + \overrightarrow{F}_{lift,s} + \overrightarrow{F}_{vm,s}) \end{aligned} \quad (6)$$

Where, p_s is the s^{th} solids pressure, $K_{ls} = K_{sl}$ is the momentum exchange coefficient between fluid or solid phase l and solid phase s , and N is the total number of phases.

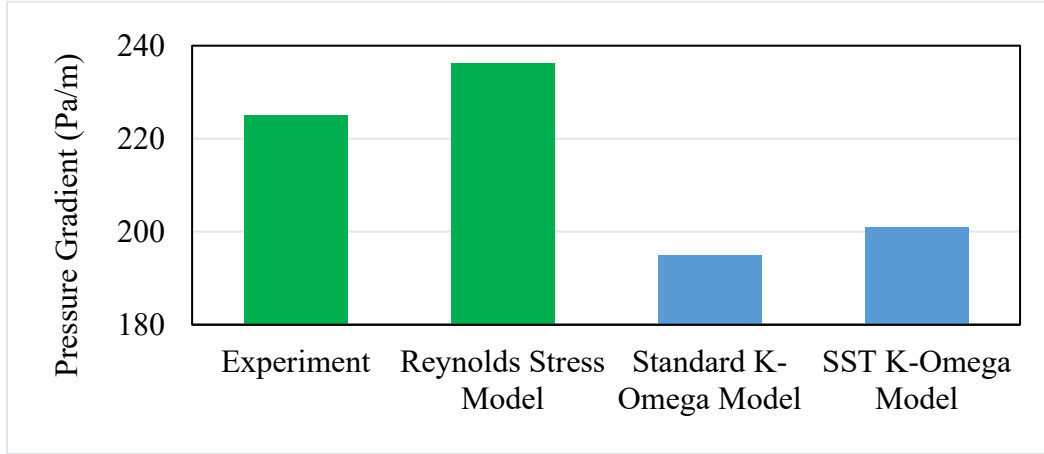


Figure 1. Optimum turbulence model analysis

Previous studies and literature indicate few comparisons between all the turbulence models like Reynolds-averaged Navier–Stokes (RANS) models: $k-\Omega$, $k-\varepsilon$ and Reynolds stress model (RSM) and Large eddy simulation (LES) for steady fluid flow through pipelines or annuli [24, 25]. Among all these turbulence models, the Reynolds stress model (RSM) is optimum to use for turbulence flow through a simple pipe. An analysis of different turbulence models is conducted using data from Kaushal et al. (2005) [26] to find the optimum model for further investigations. In Figure 1, single phase water velocity of 1 m/s is maintained through horizontal pipeline. The analysis shows the RSM as the most optimum model with least error. Considering the above points turbulent quantities for fluid flow are assumed using RSM. Abandoning the isotropic eddy-viscosity hypothesis, the RSM closes the Reynolds-averaged Navier-Stokes equation by solving the transport equations for the Reynolds stresses, together with an equation for the dissipation rate.

The exact transport equation for the Reynolds stress model (RSM) is as below:

$$\begin{aligned}
& \underbrace{\frac{\partial}{\partial t}(\rho \overline{u'_i u'_j})}_{\text{Local Time Derivative}} + \underbrace{\frac{\partial}{\partial x_k}(\rho u_k \overline{u'_i u'_j})}_{\text{Convection } (C_{ij})} = \underbrace{-\frac{\partial}{\partial x_k} \left[\rho \overline{u'_i u'_j u'_k} + p (\delta_{kj} u'_i + \delta_{ik} u'_j) \right]}_{\text{Turbulent Diffusion } (D_{T,ij})} \\
& + \underbrace{\frac{\partial}{\partial x_k} \left[u \frac{\partial y}{\partial x_k} (\overline{u'_i u'_j}) \right]}_{\text{Molecular Diffusion } (D_{L,ij})} - \underbrace{\rho \left(\overline{u'_i u'_k} \frac{\partial u_j}{\partial x_k} + \overline{u'_j u'_k} \frac{\partial u_i}{\partial x_k} \right)}_{\text{Stress Production } (P_{ij})} - \underbrace{\rho \beta (g_i \overline{u'_j \theta} + g_j \overline{u'_i \theta})}_{\text{Buoyancy Production } (G_{ij})} \\
& + \underbrace{p \left(\frac{\partial u'_i}{\partial x_j} + \frac{\partial u'_j}{\partial x_i} \right)}_{\text{Pressure Strain } (\Phi_{ij})} - \underbrace{2\mu \frac{\partial u'_i}{\partial x_k} \frac{\partial u'_j}{\partial x_k}}_{\text{Dissipation } (\epsilon_{ij})} \tag{7} \\
& \underbrace{-2\rho \Omega_k (\overline{u'_j u'_m} \epsilon_{ikm} + \overline{u'_i u'_m} \epsilon_{jkm})}_{\text{Production by system Rotation } (F_{ij})} + \underbrace{S_{user}}_{\text{User-Defined Source}}
\end{aligned}$$

Of the various terms in these exact equations, C_{ij} , $D_{L,ij}$, P_{ij} and F_{ij} do not require any modelling.

However, $D_{T,ij}$, G_{ij} , Φ_{ij} and ϵ_{ij} need to be modelled to close the equations. $D_{T,ij}$ can be modelled

by the generalized gradient-diffusion model of Daly and Harlow (1970) [27]:

$$D_{T,ij} = C_s \frac{\partial}{\partial x_k} \left(\rho \frac{\overline{ku'_k u'_l}}{\epsilon} \frac{\partial \overline{u'_i u'_j}}{\partial x_l} \right) \tag{8}$$

The expression for G_{ij} for ideal gases is as follows:

$$G_{ij} = -\frac{\mu_t}{\rho Pr_t} \left(g_i \frac{\partial \rho}{\partial x_j} + g_j \frac{\partial \rho}{\partial x_i} \right) \tag{9}$$

Where, Pr_t is the turbulent Prandtl number for energy, with a default value of 0.85 used in the simulation.

The pressure-strain term, Φ_{ij} , is modelled according to the proposal by Gibson and Launder (1978) [28], and Launder (1989) [29].

The classical approach to modelling Φ_{ij} uses the following decomposition:

$$\Phi_{ij} = \Phi_{ij,1} + \Phi_{ij,2} + \Phi_{ij,w} \quad (10)$$

Where, $\Phi_{ij,1}$ is the slow pressure-strain term, also known as the return-to-isotropy term, $\Phi_{ij,2}$ is the rapid pressure-strain term, and $\Phi_{ij,w}$ is the wall-reflection term.

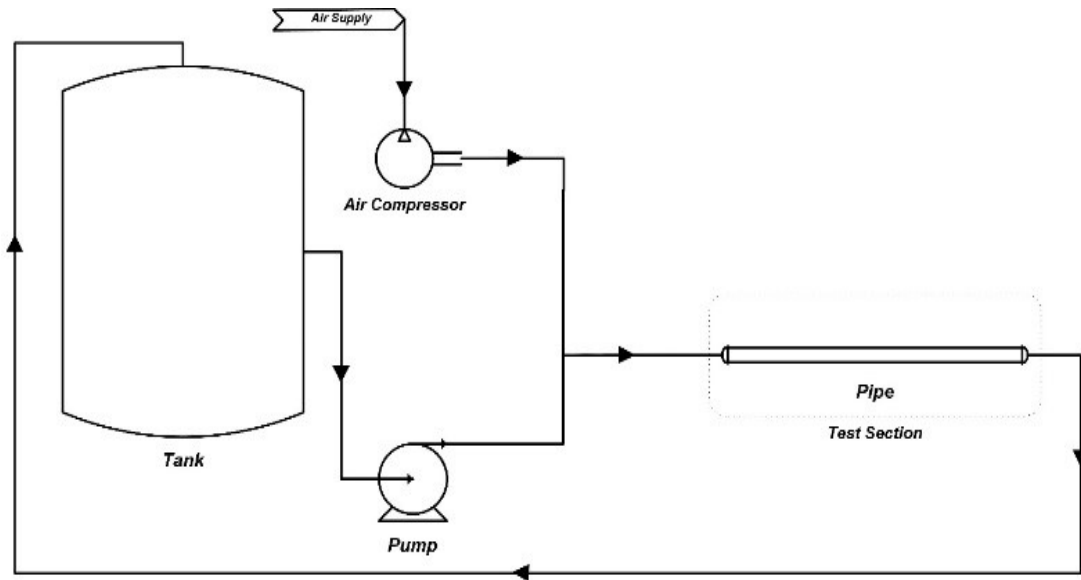
The dissipation tensor, ϵ_{ij} , is modelled as:

$$\epsilon_{ij} = \frac{2}{3} \delta_{ij} (\rho \epsilon + Y_M) \quad (11)$$

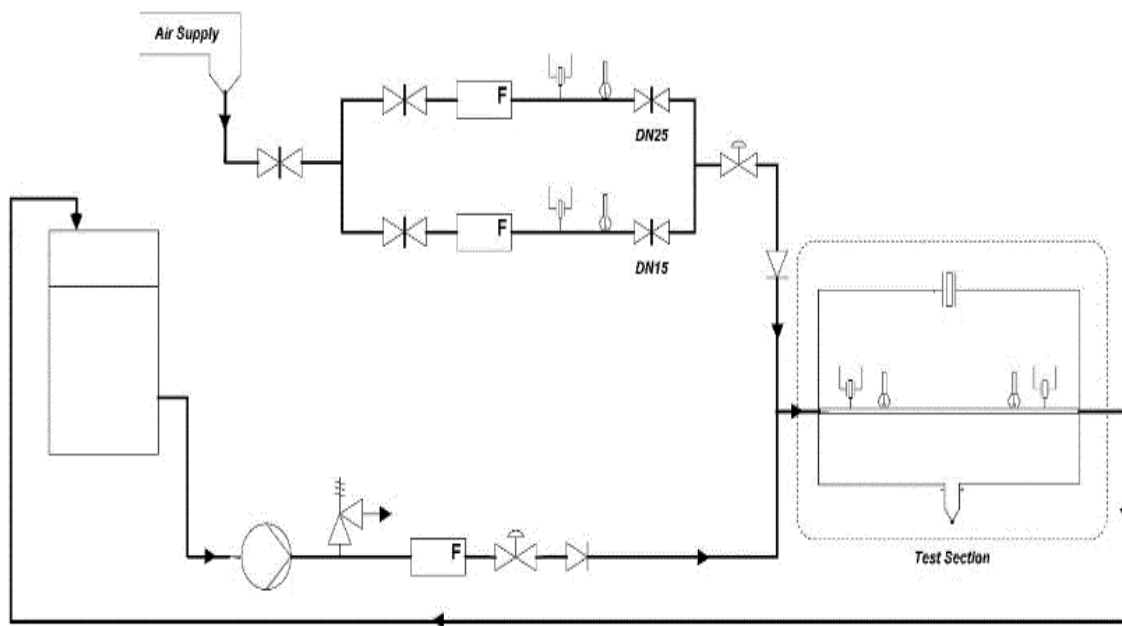
Where, $Y_M = 2\rho\epsilon M_t^2$ is an additional "dilatation dissipation" term according to the model by Sarkar and Lakshmanan (1991) [30].

Experimental Procedure

The existing flow loop at Memorial University is a 65-meter pipe open-cycle system. The liquid can be pumped from the tank through the DN 80 (3-inch pipe). The experimental flow loop set-up starts with an approximately 5-m-long clear horizontal test section, followed by 5-m-vertical clear section and a consecutive variable inclination of a 3-m test section. These horizontal, vertical and inclined pipe sections are installed in transparent PVC pipe for visualization. Instrumentation includes several pressure and temperature sensors and flow meters for the gas and pipe line to measure the individual gas and liquid flow rates. The air injection pipe is split into two different sizes, DN 15 (0.5 inch) and DN 25 (1 inch), for different volumes of air flow. Electro-pneumatic control valves are installed in the liquid and airline to facilitate control of the flow conditions and to generate different flow regimes. The control of a flow loop is implemented through a fully integrated online computer system, which also handles the data acquisition. Here in this work, data for air-water two phase slug flow through a horizontal test section will be used. Figure 2 shows the experimental setup.



(a)



(b)

Figure 2. Experimental set-up of the multiphase flow loop. (a) Simplified diagram; (b) Schematic diagram

Table 1 lists the symbols used to outline the experimental set-up.

Table 1. Symbols used in flow loop (P&ID legend)

| <u>Valves</u> | <u>Instruments</u> | <u>Equipment</u> |
|---|---|--|
|  Gate valve |  Flow meter |  Air compressor |
|  Pneumatic valve |  Pressure sensor |  Centrifugal pump |
|  Check valve |  Thermocouple |  Tank |
|  Relief valve |  dP cell sensor | |
| |  Manometer | |

Simulation methodology

The computational grids for horizontal pipe are generated using ANSYS Fluent. Meshing is finalized after conducting proper mesh independency check. Inflation is added near the wall to observe more precisely the characteristics of different parameters near the wall. Shear stress between wall surface and gas molecules is much higher and this inflation helps to create denser meshing near wall. The length of the pipe is sufficient enough in this study to achieve a fully developed flow at the outlet as minimum flow development section should be at least 50D (D = internal diameter of pipe) [31]. One of the computational grid distributions of the pipe geometry is shown in Figure 4.

ANSYS Inc. Fluent, ver. 16.2, ANSYS Inc. is used to build a CFD simulation model of pipeline flow. A convergence value of 10^{-5} has been adopted for termination of iteration, this value is selected by optimizing analysis to have the most satisfactory accuracy with less time. Figure 3 shows an analysis to discover the optimum convergence rate (between a range of 10^{-4} to 10^{-6}) using

parameters (inlet velocity) from the experiment. SIMPLE algorithm is applied with the first and second order upwind discretization method to have stability and confirm convergence in the governing equations. Upwind discretization is a method that simulates numerically the direction of the normal velocity in the flow field.

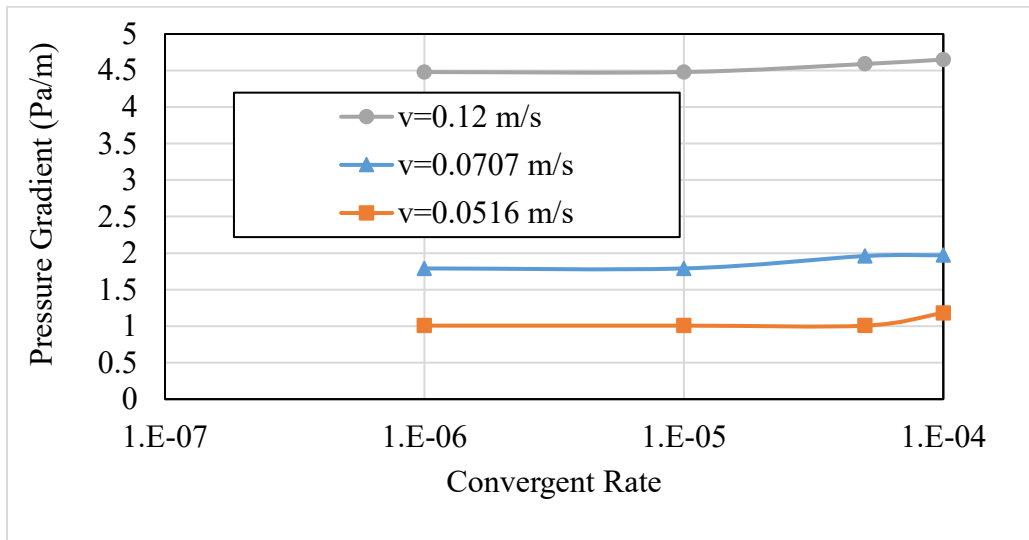


Figure 3. Optimum convergence rate analysis

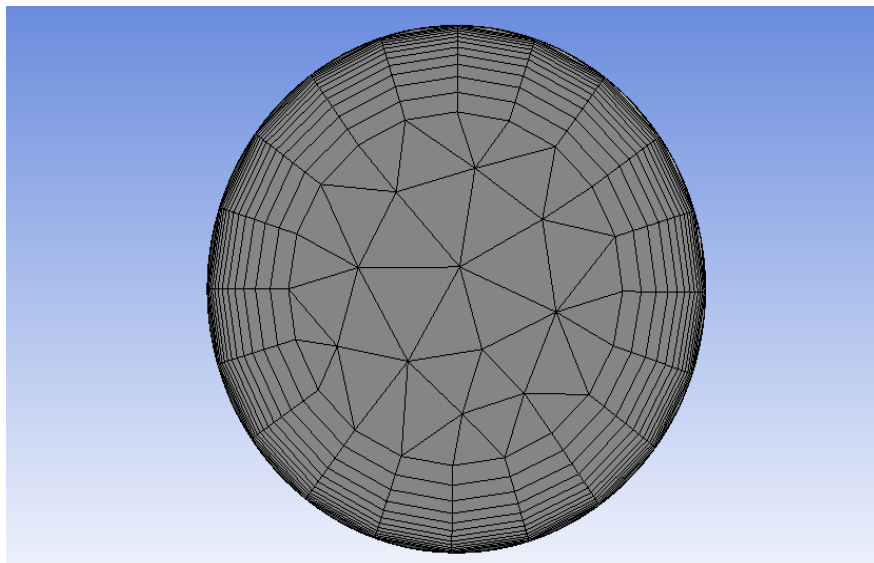


Figure 4. Mesh distribution (cross section)

Result and discussion

Validation

Two-phase air-water slug flow through an experimental flow loop at our laboratory is used to validate the CFD model. The data acquisition system used in the flow loop was designed by using Lab-VIEW 7.0. The program has a graphical user interface; Lab-VIEW interprets the incoming signals from the flow meter, thermocouple and pressure sensors. Geometry and other parameters in the CFD simulation are used according to experimental setup described in the experimental procedure section. Fluid are taken: water (density 998.2 Kg/m^3 , viscosity 0.001 Kg/m-s) and air (density 1.225 kg/m^3 , viscosity $1.789 \cdot 10^{-5} \text{ Kg/m-s}$). Figure 5 demonstrates the pressure gradients are different for different water inlet velocity with constant gas inlet velocity (0.69 m/s).

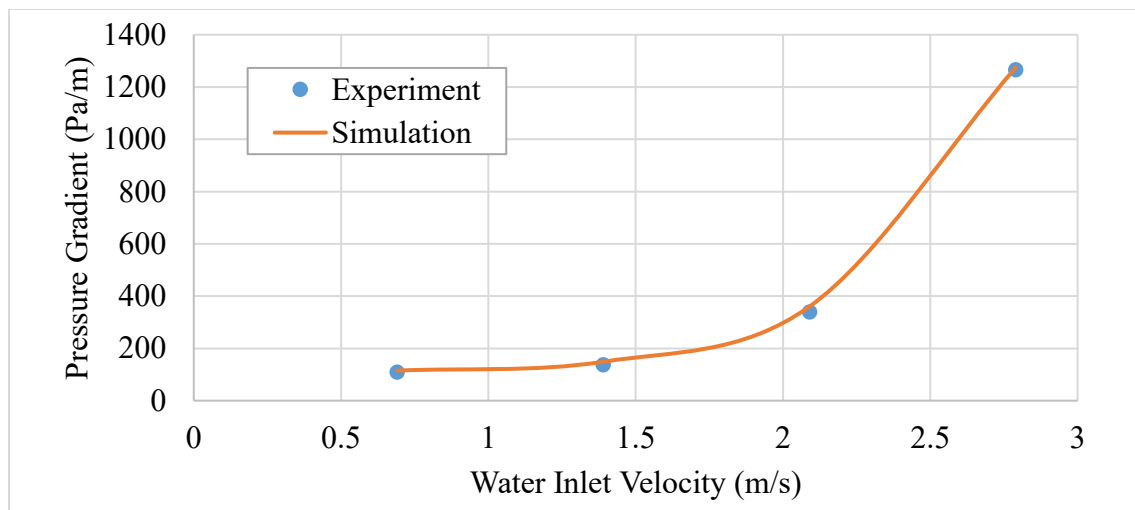


Figure 5. Comparison of pressure gradient as a function of water velocity

The local solid concentration profile of water-sand slurry flow from the simulation is compared with Roco and Shook's (1983) [32] experimental data in Figure 6. Here, the length of the pipe is 13.15 m, its diameter is 263 mm, fluid is taken: water (density 998.2 kg/m^3 , viscosity 0.001003 kg/m-s) and slurry taken silica (chemical formula SiO_2 , density 2650 kg/m^3) and wall material is

aluminium (density 2800 kg/m³, roughness 0.2 mm). Grain size or mean particle diameter is 0.165 mm with mixture velocity 3.5 m/s and four different solid volumetric concentrations: 9.95%, 18.4%, 26.8% and 33.8% respectively.

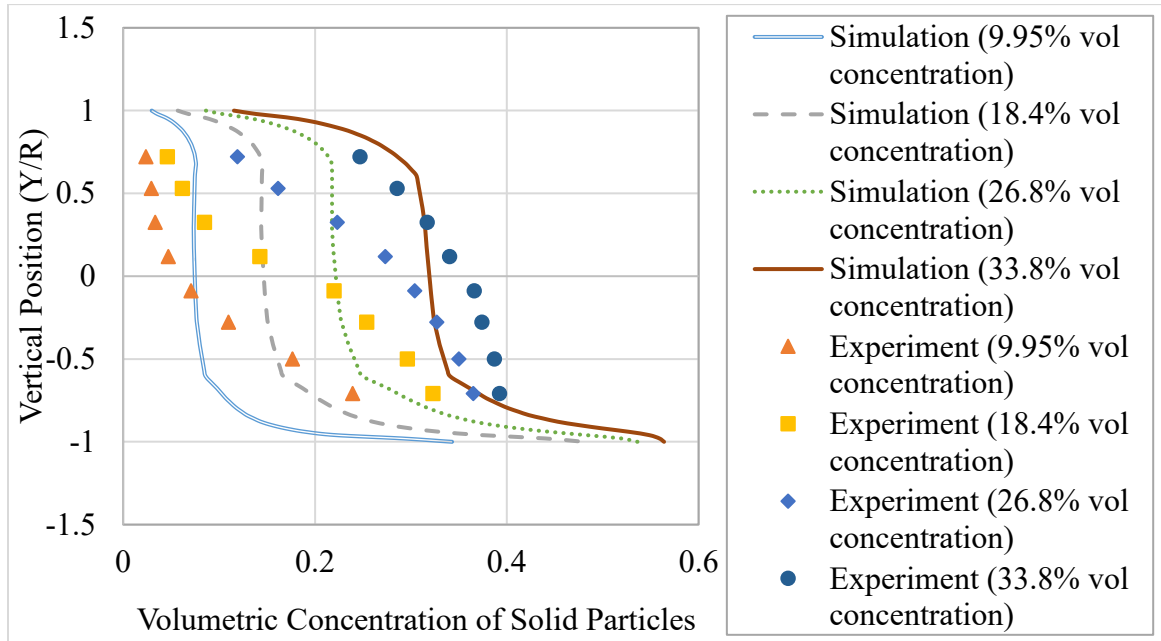


Figure 6. Comparison of simulated and measured values of local volumetric concentration of solid across vertical centreline

The simulated results are in good agreement with the experimental values. However, the simulated values deviate from the experimental values. One probable reason for these deviations could be the approximate value of the static settled concentration (packing limit) used during simulations, as the value of 0.63 used is best suited to finer grain sizes only.

The pressure gradient of air-water-sand three-phase flow from the simulation is compared with Fukuda and Shoji's (1986) [12] experimental data. In the experiment length of the pipe is 2.9 m, its diameter is 0.0416 m, fluids are taken: water (density 998.2 kg/m³, viscosity 0.001 kg/m-s), silica sand particle (density 2650 kg/m³, mean particle diameter 74 μm) and air (density 1.225

kg/m³, viscosity 1.789×10^{-5} kg/m-s). The pipe wall material is polycarbonate pipe (transparent, smooth pipe). Figure 7 shows a comparison of the pressure gradient with the solid volume concentration (C_v): 24.7% in slurry and 3 m/s slurry velocity at different gas velocities. In Figure 7, the average deviation of simulation data from experimental data is 2.1%, considering each point with maximum 4.26% error at 1.36 m/s gas velocity in the pipeline. This shows very good agreement (comparable error) with experiment.

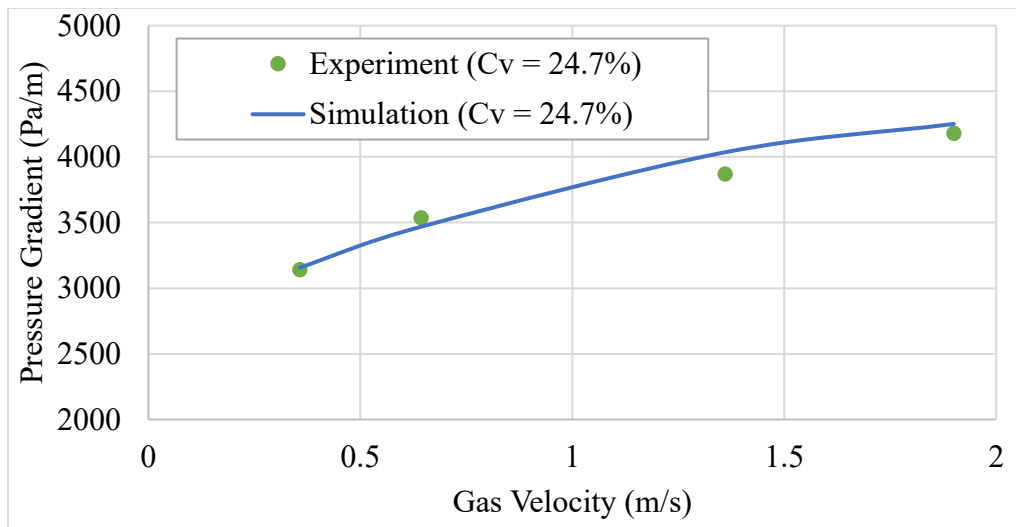
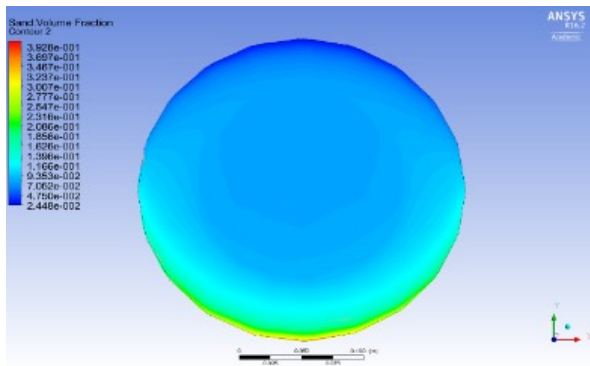


Figure 7. Comparison of pressure gradient as a function of gas velocity

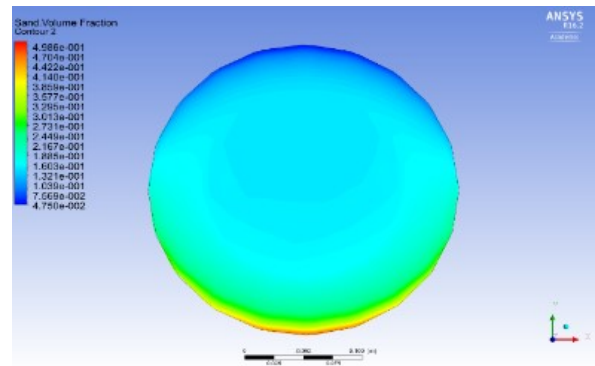
Parametric Analysis

After demonstrating very good and acceptable agreement of simulation with reference experimental results, the approach is to analyse the flow behaviour at different condition of independent parameters that affect multiphase flow through pipelines. In situ concentrations of solid and diameter of pipeline are considered here as independent variables that can affect flow behaviour.

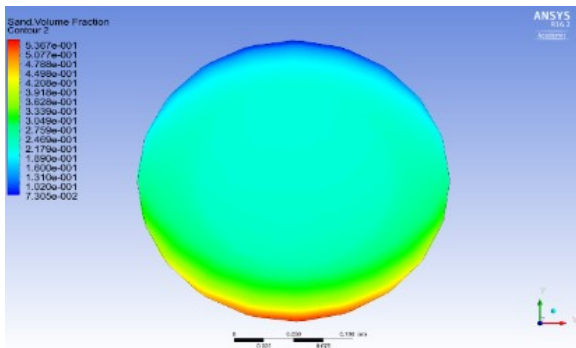
Figure 8 shows the two-phase water-slurry flow contours of the local volumetric concentration distribution of the solid phase in the vertical plane at the outlet cross-section for particle size of slurry 0.165 mm and mixture velocity of 3.5 m/s at different efflux concentrations of solid slurry. From contour analysis the region of highest solid concentration is located very near to the wall in the lower half of the pipe cross section. This happened because of gravity in horizontal pipeline which can lead to finding out the deposition velocity (i.e. minimum superficial velocity of mixture to prevent accumulation of solids or waste in the pipeline).



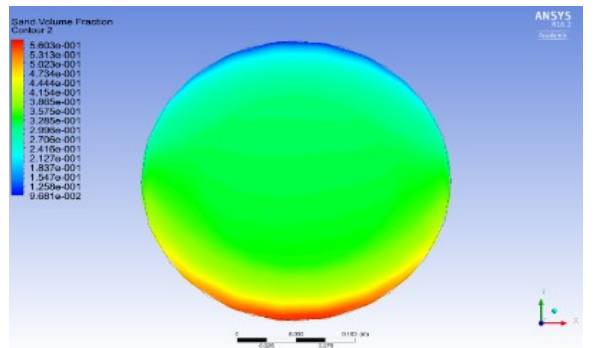
(a) Solid volumetric concentration 9.95%



(b) Solid volumetric concentration 18.4%



(c) Solid volumetric concentration 26.8%



(d) Solid volumetric concentration 33.8%

Figure 8. Solid concentration distribution in the vertical plane at the outlet

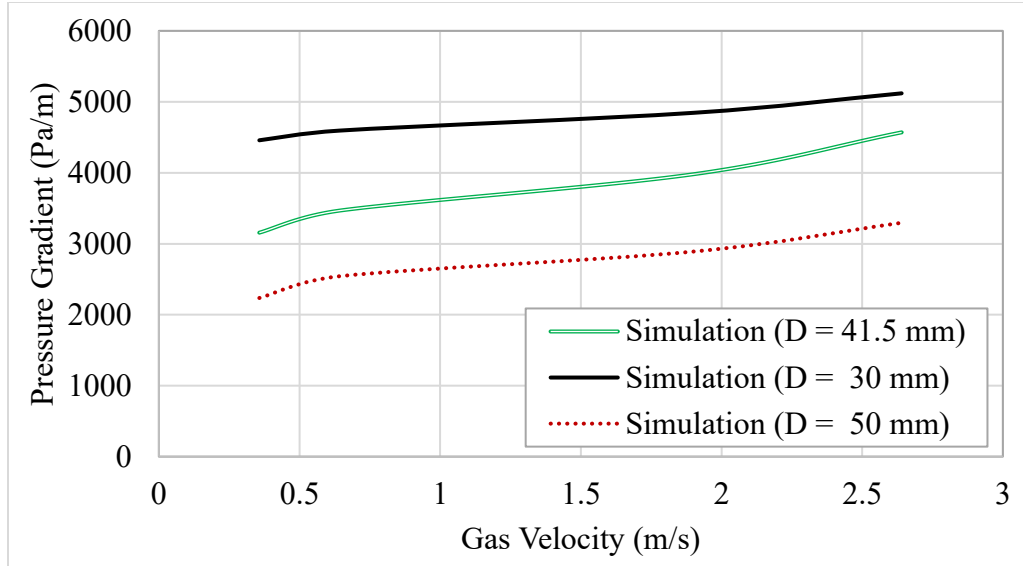


Figure 9. Pressure gradient at different gas velocity and pipe diameter

Keeping sand in situ concentration in slurry, fluid viscosity and pipe wall roughness constant in three phase air-water-slurry flow, Figure 9 graphically describes the change of pressure gradient with the change in internal pipe diameter (D) and gas velocity.

The Darcy-Weisbach equation is as follows –

$$\Delta P = \frac{fL}{D} \frac{\rho v^2}{2} \quad (12)$$

where, ΔP is pressure drop, f is friction factor, L is pipe length, D is internal diameter of the pipeline, ρ is fluid density and v is fluid velocity.

According to Equation (12), the pressure gradient decreases with the increase in internal pipe diameter, with the other parameters constant and the relation is inversely proportional. The increasing rate of pressure gradient is lower for smaller pipe diameters, but the trend of the increasing rate is almost the same. The pipeline should not be manufactured with a diameter size lower than a specific limit, which produces a maximum level of pressure drop required by industry.

Conclusion

This CFD simulation approach to multiphase flow through a horizontal pipeline demonstrates some good agreements and outcomes, with reference to experimental works. With the aim of building a model that can be applied in practical problems with fewer parameter boundary limitations, some analysis is performed under different conditions, after validating the developed model. A few of the approaches are listed below:

- Building a CFD model with Eulerian multiphase and RSM turbulence closure to simulate multiphase flow through a horizontal pipeline.
- Discussing the numerical explanation of CFD modelling and its assumptions with valid references.
- Demonstrating, with a diagram, an experimental flow loop which is sited in our laboratory.
- Simulating two-phase water-air slug flow and comparing with our own experiment.
- Validating two-phase water-sand slurry flow with reference to the experimental data.
- Validating three-phase air-water-sand flow with reference the experimental data; this also demonstrates the effect of adding air into two-phase slurry flow.
- Conducting a few parametric studies with two-phase and three-phase flow. Contour distribution of the in-situ concentration of sand and pressure gradient are used as output parameters to analyze the effects of changing parameters. The output shows similarity with developed theories and empirical correlations.

The study is ongoing with parametric analysis. CFD errors need to be reduced by focusing more on the choice of different coefficients and constants such as the coefficient of lift, coefficient of

drag, restitution coefficient and wall boundary conditions. The effect of vibration due to fluid flow will be a future task for this project.

Acknowledgements

The authors wish to acknowledge the Faculty of Engineering and Applied Science of Memorial University and ANSYS Inc. for help during this project.

References

- [1]. Geilikman, M. B., & Dusseault, M. B. (1997). Fluid rate enhancement from massive sand production in heavy-oil reservoirs. *Journal of Petroleum Science and Engineering*, 17(1), 5-18.
- [2]. Rajnauth, J., & Barrufet, M. (2012). Monetizing gas: Focusing on developments in gas hydrate as a mode of transportation. *Energy Science and Technology*, 4(2), 61-68.
- [3]. Miao, Z., Shastri, Y., Grift, T., Hansen, A., & Ting, K. (2012). Lignocellulosic biomass feedstock transportation alternatives, logistics, equipment configurations, and modeling. *Biofuels, Bioproducts and Biorefining*, 6(3), 351-362.
- [4]. Bello, O., Reinicke, K., & Teodoriu, C. (2005). Particle holdup profiles in horizontal gas-liquid-solid multiphase flow pipeline. *Chemical Engineering & Technology*, 28(12), 1546-1553.
- [5]. Mao, F., Desir, F. K., & Ebadian, M. A. (1997). Pressure drop measurement and correlation for three-phase flow of simulated nuclear waste in a horizontal pipe. *International journal of multiphase flow*, 23(2), 397-402.

- [6]. Al-Lababidi, S., Addali, A., Yeung, H., Mba, D., & Khan, F. (2009). Gas void fraction measurement in two-phase gas/liquid slug flow using acoustic emission technology. *Journal of Vibration and Acoustics*, 131(6), 064501.
- [7]. Czapp, M., Utschick, M., Rutzmoser, J., & Sattelmayer, T. (2012, July). Investigations on slug flow in a horizontal pipe using stereoscopic particle image velocimetry and CFD simulation with volume of fluid method. In *2012 20th International Conference on Nuclear Engineering and the ASME 2012 Power Conference* (pp. 477-486). American Society of Mechanical Engineers.
- [8]. Pouranfard, A. R., Mowla, D., & Esmailzadeh, F. (2015). An experimental study of drag reduction by nanofluids in slug two-phase flow of air and water through horizontal pipes. *Chinese Journal of Chemical Engineering*, 23(3), 471-475.
- [9]. Sanders, R., Schaan, J., & McKibben, M. (2007). Oil sand slurry conditioning tests in a 100 mm pipeline loop. *Canadian Journal of Chemical Engineering*, 85(5), 756-764.
- [10]. Scott, D. S., & Rao, P. K. (1971). Transport of solids by gas-liquid mixtures in horizontal pipes. *The Canadian Journal of Chemical Engineering*, 49(3), 302-309.
- [11]. Toda, M., Shimazaki, K., & Maeda, S. (1978). Pressure drop of three-phase flow in horizontal pipes. *Kagaku Kogaku Ronbunshu*, 4, 56-62.
- [12]. Fukuda, T., & Shoji, Y. (1986). Pressure drop and heat transfer for tree phase flow: 1st report, flow in horizontal pipes. *Bulletin of JSME*, 29(256), 3421-3426.
- [13]. Kago, T., Saruwatari, T., Kashima, M., Morooka, S., & Kato, Y. (1986). Heat transfer in horizontal plug and slug flow for gas-liquid and gas-slurry systems. *Journal of Chemical Engineering of Japan*, 19(2), 125-131.

- [14]. Toda, M., & Konno, H. (1987). Fundamentals of gas-liquid-solid three phase flow. *Japanese Journal of Multiphase Flow*, 1(2), 139-156.
- [15]. Gillies, R. G., McKibben, M. J., & Shook, C. A. (1997). Pipeline flow of gas, liquid and sand mixtures at low velocities. *Journal of Canadian Petroleum Technology*, 36(09).
- [16]. Bello, O. O., Udong, I. N., Falcone, G., & Teodoriu, C. (2010, January). Hydraulic analysis of gas/oil/sand flow in horizontal wells. In *SPE Latin American and Caribbean Petroleum Engineering Conference*. Society of Petroleum Engineers.
- [17]. Rahman, M. A., Adane, K. F., & Sanders, R. S. (2013). An improved method for applying the Lockhart–Martinelli correlation to three-phase gas–liquid–solid horizontal pipeline flows. *The Canadian Journal of Chemical Engineering*, 91(8), 1372-1382.
- [18]. Annaland, M., Deen, N. G., & Kuipers, J. A. M. (2005). Numerical simulation of gas–liquid–solid flows using a combined front tracking and discrete particle method. *Chemical Engineering Science*, 60(22), 6188-6198.
- [19]. Washino, Tan, Salman, & Hounslow. (2011). Direct numerical simulation of solid–liquid–gas three-phase flow: Fluid–solid interaction. *Powder Technology*, 206(1), 161-169.
- [20]. Liu, X., Aramaki, Y., Guo, L., & Morita, K. (2015). Numerical simulation of gas–liquid–solid three-phase flow using particle methods. *Journal of Nuclear Science and Technology*, 52(12), 1480-1489.
- [21]. Orell, A. (2007). The effect of gas injection on the hydraulic transport of slurries in horizontal pipes. *Chemical Engineering Science*, 62(23), 6659-6676.
- [22]. Alder, B. J., & Wainwright, T. E. (1960). Studies in molecular dynamics. II. Behavior of a small number of elastic spheres. *The Journal of Chemical Physics*, 33(5), 1439-1451.

- [23]. Syamlal, M., Rogers, W., & O'Brien, T. J. (1993). MFIx documentation: Theory guide. National Energy Technology Laboratory, Department of Energy, Technical Note DOE/METC-95/1013 and NTIS/DE95000031.
- [24]. Vijiapurapu, S., & Cui, J. (2010). Performance of turbulence models for flows through rough pipes. *Applied Mathematical Modelling*, 34(6), 1458-1466.
- [25]. Markatos, N. C. (1986). The mathematical modelling of turbulent flows. *Applied Mathematical Modelling*, 10(3), 190-220.
- [26]. Kaushal, D. R., Sato, K., Toyota, T., Funatsu, K., & Tomita, Y. (2005). Effect of particle size distribution on pressure drop and concentration profile in pipeline flow of highly concentrated slurry. *International Journal of Multiphase Flow*, 31(7), 809-823.
- [27]. Daly, B. J., & Harlow, F. H. (1970). Transport equations in turbulence. *Physics of Fluids (1958-1988)*, 13(11), 2634-2649.
- [28]. Gibson, M. M., & Launder, B. E. (1978). Ground effects on pressure fluctuations in the atmospheric boundary layer. *Journal of Fluid Mechanics*, 86(03), 491-511.
- [29]. Launder, B. E. (1989). Second-moment closure: present... and future?- *International Journal of Heat and Fluid Flow*, 10(4), 282-300.
- [30]. Sarkar, S., & Lakshmanan, B. (1991). Application of a Reynolds stress turbulence model to the compressible shear layer. *AIAA Journal*, 29(5), 743-749.
- [31]. Brown, N. P., & Heywood, N. I. (Eds.). (1991). *Slurry Handling: Design of solid-liquid systems*. Springer Science & Business Media.
- [32]. Roco, M. C., & Shook, C. A. (1983). Modeling of slurry flow: the effect of particle size. *The Canadian Journal of Chemical Engineering*, 61(4), 494-503.

Appendix 4. Data Tables

Table 1. Parametric Study Chart with Single Phase Fluid (Chapter 2)

| Controlled Variables | | | CFD Results |
|--|---------------------------|------------------|-----------------------------|
| Reynolds number ($Re=d_H V \rho / \mu$) | Rotational speed (rpm) | Eccentricity (%) | Pressure gradient (Pa/m) |
| 20000 | 0 | 0 | 82 |
| 40000 | 0 | 0 | 150 |
| 50000 | 0 | 0 | 230 |
| 60000 | 0 | 0 | 320 |
| 80000 | 0 | 0 | 557.575 |
| 100000 | 0 | 0 | 920.161 |
| 20000 | 50 | 0 | 103 |
| 40000 | 50 | 0 | 158 |
| 50000 | 50 | 0 | 234 |
| 60000 | 50 | 0 | 324 |
| 80000 | 50 | 0 | 562.112 |
| 100000 | 50 | 0 | 923.5 |
| 20000 | 100 | 0 | 165 |
| 40000 | 100 | 0 | 209 |
| 50000 | 100 | 0 | 269 |
| 60000 | 100 | 0 | 345 |

| | | | |
|--------|-----|----|---------|
| 80000 | 100 | 0 | 595.795 |
| 100000 | 100 | 0 | 933.455 |
| 20000 | 150 | 0 | 275 |
| 40000 | 150 | 0 | 293 |
| 50000 | 150 | 0 | 343 |
| 60000 | 150 | 0 | 407 |
| 80000 | 150 | 0 | 645.529 |
| 100000 | 150 | 0 | 966.1 |
| 20000 | 0 | 25 | 77 |
| 40000 | 0 | 25 | 140 |
| 50000 | 0 | 25 | 214 |
| 60000 | 0 | 25 | 299 |
| 80000 | 0 | 25 | 555.578 |
| 100000 | 0 | 25 | 902.474 |
| 20000 | 50 | 25 | 97 |
| 40000 | 50 | 25 | 150 |
| 50000 | 50 | 25 | 221 |
| 60000 | 50 | 25 | 304 |
| 80000 | 50 | 25 | 559.412 |
| 100000 | 50 | 25 | 906.422 |
| 20000 | 100 | 25 | 169 |
| 40000 | 100 | 25 | 206 |
| 50000 | 100 | 25 | 259 |

| | | | |
|--------|-----|----|---------|
| 60000 | 100 | 25 | 327 |
| 80000 | 100 | 25 | 542.354 |
| 100000 | 100 | 25 | 916.803 |
| 20000 | 150 | 25 | 291 |
| 40000 | 150 | 25 | 298 |
| 50000 | 150 | 25 | 340 |
| 60000 | 150 | 25 | 395 |
| 80000 | 150 | 25 | 582.623 |
| 100000 | 150 | 25 | 951.93 |
| 20000 | 0 | 50 | 80 |
| 40000 | 0 | 50 | 150 |
| 50000 | 0 | 50 | 238 |
| 60000 | 0 | 50 | 342 |
| 80000 | 0 | 50 | 639.231 |
| 100000 | 0 | 50 | 955.782 |
| 20000 | 50 | 50 | 112 |
| 40000 | 50 | 50 | 178 |
| 50000 | 50 | 50 | 263 |
| 60000 | 50 | 50 | 364 |
| 80000 | 50 | 50 | 644.75 |
| 100000 | 50 | 50 | 965.534 |
| 20000 | 100 | 50 | 203 |
| 40000 | 100 | 50 | 251 |

| | | | |
|--------|-----|----|---------|
| 50000 | 100 | 50 | 323 |
| 60000 | 100 | 50 | 416 |
| 80000 | 100 | 50 | 689.054 |
| 100000 | 100 | 50 | 1003.29 |
| 20000 | 150 | 50 | 355 |
| 40000 | 150 | 50 | 373 |
| 50000 | 150 | 50 | 428 |
| 60000 | 150 | 50 | 505 |
| 80000 | 150 | 50 | 750.208 |
| 100000 | 150 | 50 | 1056.07 |
| 20000 | 0 | 75 | 71 |
| 40000 | 0 | 75 | 135 |
| 50000 | 0 | 75 | 215 |
| 60000 | 0 | 75 | 310 |
| 80000 | 0 | 75 | 574.076 |
| 100000 | 0 | 75 | 907.722 |
| 20000 | 50 | 75 | 123 |
| 40000 | 50 | 75 | 197 |
| 50000 | 50 | 75 | 288 |
| 60000 | 50 | 75 | 395 |
| 80000 | 50 | 75 | 680.247 |
| 100000 | 50 | 75 | 1013.64 |
| 20000 | 100 | 75 | 231 |

| | | | |
|--------|-----|----|---------|
| 40000 | 100 | 75 | 296 |
| 50000 | 100 | 75 | 388 |
| 60000 | 100 | 75 | 501 |
| 80000 | 100 | 75 | 810.132 |
| 100000 | 100 | 75 | 1166.54 |
| 20000 | 150 | 75 | 401 |
| 40000 | 150 | 75 | 449 |
| 50000 | 150 | 75 | 528 |
| 60000 | 150 | 75 | 631 |
| 80000 | 150 | 75 | 948.062 |
| 100000 | 150 | 75 | 1313.03 |

Table 2. Parametric Study Chart with Two Phase Fluid (Chapter 2)

| Controlled Variables | | | | | CFD Results | |
|--|---------------------------|------------------|----------------------------------|--------------------|--------------------------|--|
| Reynolds number ($Re=d_H V \rho / \mu$) | Rotational speed (rpm) | Eccentricity (%) | Particle Input Concentration (%) | Particle Size (mm) | Pressure gradient (Pa/m) | Maximum Bed Concentration near bottom wall (%) |
| 40000 | stationary | Concentric | 5 | 0.05 | 766.966 | 58.12 |
| 70000 | stationary | Concentric | 5 | 0.05 | 848.724 | 22.09 |
| 100000 | stationary | Concentric | 5 | 0.05 | 1120.29 | 12.38 |
| 200000 | stationary | Concentric | 5 | 0.05 | 3126.42 | 7.49 |
| 40000 | stationary | Concentric | 20 | 0.05 | 767.134 | 58.14 |
| 70000 | stationary | Concentric | 20 | 0.05 | 848.557 | 22.04 |
| 100000 | stationary | Concentric | 20 | 0.05 | 1120.29 | 12.36 |
| 200000 | stationary | Concentric | 20 | 0.05 | 3118.21 | 7.47 |
| 40000 | stationary | Concentric | 5 | 0.1 | 767.674 | 58 |
| 70000 | stationary | Concentric | 5 | 0.1 | 837.6 | 42.1 |
| 100000 | stationary | Concentric | 5 | 0.1 | 1112.26 | 25.91 |
| 200000 | stationary | Concentric | 5 | 0.1 | 3120.31 | 10.15 |
| 40000 | stationary | Concentric | 20 | 0.1 | 761.902 | 52.73 |
| 70000 | stationary | Concentric | 20 | 0.1 | 837.166 | 42.15 |
| 100000 | stationary | Concentric | 20 | 0.1 | 1111.41 | 26.02 |
| 200000 | stationary | Concentric | 20 | 0.1 | 3129.55 | 10.16 |

| | | | | | | |
|--------|------------|------------|----|-------|---------|-------|
| 40000 | stationary | Concentric | 5 | 0.005 | 759.968 | 5.27 |
| 70000 | stationary | Concentric | 5 | 0.005 | 848.862 | 5.14 |
| 100000 | stationary | Concentric | 5 | 0.005 | 1121.32 | 5.1 |
| 200000 | stationary | Concentric | 5 | 0.005 | 3143.08 | 5.06 |
| 40000 | stationary | Concentric | 20 | 0.005 | 759.924 | 5.27 |
| 70000 | stationary | Concentric | 20 | 0.005 | 848.871 | 5.14 |
| 100000 | stationary | Concentric | 20 | 0.005 | 1121.6 | 5.1 |
| 200000 | stationary | Concentric | 20 | 0.005 | 3119.51 | 5.06 |
| 40000 | 150 | Concentric | 5 | 0.05 | 812.232 | 57.79 |
| 70000 | 150 | Concentric | 5 | 0.05 | 888.334 | 21.84 |
| 100000 | 150 | Concentric | 5 | 0.05 | 1162.98 | 12.33 |
| 200000 | 150 | Concentric | 5 | 0.05 | 3151.97 | 7.48 |
| 40000 | 150 | Concentric | 20 | 0.05 | 812.265 | 57.74 |
| 70000 | 150 | Concentric | 20 | 0.05 | 888.189 | 21.65 |
| 100000 | 150 | Concentric | 20 | 0.05 | 1162.52 | 12.32 |
| 200000 | 150 | Concentric | 20 | 0.05 | 3151.46 | 7.47 |
| 40000 | 150 | Concentric | 5 | 0.1 | 808.946 | 53.66 |
| 70000 | 150 | Concentric | 5 | 0.1 | 886.414 | 41.42 |
| 100000 | 150 | Concentric | 5 | 0.1 | 1155.53 | 25.81 |
| 200000 | 150 | Concentric | 5 | 0.1 | 3160.58 | 10.17 |
| 40000 | 150 | Concentric | 20 | 0.1 | 810.85 | 51.43 |
| 70000 | 150 | Concentric | 20 | 0.1 | 886.051 | 41.47 |
| 100000 | 150 | Concentric | 20 | 0.1 | 1156.06 | 25.85 |

| | | | | | | |
|--------|------------|------------|----|-------|---------|-------|
| 200000 | 150 | Concentric | 20 | 0.1 | 3149.8 | 10.16 |
| 40000 | 150 | Concentric | 5 | 0.005 | 799.978 | 5.27 |
| 70000 | 150 | Concentric | 5 | 0.005 | 882.585 | 5.14 |
| 100000 | 150 | Concentric | 5 | 0.005 | 1162.34 | 5.1 |
| 200000 | 150 | Concentric | 5 | 0.005 | 3166.04 | 5.06 |
| 40000 | 150 | Concentric | 20 | 0.005 | 799.909 | 5.27 |
| 70000 | 150 | Concentric | 20 | 0.005 | 882.953 | 5.14 |
| 100000 | 150 | Concentric | 20 | 0.005 | 1162.38 | 5.1 |
| 200000 | 150 | Concentric | 20 | 0.005 | 3146.69 | 5.06 |
| 85000 | stationary | 50 | 5 | 0.05 | 1042.12 | 33.71 |
| 100000 | stationary | 50 | 5 | 0.05 | 1198.23 | 26.03 |
| 200000 | stationary | 50 | 5 | 0.05 | 3255.59 | 9.96 |
| 300000 | stationary | 50 | 5 | 0.05 | 6848.14 | 7.76 |
| 85000 | stationary | 50 | 20 | 0.05 | 1055.6 | 33.46 |
| 100000 | stationary | 50 | 20 | 0.05 | 1206.28 | 24.9 |
| 200000 | stationary | 50 | 20 | 0.05 | 3278.31 | 9.9 |
| 300000 | stationary | 50 | 20 | 0.05 | 6693.65 | 7.78 |
| 85000 | stationary | 50 | 5 | 0.1 | 1011.03 | 26.39 |
| 100000 | stationary | 50 | 5 | 0.1 | 1263.45 | 23.56 |
| 200000 | stationary | 50 | 5 | 0.1 | 3170.89 | 9.91 |
| 300000 | stationary | 50 | 5 | 0.1 | 6479.87 | 6.83 |
| 85000 | stationary | 50 | 20 | 0.1 | 1016.64 | 30.3 |
| 100000 | stationary | 50 | 20 | 0.1 | 1179.16 | 23.6 |

| | | | | | | |
|--------|------------|----|----|-------|---------|-------|
| 200000 | stationary | 50 | 20 | 0.1 | 3180.33 | 10.62 |
| 300000 | stationary | 50 | 20 | 0.1 | 6636.22 | 7.2 |
| 85000 | stationary | 50 | 5 | 0.005 | 1036.05 | 5.35 |
| 100000 | stationary | 50 | 5 | 0.005 | 1192.55 | 5.3 |
| 200000 | stationary | 50 | 5 | 0.005 | 3184.09 | 5.15 |
| 300000 | stationary | 50 | 5 | 0.005 | 6544.09 | 5.1 |
| 85000 | stationary | 50 | 20 | 0.005 | 1035.73 | 5.36 |
| 100000 | stationary | 50 | 20 | 0.005 | 1195.77 | 5.3 |
| 200000 | stationary | 50 | 20 | 0.005 | 3186.63 | 5.15 |
| 300000 | stationary | 50 | 20 | 0.005 | 6519.47 | 5.1 |
| 85000 | 150 | 50 | 5 | 0.05 | 1095.77 | 32.5 |
| 100000 | 150 | 50 | 5 | 0.05 | 1259.55 | 24.06 |
| 200000 | 150 | 50 | 5 | 0.05 | 3342.23 | 10.21 |
| 300000 | 150 | 50 | 5 | 0.05 | 6794.4 | 7.72 |
| 85000 | 150 | 50 | 20 | 0.05 | 1096.93 | 29.37 |
| 100000 | 150 | 50 | 20 | 0.05 | 1277.49 | 22.62 |
| 200000 | 150 | 50 | 20 | 0.05 | 3352.92 | 9.85 |
| 300000 | 150 | 50 | 20 | 0.05 | 6849.01 | 7.55 |
| 85000 | 150 | 50 | 5 | 0.1 | 1075.24 | 25.28 |
| 100000 | 150 | 50 | 5 | 0.1 | 1226.04 | 24.57 |
| 200000 | 150 | 50 | 5 | 0.1 | 3196.13 | 9.8 |
| 300000 | 150 | 50 | 5 | 0.1 | 6533.21 | 6.94 |
| 85000 | 150 | 50 | 20 | 0.1 | 1071.57 | 25.25 |

| | | | | | | |
|--------|-----|----|----|-------|---------|-------|
| 100000 | 150 | 50 | 20 | 0.1 | 1244.69 | 22.86 |
| 200000 | 150 | 50 | 20 | 0.1 | 3216.8 | 10.19 |
| 300000 | 150 | 50 | 20 | 0.1 | 6656.04 | 7.32 |
| 85000 | 150 | 50 | 5 | 0.005 | 1092.88 | 5.35 |
| 100000 | 150 | 50 | 5 | 0.005 | 1257.26 | 5.29 |
| 200000 | 150 | 50 | 5 | 0.005 | 3246.63 | 5.15 |
| 300000 | 150 | 50 | 5 | 0.005 | 6567.77 | 5.1 |
| 85000 | 150 | 50 | 20 | 0.005 | 1091.97 | 5.35 |
| 100000 | 150 | 50 | 20 | 0.005 | 1261.21 | 5.29 |
| 200000 | 150 | 50 | 20 | 0.005 | 3243.02 | 5.15 |
| 300000 | 150 | 50 | 20 | 0.005 | 6561.63 | 5.1 |